

**Development of Large-Capacity Optical Path Networks
Using Ultra-Dense Wavelength Division Multiplexing**

超高密度波長分割多重を用いた
大容量光パスネットワークに関する研究

SHIRAKI Ryuta

白木 隆太

Department of Information and Communication Engineering

Nagoya University

Table of Contents

| | |
|---|----|
| Table of Contents | 2 |
| List of Figures | 6 |
| List of Tables..... | 8 |
| Chapter 1 Introduction..... | 9 |
| 1.1 Background | 9 |
| 1.2 Ultra-dense WDM network and its problem..... | 9 |
| 1.3 Purpose of this study..... | 10 |
| 1.3.1 Digital signal processing | 10 |
| 1.3.2 Network design..... | 11 |
| 1.3.3 Network control | 12 |
| 1.4 Organization of dissertation | 13 |
| References | 14 |
| Chapter 2 Optical path network | 17 |
| 2.1 Overview of optical path networks | 17 |
| 2.2 Digital coherent optical transmission | 19 |
| 2.2.1 Quadrature amplitude modulation | 20 |
| 2.2.2 Polarization-division multiplexing..... | 21 |
| 2.3 Optical cross-connect..... | 22 |
| 2.3.1 Architecture of optical cross-connect | 22 |
| 2.3.2 Splitters and couplers..... | 24 |
| 2.3.3 Wavelength-selective switch..... | 24 |
| 2.4 Network control | 26 |
| 2.4.1 Wavelength continuity constraint | 26 |
| 2.4.2 Network-resource assignment | 26 |
| 2.4.3 Network scenarios | 28 |

| | |
|--|----|
| 2.5 Summary..... | 28 |
| References | 29 |
| Chapter 3 Ultra-dense WDM network..... | 31 |
| 3.1 Ultra-dense WDM..... | 31 |
| 3.2 Spectrum-narrowing effect | 32 |
| 3.3 Noise enhancement in DSP circuit..... | 35 |
| 3.4 Spectrum narrowing in networking..... | 36 |
| 3.5 Grouped routing..... | 39 |
| 3.6 Mismatch with WSS resolution | 41 |
| 3.7 Summary..... | 41 |
| References | 42 |
| Chapter 4 Digital signal processing mitigating spectrum narrowing..... | 44 |
| 4.1 Introduction..... | 44 |
| 4.2 Conventional demodulation method..... | 45 |
| 4.2.1 Sequence estimation | 45 |
| 4.2.2 ISI-imposing filter..... | 46 |
| 4.3 Symbol decision based on machine learning | 47 |
| 4.3.1 Machine learning for symbol decision..... | 47 |
| 4.3.2 Neural network | 47 |
| 4.4 Proposed demodulation method..... | 49 |
| 4.5 Simulation..... | 50 |
| 4.5.1 Simulation setup | 50 |
| 4.5.2 Simulation result | 52 |
| 4.6 Conclusion | 58 |
| References | 58 |
| Chapter 5 Design for ultra-dense WDM networks..... | 62 |
| 5.1 Introduction..... | 62 |

| | |
|---|-----|
| 5.2 Coarsely granular routing | 63 |
| 5.3 Filter-less drop operation | 63 |
| 5.4 Design scheme of ultra-dense WDM networks | 65 |
| 5.4.1 Concept..... | 65 |
| 5.4.2 Network design algorithm | 66 |
| 5.5 Simulations..... | 69 |
| 5.5.1 Simulation setup | 69 |
| 5.5.2 Simulation result | 70 |
| 5.6 Conclusion | 74 |
| References | 74 |
| Chapter 6 Control in ultra-dense WDM networks | 77 |
| 6.1 Introduction | 77 |
| 6.2 Proposed path control scheme for ultra-dense WDM networks..... | 78 |
| 6.2.1 Path bundling..... | 78 |
| 6.2.2 Wavelength assignment aware of signal-spectrum narrowing..... | 79 |
| 6.2.3 Filter-less drop operation for path bundling | 79 |
| 6.2.4 Wavelength-assignment algorithm..... | 80 |
| 6.3 Simulations..... | 82 |
| 6.4 Transmission experiments | 88 |
| 6.5 Conclusion | 93 |
| References | 93 |
| Chapter 7 Integration..... | 95 |
| 7.1 ML-based DSP assuming impairment-aware wavelength assignment..... | 95 |
| 7.2 Network design based on sub-networks | 99 |
| 7.3 Dynamic path control in ultra-dense WDM networks | 99 |
| 7.4 Conclusion | 101 |
| Chapter 8 Conclusion | 102 |

| | |
|---------------------------|-----|
| Acknowledgement..... | 103 |
| List of Publications..... | 104 |

List of Figures

| | |
|---|----|
| Figure 1.1 Organization of the dissertation. | 13 |
| Figure 2.1 Optical path network. | 18 |
| Figure 2.2 Typical digital coherent receiver..... | 19 |
| Figure 2.3 Examples of QAM signals on a complex plane. | 20 |
| Figure 2.4 Schematic of polarization-division multiplexing. | 21 |
| Figure 2.5 Configurations of optical nodes. | 23 |
| Figure 2.6 Example of the operations of a splitter and a coupler. | 24 |
| Figure 2.7 Example of the operations of a WSS..... | 25 |
| Figure 2.8 Wavelength continuity constraint. | 26 |
| Figure 2.9 An example of network resource assignment. | 27 |
| Figure 3.1 Spectrum narrowing effect | 33 |
| Figure 3.2 Inter-symbol interference | 34 |
| Figure 3.3 Interaction between spectrum narrowing and ASE noise in a network..... | 34 |
| Figure 3.4 Noise enhancement induced by ISI-suppressing filter. | 35 |
| Figure 3.5 The operations with/without spectrum narrowing for a B&S node..... | 37 |
| Figure 3.6 The operations with/without spectrum narrowing for a R&S node..... | 38 |
| Figure 3.7 Grouped routing..... | 39 |
| Figure 3.8 Fiber capacity variation subject to GRE width. | 40 |
| Figure 3.9 The limited WSS-passband resolution..... | 41 |
| Figure 4.1 An example of maximum likelihood sequence estimation | 46 |
| Figure 4.2 A unit of NN..... | 48 |
| Figure 4.3 The basic NN model..... | 48 |
| Figure 4.4 Proposed demodulation framework. | 49 |
| Figure 4.5 Bidirectional RNN model..... | 50 |
| Figure 4.6 Simulation setup. | 52 |
| Figure 4.7 The transition of learning accuracy of bi-RNN..... | 53 |
| Figure 4.8 Evaluation of the BER performances of RNN structures. | 53 |
| Figure 4.9 Evaluation of the ISI-imposing filter ability | 54 |
| Figure 4.10 The time-sequence dependency of bi-RNN performance. | 54 |
| Figure 4.11 A constellation map after RNN model based on regression. | 55 |
| Figure 4.12 Demodulation performances of classification-/regression-based RNN. | 56 |
| Figure 4.13 BER vs. transmission distance in ultra-dense WDM network. | 57 |
| Figure 4.14 BER vs. transmission distance in quasi-Nyquist WDM network..... | 57 |

| | |
|---|-----|
| Figure 5.1 Filter-less drop..... | 64 |
| Figure 5.2 Proposed sub-network-based network design scheme | 65 |
| Figure 5.3 Comparison of spectrum-narrowing occurrences..... | 66 |
| Figure 5.4 An example of sub-networks. | 71 |
| Figure 5.5 Variations of the number of fibers. | 73 |
| Figure 6.1 Bundling of multiple paths. | 79 |
| Figure 6.2 Flowchart of the proposed wavelength-assignment algorithm. | 81 |
| Figure 6.3 Spectral-efficiency degradation due to spectrum narrowing..... | 84 |
| Figure 6.4 Spectral-efficiency degradation due to path bundling..... | 85 |
| Figure 6.5 Spectral efficiency as a function of traffic intensity, where the traffic distribution is uniform..... | 86 |
| Figure 6.6 Spectral efficiency as a function of traffic intensity, where the traffic distribution is centralized..... | 87 |
| Figure 6.7 Experimental setup..... | 90 |
| Figure 6.8 BER characteristics for 400-Gbps signals..... | 92 |
| Figure 7.1 Simulation setup. | 96 |
| Figure 7.2 BER vs. transmission distance for ultra-dense WDM networks..... | 98 |
| Figure 7.3 BER vs. transmission distance for quasi-Nyquist WDM networks..... | 99 |
| Figure 7.4 Blocking-ratio variations..... | 101 |

List of Tables

| | |
|---|----|
| Table 3.1 WDM schemes | 32 |
| Table 5.1 Variables and parameters for ILP-based network design scheme..... | 67 |
| Table 5.2 Tested physical topologies and their characteristics..... | 70 |
| Table 5.3 Network configurations..... | 70 |
| Table 6.1 Comparison of networking schemes..... | 82 |
| Table 6.2 Transmittable distance for 400-Gbps signals..... | 91 |

Chapter 1

Introduction

1.1 Background

Optical fiber technology firstly got attracted in 1966; C. K. Kao reported that the fundamental limitation for optical fiber loss is below 20 dB/km, which arouse much controversy to find low-loss materials for decades [1]. In 1987, an erbium-doped fiber amplifier (EDFA) enabling optical amplification around at 1.55 μm waveband suitable for low-loss optical fiber transmission innovates the optical fiber technology [2, 3]. In the 1990s, the capacity of an optical fiber is drastically enhanced by wavelength-division multiplexing (WDM) technology, where multiple optical signals with different wavelength channels are transmitted simultaneously in a single optical fiber [4-6]. Since the early 2000s, the digital coherent transmission system re-innovates optical fiber communication systems [7, 8]. The digital signal processing (DSP) circuit can remove various system impairments in the digital domain. The digital coherent transmission system allows us to use polarization-division multiplexing (PDM) and multi-level modulation such as quadrature phase shift keying (QPSK) and quadrature amplitude modulation (QAM). As a result, the spectral efficiency is drastically enhanced compared to the previous non-coherent systems.

Internet traffic demands have been growing over the past decades and the growth will continue or even accelerate due to recently emerging bandwidth-intensive services such as ultra-high-definition video-distribution service, cloud-computing service, big-data analysis based on machine learning (ML), and so on [9]. The capacity expansion of optical fiber communication is the never-ending challenge.

1.2 Ultra-dense WDM network and its problem

In optical fiber networks, the optical nodes using wavelength selective switches (WSSs) can transparently forward WDM signals without relying on costly optical-to-electrical and electrical-to-optical converters. The wavelength bandwidth available in optical fiber communications is limited due to characteristics of optical amplifiers. To enhance the capacity under the restriction,

a bandwidth assigned for each WDM signal needs to be reduced. Ultra-dense WDM systems, where the guard-bands inserted between WDM signals are narrower than those in the conventional dense WDM (DWDM) systems, are expected to realize higher spectral efficiency. Many studies have shown the effectiveness of ultra-dense WDM technology in point-to-point transmission systems that do not use optical nodes [10, 11]. On the other hand, its use for networking is hindered by spectrum narrowing caused by optical node traversals. In ultra-dense WDM networks, signal spectra are narrowed by a WSS used for wavelength-by-wavelength routing, which is referred to as the spectrum-narrowing effect. The spectrum narrowing can be avoided if the transfer function of a WSS is rectangular; however, actual WSS passbands have gradual cut-off characteristics, so spectrum narrowing is inevitable. To enjoy the benefit of ultra-dense WDM networks, therefore, we must mitigate or control the impact of spectrum narrowing.

1.3 Purpose of this study

The purpose of this paper is to enhance the spectral efficiency in optical networks by exploiting the ultra-dense WDM technology. To realize such networks, we focus on the following three approaches; (1) digital signal processing, (2) network design, and (3) network control.

1.3.1 Digital signal processing

The advent of digital coherent optical communication technology, which combines DSP and coherent optical receivers, has dramatically increased the capacity of optical networks. A phase/polarization-diversity optical receiver can extract in-phase and quadrature components of the electric field in both polarization modes. Then, the obtained analog signals are converted into digital signals by a high-speed analog-to-digital converter (ADC). In the digital domain, the signal is regenerated by chromatic-dispersion (CD) compensation, polarization-mode demultiplexing, and carrier-phase estimation. This enables the adoption of multi-level modulation techniques, *e.g.*, PSK and QAM, and polarization-division multiplexing. As a result, communication capacity increases more than 10 times greater than that of conventional non-coherent systems. On the other hand, the transmission capacity depends greatly on the performance of the DSP algorithm executed inside the receiver.

Spectrum narrowing caused in ultra-dense WDM networks is also expected to be eliminated by a DSP circuit. If only the spectrum-narrowing effect degrades the signal quality, the digital filter with the inverse transfer function can perfectly compensate for the spectrum narrowing. In

practical systems, however, the spectrum narrowing interacts with amplified spontaneous emission (ASE) noise generated by optical amplifiers. As a result, perfect compensation for the spectrum narrowing is no longer attainable. Several DSP methods for this problem has been reported [12, 13]. The work in [12] developed the demodulation method collaborating the fixed digital filter and sequence estimation to suppress the impact of spectrum narrowing. Although the approach improved the robustness against the spectrum narrowing for the specific channel model, the fixed digital filter and sequence estimation cannot adapt to various channel models. The work in [13] studied a machine learning (ML) based DSP method adaptive to the variable channel model. However, it did not take the interaction between spectrum narrowing and ASE noise into consideration.

To suppress the interactive impact of spectrum narrowing and ASE noise for arbitrary channel model, we proposed a new DSP method based on ML. By using a recurrent neural network (RNN) to learn the signal deterioration pattern, the signal can be appropriately demodulated even under the interactive effect of spectrum narrowing and ASE noise. The proposal has improved the robustness against spectral narrowing and succeeded in expanding the applicable area of ultra-dense WDM. Since the proposed method can be realized only with a slight change in the DSP circuit of the present receiver, the introduction of the proposed method to commercial systems can be expected to be installed at an early stage.

1.3.2 Network design

In the conventional optical fiber networks using electrical switches, the high power consumption was a bottleneck for enhancing the throughput of optical nodes [14]. Transport systems based on electrical switches necessitate optical-electrical-optical (O-E-O) conversion, which results in high power consumption. The next-generation network using optical switches, on the other hand, reduces the power consumption by eliminating O-E-O conversions. In such systems, an optical cross-connect in an optical node flexibly controls routes of WDM signals wavelength-by-wavelength in the optical domain. Such a transparent process contributes to the significant reduction of power consumption. For example, to process 1000-port switch in which each port is responsible for a 1 Tbps signal, an optical switch consumes less than 1 kW, while an electrical switches consumes about 6000 kW [15, 16].

In ultra-dense WDM networks, signals suffer from spectrum narrowing caused at optical nodes. An optical signal is impaired when the optical-node operation for routing is applied to the optical signals adjacent in the frequency domain. As a result, conventional network design schemes used for DWDM networks cannot be applied to ultra-dense WDM networks. This motivates us to

develop network architecture that can easily manage the effects of spectrum narrowing while retaining the routing flexibility. So far, many network design schemes considering the impact of spectrum narrowing have been reported. In [17, 18], the available frequency range is divided into several wavebands, and a broad guardband is inserted only between the wavebands. Optical signals in the same waveband are routed together, *i.e.*, coarsely granular routing, while an optical signal in a waveband can be dropped/added on a wavelength basis. With this hierarchical optical network design, the spectrum narrowing is induced only by wavelength-granular add/drop operation. Note that ultra-dense WDM is expected to offer higher spectral efficiency compared to [17]; however, it necessitates more sophisticated network design scheme since the number of possible spectrum-narrowing events is much larger.

In order to resolve this problem, we proposed a network design scheme enabling introduction of ultra-dense WDM. In our proposal, the wavelength-granular routing and the fiber-granular routing are combined so as to minimize the effect of spectral narrowing while realizing an appropriate routing flexibility. By formulating the conditions of connection based on integer linear programming (ILP), the configurations for cross-connects are optimized. As a result, ultra-dense WDM can be applied even to complicated network topologies that would be severely affected by spectral narrowing. The proposed scheme is applicable not only to the existing optical cross-connects but also to cost-efficient fiber cross-connects (FXCs) that are expected to be introduced in the future.

1.3.3 Network control

In current optical path networks, a wavelength assigned to each WDM signal cannot be converted into another wavelength along the transmission line to retain the transparent processes. In other words, the optical signal must use the same wavelength from the transmitter to the receiver, which is referred to as the wavelength continuity constraint. The pair of route and wavelength must be controlled for numerous optical signals under the constraint. The routing and wavelength assignment (RWA) task is categorized as NP-hard [19]. Furthermore, the spectrum-narrowing effect induced in the ultra-dense WDM networks strictly shortens the signal transmission reach. To effectively manage the optical fiber resources being depleted, we need to develop a sophisticated RWA algorithm aware of transmission impairments. Several impairment-aware algorithms have been studied [20-22]. The work shown in [20] studied the network control method considering multiple physical-layer impairments, such as power loss, ASE noise, and self-phase modulation (SPM). However, it did not assume the spectrum narrowing effect induced in ultra-dense WDM networks. Since the impact of spectrum narrowing cannot be fully eliminated

by any DSP algorithm, the impact of spectrum narrowing needs to be controlled in order to introduce ultra-dense WDM into a network. Considering the above background, we proposed an RWA algorithm that controls the expectation of spectrum narrowing caused in ultra-dense WDM networks. With the method, the number of spectrum-narrowing events for each optical path is controlled so as not to exceed the limit. The effectiveness of the proposal is verified through network simulations and transmission experiments. Our proposal can realize highly dense WDM networks without relying upon state-of-the-art hardware.

1.4 Organization of dissertation

This dissertation is organized with 8 chapters, and covers a comprehensive overview on the optical path networks. Chapter 1 presented the introduction of this dissertation. Chapter 2 describes a comprehensive review of the optical path networks. Chapter 3 presents the detail of ultra-dense WDM network. As mentioned in Section 1.3, we focus on three topics for the ultra-dense WDM networking. Chapter 4, Chapter 5, and Chapter 6 will be dedicated to each of the topics. In Chapter 4, the DSP method to mitigate the spectrum narrowing is described. Chapter 5 reports the network design scheme for ultra-dense WDM networks. Chapter 6 presents the network control method, where the optical paths are intellectually managed. After detailing each key technology, the integrated network architecture enabling ultra-dense WDM networks is presented in Chapter 7. The general conclusion is provided in Chapter 8.

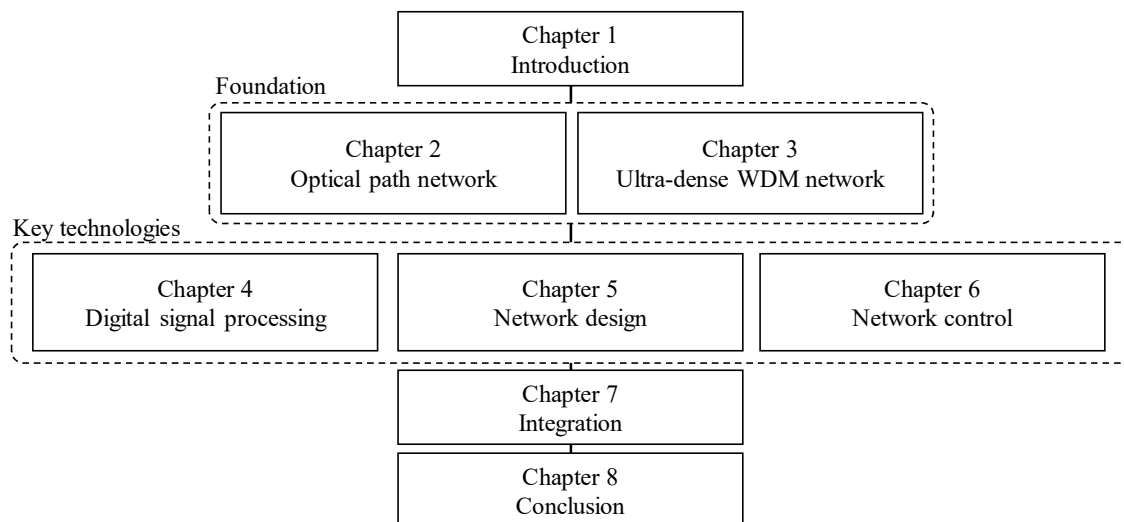


Figure 1.1 Organization of the dissertation.

References

- [1] K. C. Kao and G. A. Hockham, "Dielectric-fibre surface waveguides for optical frequencies," *Proceedings of the Institution of Electrical Engineers*, vol. 113, no.7, pp. 1151-1158 (1966).
- [2] E. Desurvire, J. R. Simpson, and P. C. Becker, "High-gain erbium-doped traveling-wave fiber amplifier," *Optica Optics Letters*, vol. 12, no. 11, pp. 888-890 (1987).
- [3] M. Nakazawa, Y. Kimura, and K. Suzuki, "Soliton amplification and transmission with an Er³⁺-doped fiber repeater pumped by InGaAsP laser diodes," in *Technical Digest of Optical Fiber Communication Conference (OFC)*, paper PD2 (1989).
- [4] P. C. Becker, N. A. Olsson, J. R. Simpson, *Erbium-doped fiber amplifier*, Academic Press (1999).
- [5] C.A. Brackett, "Dense wavelength division multiplexing networks: Principles and applications," *IEEE Journal on Selected Areas in Communications*, vol. 8, no. 6, pp. 948-964 (1990).
- [6] K. Hagimoto, K. Iwashita, A. Takada, M. Nakazawa, M. Saruwatari, K. Aida, K. Nakazawa, and M. Horiguchi, "A 212 km non-repeated transmission experiment at 1.8 Gb/s using LD pumped Er³⁺-doped fiber amplifiers in an IM/directed-detection repeater system," in *Technical Digest of Optical Fiber Communication Conference (OFC)*, paper PD15, (1989).
- [7] G. P. Agrawal, *Fiber-optic communication systems*, Wiley-Interscience (2002).
- [8] T. Okoshi, "Recent advances in coherent optical fiber communication systems," *IEEE Journal of Lightwave Technology*, vol. 5, pp. 44-52 (1987).
- [9] Cisco Visual Networking Index (VNI) White paper, "Forecast and methodology, 2017–2022," (2019).
- [10] S. Kilmurray, T. Fehenberger, P. Bayvel, and Ri Killey, "Comparison of the nonlinear transmission performance of quasi-Nyquist WDM and reduced guard interval OFDM," *Optica Optics Express*, vol. 20, no. 4, pp. 4198-4205 (2012).
- [11] G. Bosco, V. Curri, A. Carena, P. Poggiolini, and F. Forghieri, "On the performance of Nyquist-WDM terabit superchannels based on PM-BPSK, PM-QPSK, PM-8QAM or PM-16QAM subcarriers," *IEEE Journal of Lightwave Technology*, vol. 29, pp. 53-61 (2011).
- [12] S. Yamaoka, Y. Mori, H. Hasegawa, and K. Sato, "Novel demodulation framework based on

quadrature duo-binary/quaternary/octernary spectrum shaping and MLSE for mitigating spectrum narrowing caused by node traversals,” in Proc. ECOC, Rome, Italy, Sept. 2018, pp. Mo4F.5.

- [13] M. Schaedler, F. Pittalà, G. Böcherer, C. Bluemm, M. Kuschnerov, and S. Pachnicke, “Recurrent neural network soft-demapping for nonlinear ISI in 800Gbit/s DWDM coherent optical transmissions,” *IEEE/Optica Journal of Lightwave Technology*, vol. 39, no. 16, pp. 5278-5286 (2021).
- [14] W. Vereecken, W. Van Heddeghem, M. Deruyck, B. Puype, B. Lannoo, W. Joseph, D. Colle, L. Martens, and P. Demeester, “Power consumption in telecommunication networks: overview and reduction strategies,” *IEEE Communications Magazine*, vol. 49, no. 6, pp. 62-69 (2011).
- [15] S. Namiki, “Introduction to VICTORIES – challenges for dynamic optical path network,” International Symposium on VICTORIES Project & workshop (2014).
- [16] D. Sinefeld, S. Shalva Ben-Ezra, and D. M. Marom, “Nyquist-WDM filter shaping with a high-resolution colorless photonic spectral processor,” *Optica Optics Letters*, vol. 38, no. 17, pp. 3268-3271 (2013).
- [17] Y. Terada, Y. Mori, H. Hasegawa, and K. Sato, “Highly spectral efficient networks based on grouped optical path routing,” *Optica Optics Express*, vol. 24, pp. 6213-6228 (2016).
- [18] J. M. Fàbrega, M. S. Moreolo, L. Martín, A. C. Piat, E. Riccardi, D. Roccatò, N. Sambo, F. Cugini, L. Potí, S. Yan, E. Hugues-Salas, D. Simeonidou, M. Gunkel, R. Palmer, S. Fedderwitz, D. Rafique, T. Rahman, H. de Waardt, and A. Napoli, "On the filter narrowing issues in elastic optical networks," *IEEE/Optica Journal of Optical Communications and Networking*, vol. 8, no. 7, pp. A23 - A33 (2016).
- [19] I. Chlamtac, A. Ganz, and G. Karmi, “Lightpath communications: an approach to high bandwidth optical WAN’s,” *IEEE Trans. Commun.*, Vol. 40, pp. 1171–1182 (1992).
- [20] S. Behera, A. Deb, G. Das, Member, and B. Mukherjee “Impairment aware routing, bit loading, and spectrum allocation in elastic optical networks,” *IEEE Journal of Lightwave Technology Letter*, vol. 37, no. 13, pp. 3009-3020 (2019).
- [21] J. Zhao, B. Bao, H. Yang, E. Oki, and B. C. Chatterjee, “A holding-time- and impairment-aware shared spectrum allocation in mixed-line-rate elastic optical networks,” *Journal of Optical Communications and Networking*, vol. 11, no. 6, pp. 322-332 (2018).

- [22] C. V. Saradhi and Suresh Subramaniam, "Physical layer impairment aware routing (PLIAR) in wdm optical networks: issues and challenges," *IEEE Communications Surveys and Tutorials*, vol. 11, no. 4, pp. 109-130 (2009).

Chapter 2

Optical path network

Optical path network is a cornerstone of the information and communication society. All kinds of digital services, such as social media services, video streaming services, cloud computing services, and so on, depends on optical path networks. To effectively utilize costly optical fibers, the WDM technologies has been extensively studied and implemented in commercial systems. There are various elaborated components and technologies for effective use of optical path network. In this chapter, the fundamentals of optical path networks are described.

2.1 Overview of optical path networks

A typical optical path network is mainly composed of three elements: optical fibers, optical amplifiers, and optical nodes as shown in Figure 2.1. To provide a high-capacity communication infrastructure, wavelength-division multiplexing (WDM) transmission has already been commercially introduced in optical path networks. This technology enables the transmission of multiple optical signals with different wavelength channels simultaneously in an optical fiber [1, 2]. An optical path corresponds to one communication connection, and characterizes the route and resources assigned for the optical signal.

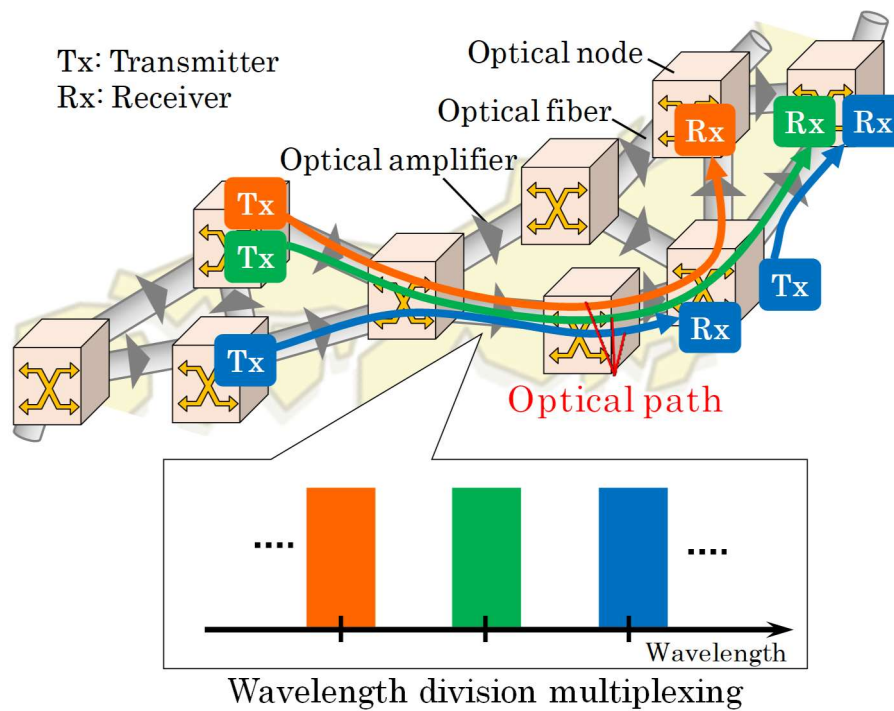


Figure 2.1 Optical path network.

An optical fiber is a medium propagating a lightwave. The most commonly used optical fiber is a standard single-mode fiber (SSMF) made of silica glass, where the propagation loss around the bandwidth of $1.55\mu\text{m}$ is now less than 0.2 dB/km [3].

Optical amplifiers are deployed to compensate power loss yielded by traversing devices. All optical amplifiers have limited bandwidth characteristics for amplification. Among the various optical amplifiers, an erbium-doped optical amplifier (EDFA) is mainly utilized because the gain profile is suitable for the bandwidth where the propagation loss of SSMF is minimized [4, 5]. Optical amplifiers add one of the main signal degradation factors of amplified-spontaneous-emission (ASE) noise. The ASE noise cannot be eliminated by any processes. Therefore, the impact of ASE noise needs to be minimized by keeping the signal power high. The ASE noise is modeled as the additive white Gaussian noise (AWGN).

An optical node consists of optical transmitters, an optical cross-connect, and optical receivers. At an optical transmitter, a WDM signal is generated and sent to the optical network. In optical cross-connect, the direction of each optical signal is controlled without power-consuming optical-electrical-optical (O-E-O) conversion. Then, the transmitted signals are exported to optical receivers. All of the processes are conducted in the optical domain.

2.2 Digital coherent optical transmission

Until the 2000s, intensity modulation / direct detection (IM-DD) had been used in optical fiber communications. In the IM-DD system, an intensity-modulated signal that allocates bits only for intensity carries information. At the receiver, the intensity information is directly obtained by square-law detection of the optical electric field using a photodiode.

Since the 2000s, the digital coherent optical receiver has been attracted for high-speed and high-capacity optical communication systems [6, 7]. Figure 2.2 shows the schematic of the digital coherent optical receiver. A digital coherent receiver system is realized by coherent detection and digital signal processing (DSP) technology. First, the received polarization-division multiplexed (PDM) signal is demultiplexed by a polarization demultiplexer. Next, the signals for both polarizations are separated into in-phase and quadrature-phase components. This process is realized by interfering with a signal lightwave and a lightwave generated by a local oscillator (LO) using 90-degree optical hybrid circuit. Here, the analog signals are converted into digital signals using analog-to-digital converter (ADC). Then, DSP circuit conducts equalization, chromatic-dispersion (CD) compensation, polarization mode dispersion (PMD) compensation, and phase estimation. Since the complex electric value contains both the amplitude information and phase information of the signal, any multi-level modulation method such as quadrature phase shift keying (QPSK) and quadrature amplitude modulation (QAM) can be utilized. In addition, PDM is also available, which doubles the fiber capacity.

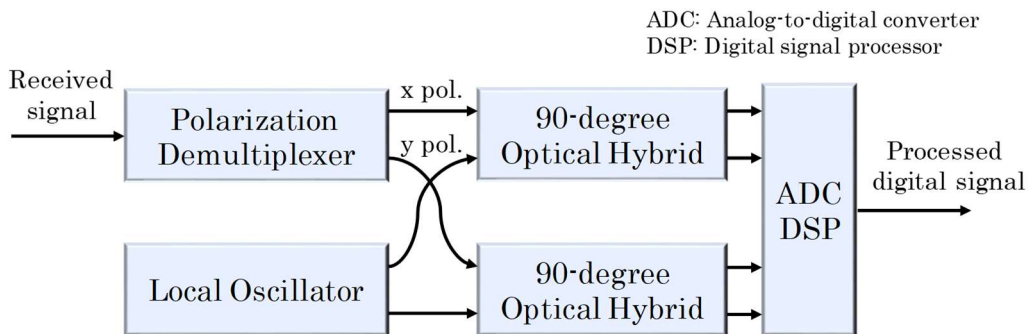


Figure 2.2 Typical digital coherent receiver.

2.2.1 Quadrature amplitude modulation

Figure 2.3 shows the constellation map of a general 4-/16-/64-QAM signal, where M of M -QAM is called the modulation order. Figure 2.3(a) and Figure 2.3(b) show the constellation maps for the signal with noise and signal without noise. A QAM signal transmits bit information using the modulation parameters of phase and intensity. By setting the modulation order to M , the amount of information bit per symbol can be $\log_2 M$ bits. Note that 4-QAM and QPSK are the same modulation method. The spectral efficiency can be enhanced as the modulation order increases. However, since the Euclid distance between symbols on a complex plane shortens, decision errors are more likely to occur as shown in Figure 2.3(b). Although the Euclid distance between symbols can be elongated by increasing the signal power, the high signal power induces signal waveform distortion through fiber nonlinearity referred to as the Kerr effect, which includes self-phase modulation (SPM), cross-phase modulation (XPM), and four-wave mixing (FWM) [8]. Therefore, the signal quality worsens as the modulation order increases, which results in the possible transmission distance shorter [9].

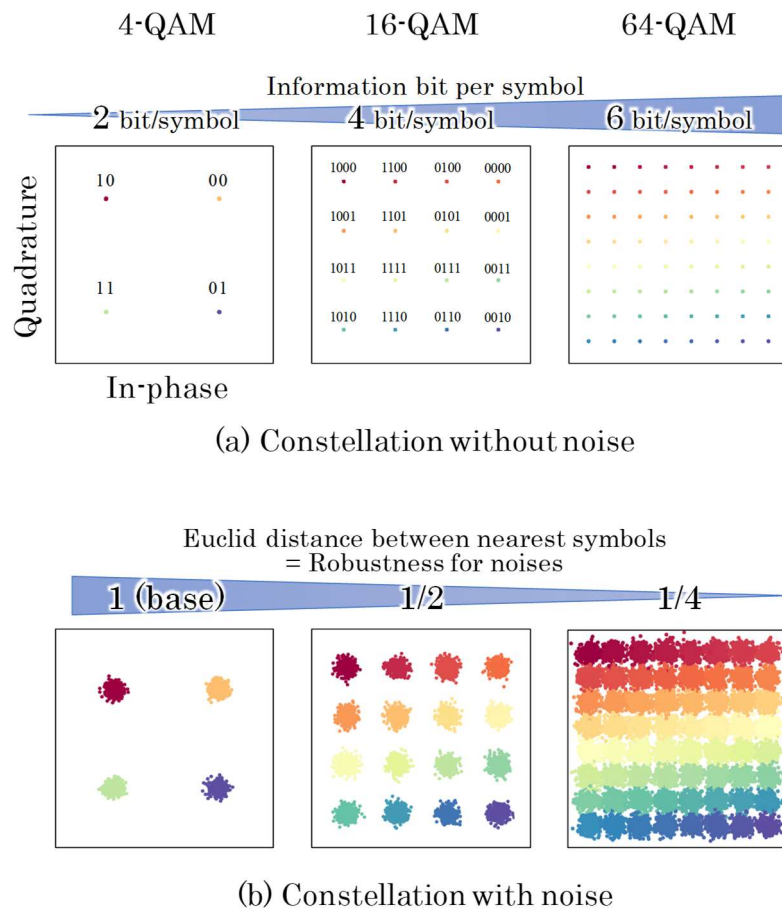


Figure 2.3 Examples of QAM signals on a complex plane.

2.2.2 Polarization-division multiplexing

Since a lightwave is a transverse wave, optical signals can be multiplexed on polarization modes, *i.e.*, polarization-division multiplexing (PDM). Figure 2.4 shows the schematic of PDM. Two lightwaves with orthogonal polarization states are propagated in one path. Since the practical optical fiber has a slightly elliptical structure, *i.e.*, birefringence, the propagation characteristics for each polarization state is different. As a result, the optical receiver can only obtain the signal mixed up by two PDM signals, *i.e.*, polarization-mode dispersion (PMD). Furthermore, the state of polarization (SOP) fluctuates through all time. In order to exploit the PDM technology, the polarization demultiplexing process hence necessitates the adaptive control. In digital coherent optical transmission, DSP circuit in the optical receiver realize the adaptive polarization demultiplexing and PMD compensation.

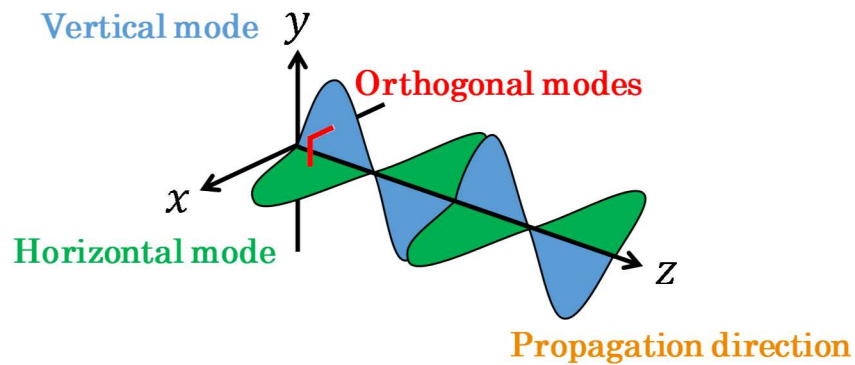


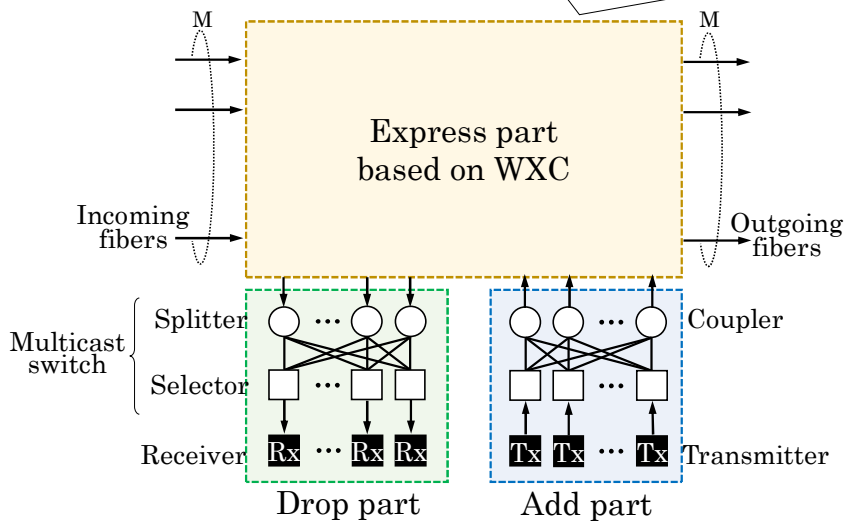
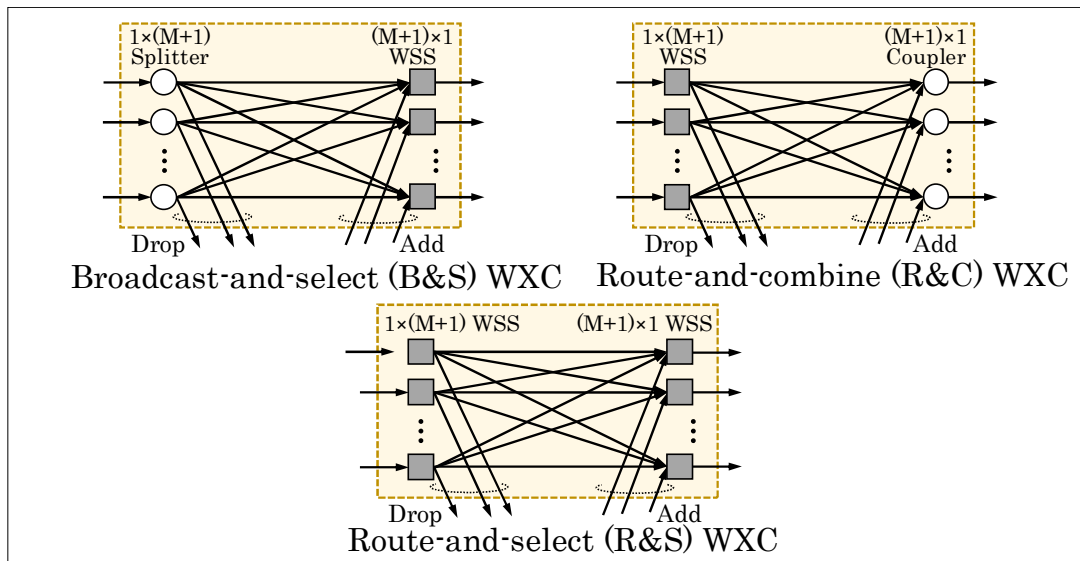
Figure 2.4 Schematic of polarization-division multiplexing.

2.3 Optical cross-connect

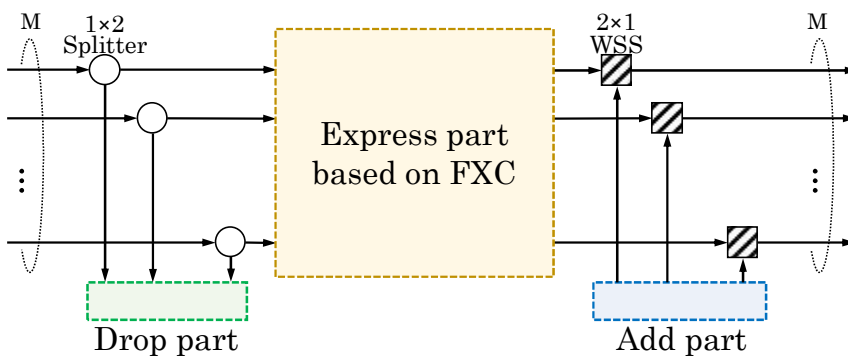
2.3.1 Architecture of optical cross-connect

An optical cross-connect realizes the switching of direction for all optical signals without O-E-O conversion. Figure 2.5 shows the typical node configurations. An optical node consists of an express part, a drop part, and an add part. In the drop part, signals are dropped as necessary and delivered to their corresponding receivers through multicast switches consisting of optical splitters and selectors, *i.e.*, drop operation. In the add part, signals generated by transmitters are sent to their target outgoing fibers through multicast switches and combined with express signals, *i.e.*, add operation. In the express part, signals arrived at the cross-connect are forwarded to arbitrary output port for routing, *i.e.*, express operation.

The express part can be either wavelength cross-connect (WXC) based on WSSs or fiber cross-connect (FXC) based on optical selectors. As shown in Figure 2.5(a), a WXC can comprise WSSs, splitters, and couplers [10, 11]. In the broadcast-and-select (B&S) architecture, splitters are located at the input side and WSSs at the output side. The route-and-combine (R&C) configuration places WSSs at the input side and couplers at the output side. When WSSs are adopted for both input and output sides, the architecture is referred to as the route-and-select (R&S) configuration. In Figure 2.5(b), on the other hand, the FXC-based express part can consist of an optical switch based on micro-electro-mechanical system (MEMS) or that based on piezoelectric actuation [12-14]. As the express part does not have any wavelength selectivity, all the express paths in an input fiber are routed to the same output fiber. To add/drop signals on a wavelength basis, therefore, the node necessitates additional splitters and/or WSSs outside the FXC-based express part; the splitters and WSSs can be low cost because the port count of 1×2 is sufficient to drop/add signals. The FXC-based nodes have scalability in terms of port count, *e.g.*, the port count of over 300×300 is commercially available.



(a) WXC-based optical-node configurations



(b) FXC-based optical-node configurations

Figure 2.5 Configurations of optical nodes.

2.3.2 Splitters and couplers

Figure 2.6 shows the examples of splitter and coupler. A splitter is a device that distributes one input optical signal to multiple output ports. On the other hand, an optical coupler is a device that combines multiple input signals into one output destination. A splitter and a coupler is the same devices; they are distinguished by which port is used as input/output.

A splitter with 1 input port and N output port is referred to as a $1 \times N$ splitter, vice versa for an optical coupler. The loss of the optical coupler is expressed as $10\log_{10}N + \alpha$ [dB], where the first term is called the principle loss, and the second term is called the excess loss. Excess loss is usually about 1 dB.

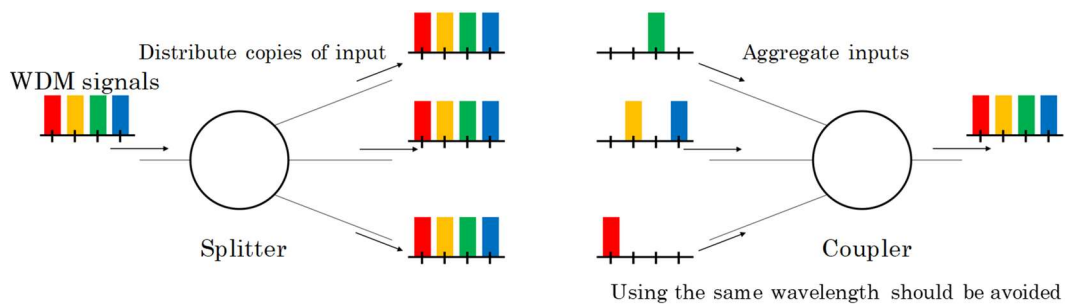


Figure 2.6 Example of the operations of a splitter and a coupler.

2.3.3 Wavelength-selective switch

Figure 2.7 shows the examples of wavelength-selective switches (WSSs) operations [15]. A WSS is a reversible device. By using a WSS as a $1 \times N$ device, the input WDM signals can be flexibly routed to any output ports wavelength by wavelength. By using a WSS as a $N \times 1$ device, on the other hand, the arbitrary input signals are selectively exported into one output port. Other WDM signals not selected are attenuated by optical filters. The optical filters cannot completely attenuate the optical signals; thus, the remaining optical signal is added to the target optical signal as in-band crosstalk. Since the target signal is exported to one output port, the loss does not theoretically increase as the output port increases. The loss of the WSS is about 7 dB.

The commercially available WSSs are implemented by using micro-electro-mechanical systems (MEMS) or liquid-crystal-on-silicon (LCOS) technologies. Since the route of each WDM signal is controlled by MEMS or LCOS, the wavelength setting granularity is limited; the minimum unit for wavelength controlling is a grid. ITU-T standardized the flexible grid of 12.5 GHz [16]. This

limitation restricts that the passband bandwidth of optical filtering must be multiples of 12.5 GHz. Even under the grid limitation, a WSS has higher functionality and less signal loss compared to splitters and couplers, which results in the dynamic flexible optical-path networking [17-20].

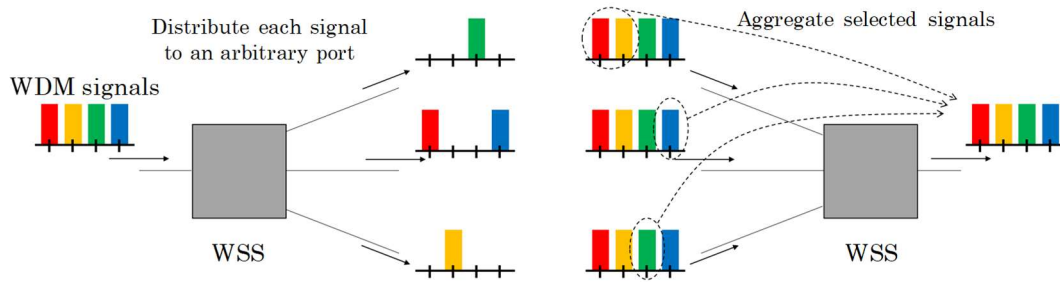


Figure 2.7 Example of the operations of a WSS.

2.4 Network control

2.4.1 Wavelength continuity constraint

To setup an optical path, the network operator must assign an available physical route and wavelength to establish the new optical path. This process is called routing and wavelength assignment (RWA). For the optical path network without costly O-E-O conversion, each optical path must occupy the same wavelength through the whole transmission, this characteristic is referred to as the wavelength continuity constraint [21]. Figure 2.8 shows the example of wavelength continuity constraint. In this example, each optical fiber can carry two optical signals shown as blue and orange lines. The different wavelength is assigned to different optical paths. As shown in Figure 2.8, even if both of the optical fiber #1 and #2 has a vacant wavelength resource, a path from node #1 to node #3 cannot be established unless the existing optical path is disrupted. Therefore, the all pairs of route and wavelength assigned to each optical path need to be carefully selected considering the wavelength continuity constraint; this task is known as NP-complete [22].

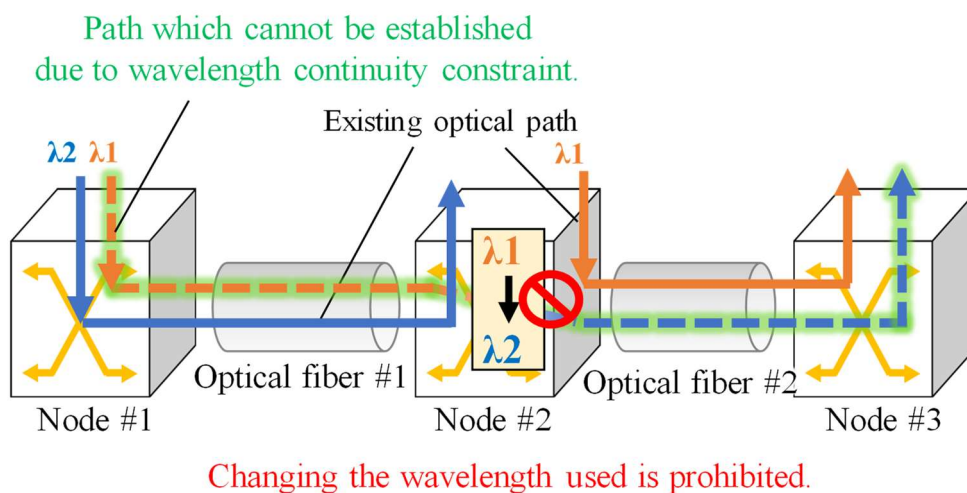


Figure 2.8 Wavelength continuity constraint.

2.4.2 Network-resource assignment

Figure 2.9 shows an example of network resource assignment. When an optical path setup request arrives, a pair of route and wavelength is selected to be assigned. There are two types of routes. To make a connection between a source node and a destination node of a setup request, a route defined as optical nodes that the new signal traverses is selected as shown in Figure 2.9 (a); this route is referred to as a node route. Here, a link between each pair of adjacent optical nodes has

several optical fibers as shown in Figure 2.9 (b). Therefore, it is necessary to decide which optical fibers the signal passes through; the route is called a fiber route. In the wavelength domain, an optical fiber can accommodate multiple WDM signals. The available wavelength range of the commercially utilized EDFA is limited in 4.8 THz. When all signals demand the bandwidth of 50 GHz in the fixed grid, the number of wavelength candidate is 96 ($4,800 \text{ GHz} / 50 \text{ GHz}$) [16]. The used wavelength slot is selected from the available slots considering the wavelength continuity constraint as shown in Figure 2.9 (c). The task of selecting the pair of route and wavelength slot is called a routing and wavelength assignment (RWA) task. Since the simple RWA algorithm results in the network utilization ratio of about 70%, it is necessary to pursue the better RWA algorithm that improves the network capacity.

As for the advanced network control tasks, the bandwidth to each optical signal is flexibly assigned on the flexible grid [16]. In the flexible grid, the bandwidth assigned for each signal is a multiple of 12.5 GHz, hence the number of wavelength slots is 384 ($4,800 \text{ GHz} / 12.5 \text{ GHz}$). To discriminate with the RWA task, this task is traditionally called route and spectrum assignment (RSA) task [23]. Furthermore, the modulation format that defines the transmission distance and spectral efficiency is flexibly selected for each demand; this task is called a route, modulation, and spectrum assignment (RMSA) [24].

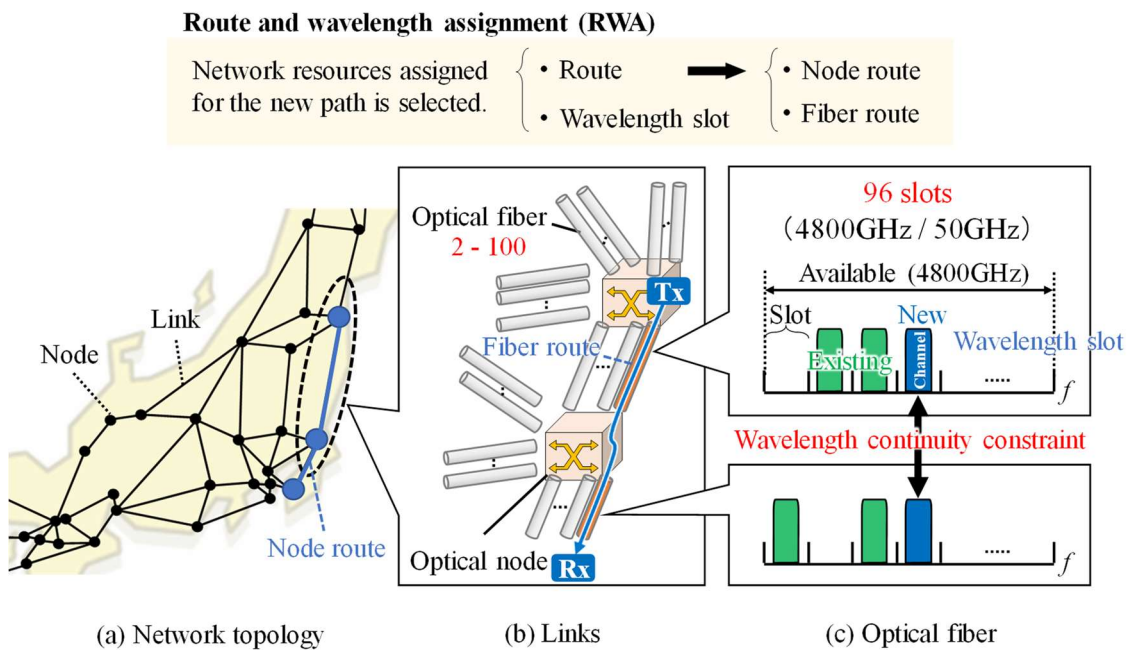


Figure 2.9 An example of network resource assignment.

2.4.3 Network scenarios

At the beginning of employing an optical path network, various parameters, *e.g.*, the number of fibers in each link, the optical cross-connect setting, the locations of optical amplifier, and so on, need to be configured. This initial process is referred to as the network design. In this process, such network parameters are statically optimized all at once against a certain amount of traffic demands that is expected to be arrived. Also, the policy for network control can be configured for the effective network control in this phase.

After the network design operations, optical paths are setup in response to the arriving path-setup requests. Since the network controller is immature in the conventional system, all optical paths are setup at once and keep the connection for a long while, *e.g.*, every few months or years. An optical path occupies the wavelength resources even though no information bit carries on a fiber. This scenario is called a static network control scenario, and is often optimized using integer linear programming (ILP) or any heuristics. Software-defined networking (SDN), which offers logically centralized network control, is expected to enhance network capacity, particularly in the dynamic network control scenario. In dynamic networks, the optical path setup/teardown operations are provided request-by-request, *e.g.*, every few hours or weeks, which results in the enhancement of the net network capacity. In this dissertation, Chapter 5 details the proposed network design while Chapter 6 presents the proposed network control.

2.5 Summary

The fundamentals of optical path network were described. Digital coherent transmission system supports high capacity transmission systems using QAM and PDM. Optical cross-connects and optical transmitters/receivers at optical nodes control WDM signals in wavelength-by-wavelength manner. The notable technologies described in this chapter have already been introduced in the commercial systems. To further enhance the capacity for next-generation information society, ultra-dense WDM network is expected to be realized; this dissertation tackles this issue. Firstly, the pros and cons of ultra-dense WDM network is detailed in the next chapter.

References

- [1] M. Mezhoudi, R. Feldman, and R. Goudreault, "The value of multiple degree ROADMs on metropolitan network economics," in Optical Fiber Communication Conference and Exposition and the National Fiber Optic Engineers Conference (OFC/NFOEC), paper NThA4 (2006).
- [2] R.-J. Essiambre, and R. W. Tkach, "Capacity trends and limits of optical communication networks," *Proceedings of IEEE*, vol. 100, no. 5, pp. 1035-1055 (2012).
- [3] L.B. Jeunhomme, "Single-mode fiber optics: principles and applications, 2nd edition" Routledge (2019).
- [4] E. Desurvire, J. R. Simpson, and P. C. Becker, "High-gain erbium-doped traveling-wave fiber amplifier," *Optica Optics Letters*, vol. 12, no. 11, pp. 888-890 (1987).
- [5] M. Nakazawa, Y. Kimura, and K. Suzuki, "Soliton amplification and transmission with an Er³⁺-doped fiber repeater pumped by InGaAsP laser diodes," in Technical Digest of Optical Fiber Communication Conference (OFC), paper PD2 (1989).
- [6] G. P. Agrawal, "Fiber-optic communication systems," Wiley-Interscience (2002).
- [7] T. Okoshi, "Recent advances in coherent optical fiber communication systems," *IEEE Journal of Lightwave Technology*, vol. 5, pp. 44-52 (1987).
- [8] G. P. Agrawal, "Nonlinear Fiber Optics, Sixth Edition", Academic Press, 2019.
- [9] M. S. Faruk and S. J. Savory, "Digital signal processing for coherent transceivers employing multilevel formats," *IEEE/Optica Journal of Lightwave Technology*, vol. 35, no. 5, pp. 1125-1141 (2017).
- [10] B. C. Collings, "Advanced ROADM technologies and architectures," in Optical Fiber Communication Conference (OFC), San Francisco, USA, paper Tu3D.3 (2015).
- [11] S. L. Woodward, M. D. Feuler, and P. Palacharla, "ROADM-node architectures for reconfigurable photonic networks," in I. Kaminow, T. Li, and A. Willner, *Optical Fiber Telecommunications VIB*, Academic Press (2013).
- [12] P.-D. Dobbelaere, K. Falta, S. Gloeckner, and S. patra, "Digital MEMS for optical switching", *IEEE Communications Magazine*, vol. 40, no. 3, pp. 88-95 (2002).
- [13] D.-T. Neilson, R. Frahm, P. Kolodner, C.-A. Bolle, R. Ryf, J. Kim, A.-R. Papazian, C.- J. Nuzman, A. Gasparyan, N.-R. Basavanhally, V.-A. Aksyuk, and J.-V. Gates, "256×256 port

- optical cross-connect subsystem,” *IEEE Journal of Lightwave Technology*, vol. 22, no. 6, pp. 1499–1509 (2004).
- [14] Polatis, “Series 7000 - 384x384 port software-defined optical circuit switch,” <https://www.polatis.com/series-7000-384x384-port-software-controlled-optical-circuit-switch-sdn-enabled.asp>.
- [15] J. Homa and K. Bala, “ROADM architectures and their enabling WSS technology,” *IEEE Communications Magazine*, vol. 46, no. 7, pp.150-154 (2008).
- [16] ITU-T, “Spectral grids for WDM applications: DWDM frequency grid,” ITU-T Recommendation G.694.1 (2012).
- [17] M. Jinno, H. Takara, B. Kozicki, Y. Tsukishima, Y. Sone, and S. Matsuoka, “Spectrum-efficient and scalable elastic optical path network: architecture, benefits, and enabling technologies,” *IEEE Communications Magazine*, vol. 47, no. 11, pp. 66-73 (2009).
- [18] O. Gerstel, M. Jinno, A. Lord, and S. J. B. Yoo, “Elastic optical networking: A new dawn for the optical layer?” *IEEE Communications Magazine*, vol. 50, no. 2, pp. 12-20 (2012).
- [19] S. Gringeri, B. Basch, V. Shukla, R. Egorov, and T. J. Xia, “Flexible architectures for optical transport nodes and networks,” *IEEE Communications Magazine*, vol. 48, no. 7, pp. 40-50 (2010).
- [20] I. Tomkos, S. Azodolmolky, J. Sole-Pareta, D. Careglio, and E. Palkopoulou, “A tutorial on the flexible optical networking paradigm: state of the art, trends, and research challenges”, *Proceedings of the IEEE*, vol. 102, no.9, pp. 1317-1337 (2014).
- [21] H. Zang, J. P. Jue, and B. Mukherjee, “A review of routing and wavelength assignment approaches for wavelength-routed optical WDM networks,” *Springer Optical Networks Magazine*, vol. 1, no. 1, pp. 47-60 (2000).
- [22] I. Chlamtac, A. Ganz, and G. Karmi, “Lightpath communications: an approach to high-bandwidth optical WAN’s,” *IEEE Transactions on Communications*, vol. 40, no. 7, pp. 1171–1182 (1992).
- [23] M. Klinkowski and K. Walkowiak, “Routing and spectrum assignment in spectrum sliced elastic optical path network,” *IEEE Communications Letters*, vol. 15, no. 8, pp. 884-886 (2011).
- [24] L. Gong, X. Zhou, W. Lu, and Z. Zhu, “A two-population based evolutionary approach for optimizing routing, modulation and spectrum assignments (RMSA) in O-OFDM networks,” *IEEE Communications Letter*, vol. 16, no. 9, pp. 1520-1523 (2012).

Chapter 3

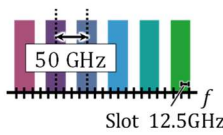
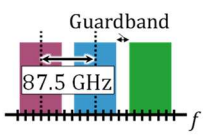
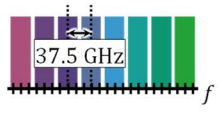
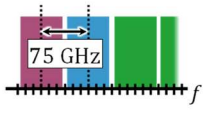
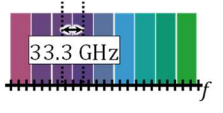
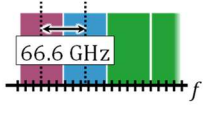
Ultra-dense WDM network

Ultra-dense WDM is expected to offer the higher spectral efficiency than the conventional DWDM. Since the bandwidth assigned for each signal can be changed without any additional devices, the introduction of ultra-dense WDM is the cost-efficient approach expanding the capacity of optical networks. On the other hand, the unideal optical-filter characteristics severely degrades the ultra-dense WDM signals. In this chapter, the pros and cons of ultra-dense WDM networks is comprehensively described.

3.1 Ultra-dense WDM

To increase the capacity of optical networks, spectral efficiency needs to be enhanced. Ultra-dense wavelength-division multiplexing (WDM) systems, where the guard-bands inserted between adjacent WDM signals are narrower than those in conventional dense WDM (DWDM) systems, are expected to realize higher spectral efficiency. Table 3.1 shows the examples of WDM schemes. In the DWDM system, the bandwidth assigned for 400-/100-Gbps signals is 87.5/50 GHz [1, 2]. In ultra-dense WDM system, on the other hand, the bandwidth assigned for 400-/100-Gbps signals is 75/37.5 GHz assuming the standardized grid of 12.5 GHz [3]. The theoretical improvements in the spectral efficiency are 16.7% for 400-Gbps signals and 33.3% for 100-Gbps signals. Quasi-Nyquist WDM is one of the ultra-dense WDM schemes neglecting the standardized grid; a 66.6-/33.3-GHz bandwidth is assigned for a 400-/100-Gbps signals. The theoretical improvements in the spectral efficiency are 31.3% for 400-Gbps signals and 50.0% for 100-Gbps signals.

Table 3.1 WDM schemes

| | | 100-Gbps (PDM-QPSK 32Gbaud) | | 400-Gbps (PDM-16QAM 64Gbaud) | |
|--------------------------------------|-----------|---|---------------------|---|--------------------|
| | | | Max # of channels | | Max # of channels |
| Dense WDM | Grid |  | 96/fiber (1) |  | 54/fiber (1) |
| Ultra-dense WDM | Grid |  | 128/fiber (1.33) |  | 64/fiber (1.17) |
| Ultra-dense WDM Quasi-Nyquist WDM | Grid-less |  | 144/fiber (1.5) |  | 72/fiber (1.31) |

Many studies have shown the effectiveness of ultra-dense WDM in point-to-point transmission systems [3, 4]. However, its use for networking is hindered by spectrum narrowing with each traversal of wavelength-selective switches (WSSs). Furthermore, the limited setting granularity of WSSs bandwidth avoids the truly spectral-efficient WDM system.

3.2 Spectrum-narrowing effect

Figure 3.1 illustrates spectrum narrowing in optical path networks; Figure 3.1(a) and Figure 3.1(b) depict spectrum narrowing caused by a 2×1 WSS and a 1×2 WSS, respectively. While high spectral efficiency is expected by adopting ultra-dense WDM, its efficient use for networking is obstructed by the spectrum-narrowing effect. When signals traverse a WSSs, the signal spectra are narrowed by filtering for wavelength routing. The spectrum narrowing can be avoided if the transfer function of a WSS is rectangular; however, actual WSS passbands have gradual cut-off characteristics, so spectrum narrowing is inevitable [5-9]. The spectrum narrowing is intensified as the guardband bandwidth decreases.

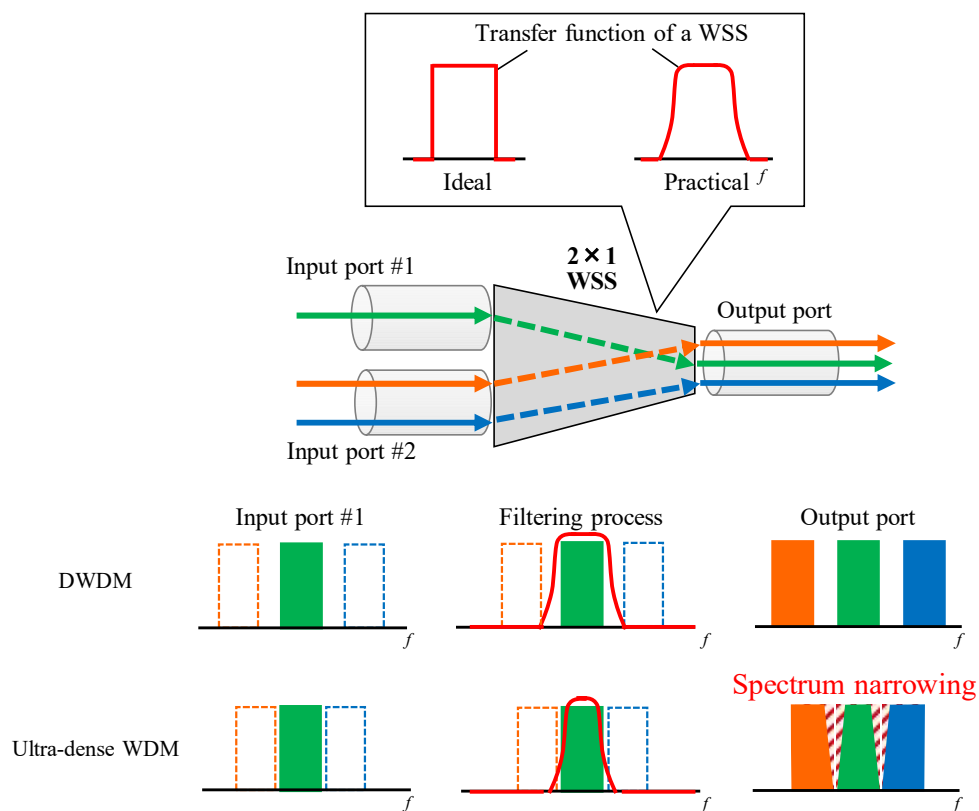


Figure 3.1(a) Spectrum narrowing in a 2×1 WSS.

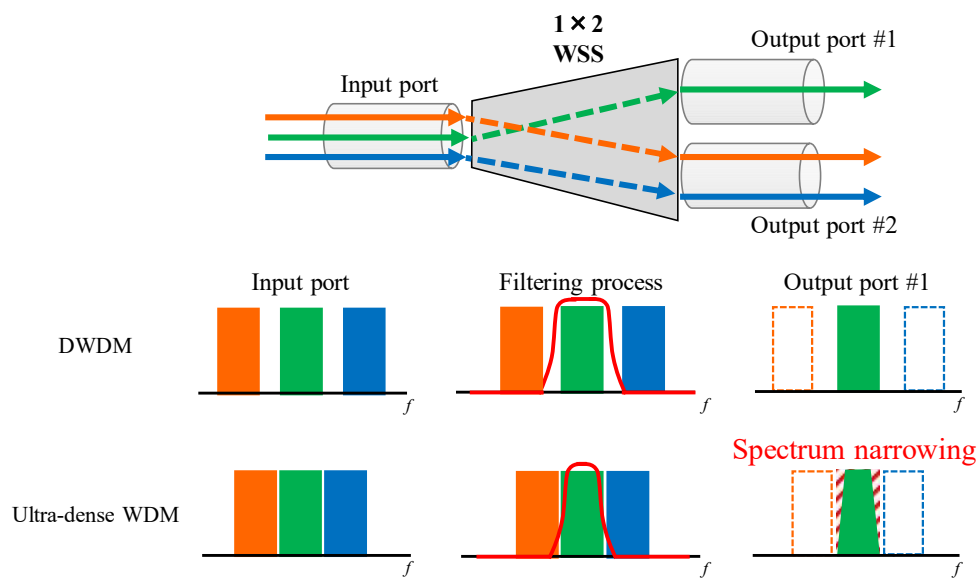


Figure 3.1(b) Spectrum narrowing in a 1×2 WSS.

Figure 3.1 Spectrum narrowing effect

Since the transfer function of WSSs does not obey the Nyquist criterion, an optical signal suffers from inter-symbol interference (ISI). Figure 3.2 shows the ISI in both a frequency domain and a time domain. The ideal signal which is not impaired by spectrum narrowing does not have any amplitude in other sample timing in a time domain. On the other hand, the signal which does not satisfy the Nyquist criterion due to spectrum narrowing has amplitude at other symbol decision timing. As a result, this ISI degrades the performance of symbol decision.

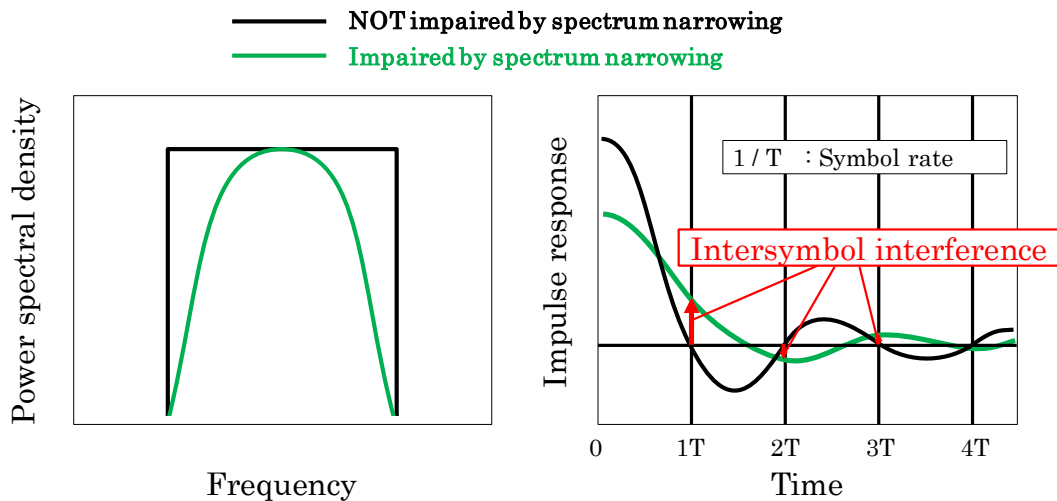


Figure 3.2 Inter-symbol interference

Optical amplifiers add amplified-spontaneous-emission (ASE) noise to the signals filtered by WSSs. Since an optical signal repeatedly undergoes such filtering-and-amplification processes, the ISI and ASE noise degrade the signal quality in an interactive manner. Figure 3.3 shows the repetitive processes of optical filtering and optical amplifications. The signal quality worsens as the number of WSS traversals increases. Consequently, the transmissible distance is severely restricted.

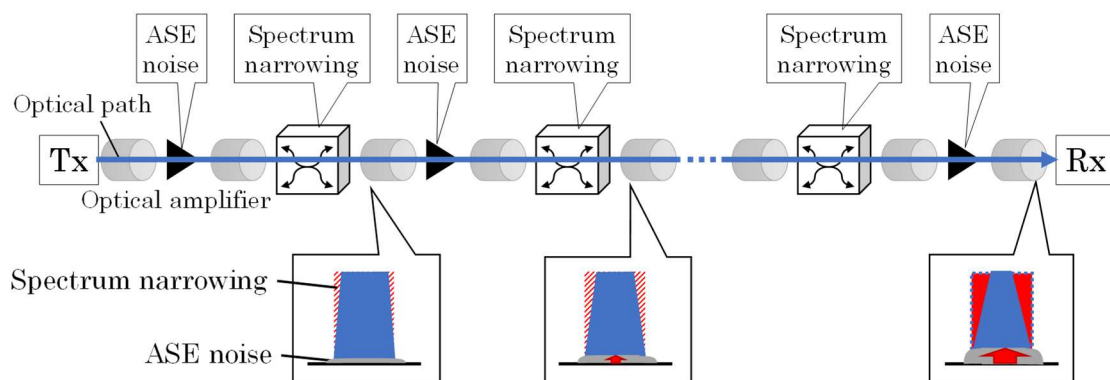


Figure 3.3 Interaction between spectrum narrowing and ASE noise in a network.

3.3 Noise enhancement in DSP circuit

In a typical DSP circuit, most of the ISI is automatically equalized by the adaptive finite impulse response (FIR) filters [10, 11]. However, since the frequency components attenuated by WSS filters are emphasized, the ISI-suppressing filter degrades the overall signal-to-noise ratio (SNR) as shown in Figure 3.4. This adaptive FIR filter simultaneously compensates for polarization-mode dispersion and IQ mismatch. As these processes are indispensable for transmission, the occurrence of the noise enhancement is hence inevitable with the ISI-suppressing filter.

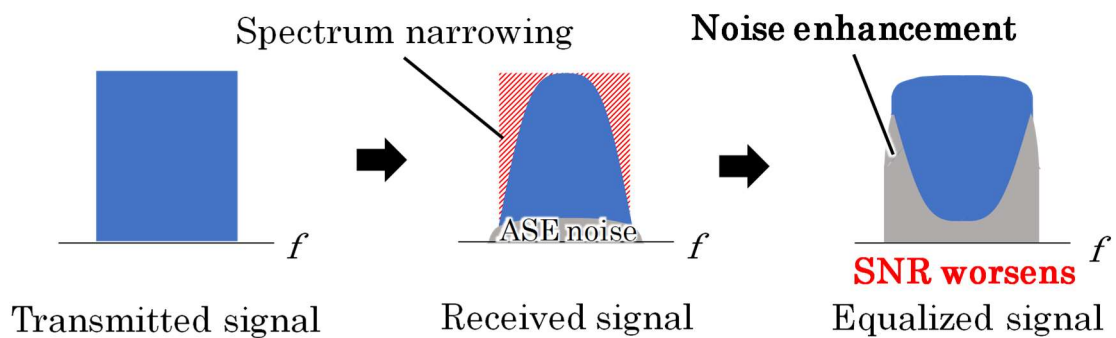


Figure 3.4 Noise enhancement induced by ISI-suppressing filter.

3.4 Spectrum narrowing in networking

Spectrum narrowing occurs at a WSS in an optical node. Figure 3.5 shows the operations that cause or do not cause spectrum narrowing in the broadcast-and-select node. In this section, we discuss the spectrum narrowing for the target signal depicted as green arrows as shown in Figure 3.5(a). When the WDM signal is added to the wavelength adjacent with that of the target signal, the target signal spectrum is narrowed by the filtering for wavelength routing as shown in Figure 3.5(b). Next, when the WDM signal whose wavelength is adjacent with that of the target signal is dropped, then the target signal also impaired by filtering as shown in Figure 3.5(c). The signal whose wavelength is adjacent to that of the target signals is called the adjacent signal hereafter. The express operations of both coupling and separating for the adjacent signal also cause the spectrum narrowing as shown in Figure 3.5(d)(e). On the other hand, if the target signal and the adjacent signal is added/dropped at the same node, the optical filter can be simultaneously applied; hence, the spectrum narrowing does not occur as shown in Figure 3.5(f)(g). Similarly, the input optical fibers and output optical fibers are the same with the target signal and the adjacent signal, the spectrum narrowing can be avoided as shown in Figure 3.5(h). In conclusion, when the target signal and the adjacent signal are split or coupled at a WSS, the target signal suffers from spectrum narrowing.

Figure 3.6 shows the operations that cause or do not cause in a route-and-select node. Similar to the occurrence situation in a B&S node, the spectrum narrowing occurs or does not occur as shown in Figure 3.6 (b) - (h). The remarkable difference with B&S node is the maximum number of spectrum narrowing in a single node is 2 for R&S node as shown in Figure 3.6 (i). As a result, B&S nodes are more sensitive against the spectrum narrowing.

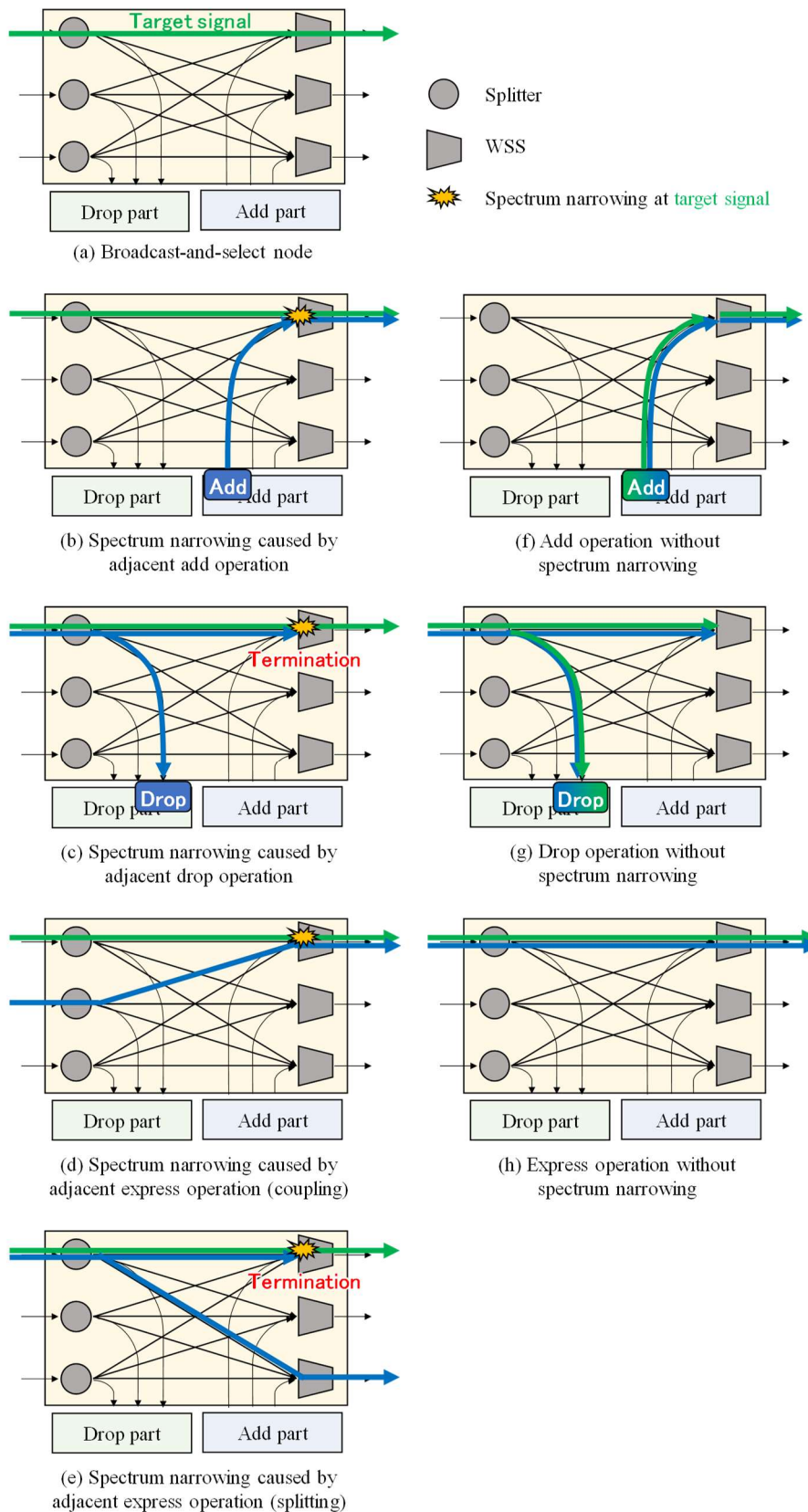


Figure 3.5 The operations with/without spectrum narrowing for a B&S node.

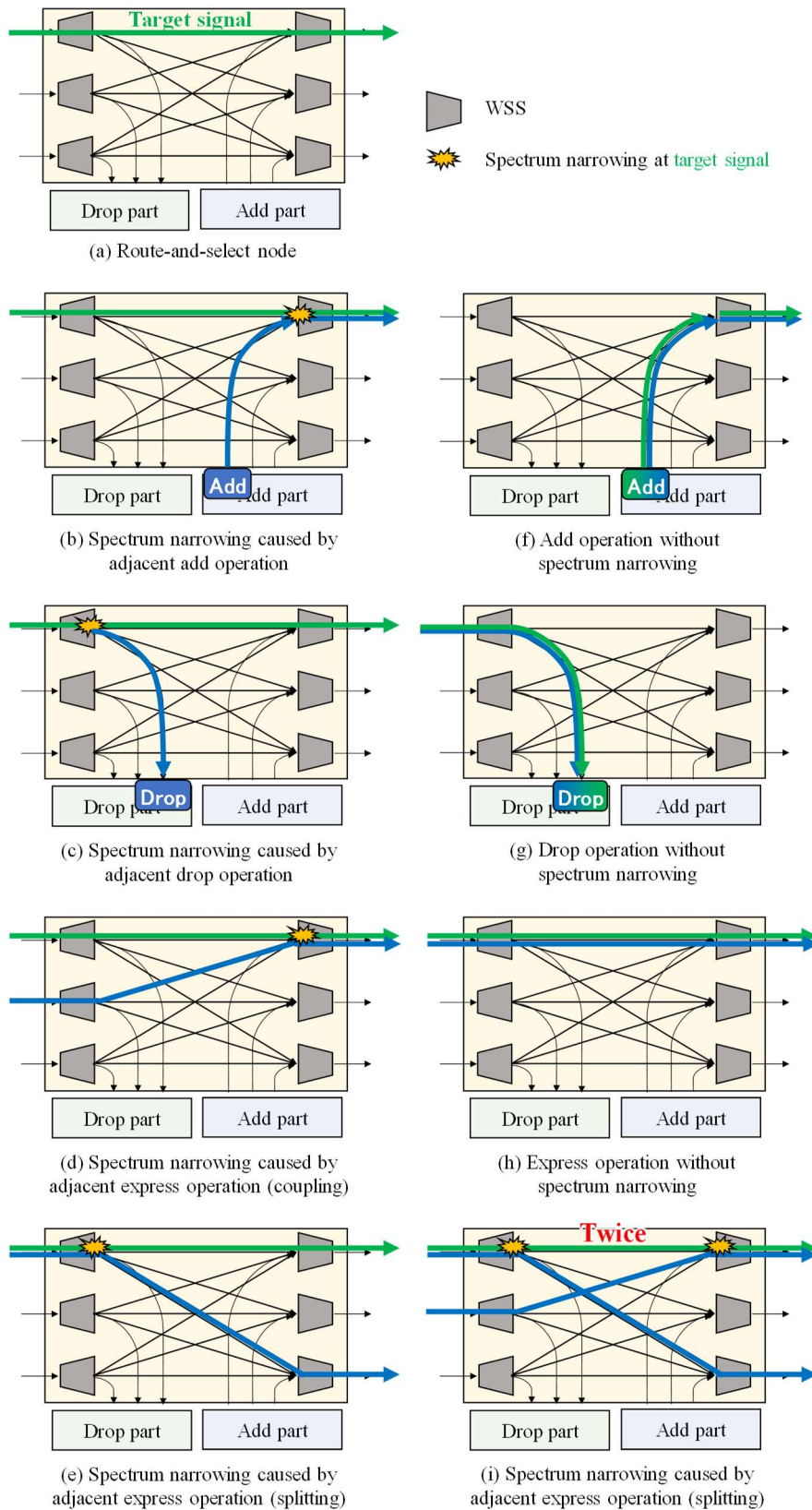


Figure 3.6 The operations with/without spectrum narrowing for a R&S node.

3.5 Grouped routing

The reduction of the bandwidth occupied by guardbands is achieved by grouping multiple paths and inserting broad guardbands only between path groups. One such scheme is grouped routing (GR) [12-16]. Figure 3.7 shows the grouped routing scheme. In this way, the available frequency range is divided into several wavebands called grouped routing entities (GREs), and a narrow guardband is inserted between the adjacent paths in a GRE. Paths in the same GRE are routed together, i.e., coarsely granular routing, while paths belonging to a GRE can be dropped/added on a wavelength basis. Hence, the spectrum narrowing is only induced by wavelength-granular add/drop operation. As widely deployed WSSs based on LCOS can create a broad passband consecutive in the frequency domain, GR can be introduced without changing any hardware.

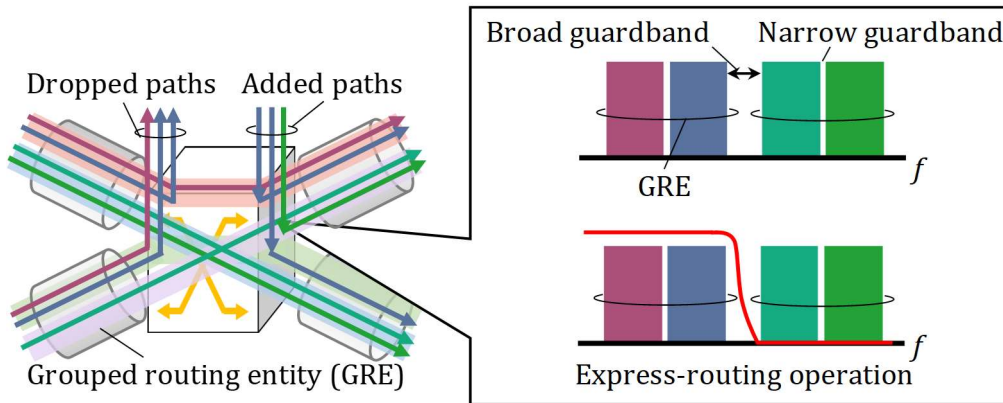


Figure 3.7 Grouped routing.

Figure 3.8 shows the enhancement of fiber capacity achieved by the GR scheme. For this evaluation, the available frequency bandwidth B_C of 4,800 GHz and the fixed-grid network using 100-Gbps signals (32-Gbaud DP-QPSK) or 400-Gbps signals (32-Gbaud dual-carrier DP-16QAM) are assumed. The assigned bandwidth for 100-/400-Gbps paths is set to 50/87.5 GHz in DWDM networks and 37.5/75 GHz in ultra-dense WDM networks; each bandwidth is described as B_D and B_{UD} , respectively. The GRE width, g , which is the number of paths per GRE, is changed. The bandwidth of each GRE, B_{GRE} , is described as

$$B_{GRE} = \begin{cases} g \times B_{UD} & \text{if } g = g_{max} \\ g \times B_{UD} + (B_D - B_{UD}) & \text{otherwise} \end{cases},$$

where g_{max} is $\lfloor B_C/B_{UD} \rfloor$ with floor function $\lfloor \cdot \rfloor$. Here, the bandwidth defined by $B_D - B_{UD}$ means the slot bandwidth additionally inserted between GREs, *i.e.*, 12.5 GHz. Using such configurations, the number of paths in a GRE, N_{GRE} , is given by

$$N_{GRE} = \left\lfloor \frac{B_C}{B_{GRE}} \right\rfloor \times g + \left\lfloor \frac{B_C - \left\lfloor \frac{B_C}{B_{GRE}} \right\rfloor \times B_{GRE}}{B_D} \right\rfloor$$

Compared to conventional WDM, *i.e.*, $g = 1$, all GRE schemes offer higher fiber capacity. So far, the number of GREs in a fiber has been set to around 10-20 to take advantage of the fiber-capacity enhancement while keeping a certain path-routing flexibility [12, 13]. If the number of GREs in each fiber is set to one, *i.e.*, $g = g_{max}$, it can be seen as ultra-dense WDM networks, which archives the highest fiber capacity; 128 wavelengths for 100-Gbps signals and 64 wavelengths for 400-Gbps signals.

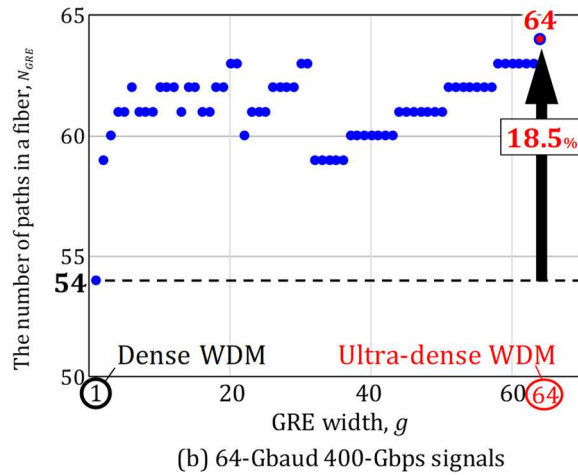
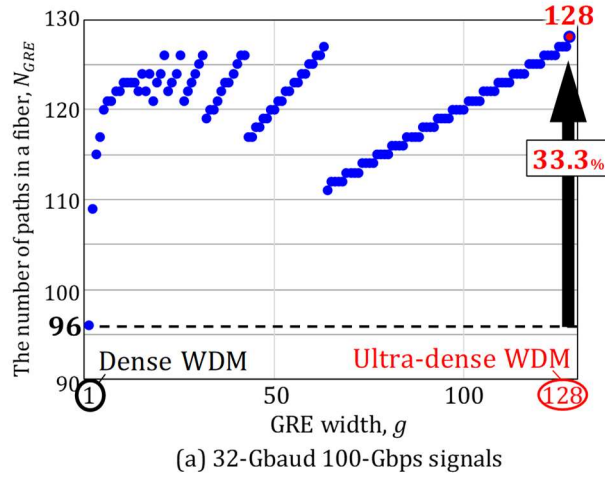


Figure 3.8 Fiber capacity variation subject to GRE width.

3.6 Mismatch with WSS resolution

Figure 3.9 shows the mismatch with frequency setting granularity of WSS and the bandwidth assigned for signals. As denoted in Section 3.1, quasi-Nyquist WDM is expected to realize the highest spectral efficiency in a practical manner. In this system, however, the bandwidth assigned for each signal is not a multiple of the grid. In this example, signals with a 66.6-GHz spacing cannot be separated by currently deployed WSSs whose frequency setting granularity is 12.5 GHz [2]. If we force a WSS to filter the signals by such inappropriate filters, the signal spectrum is severely narrowed. A quasi-Nyquist WDM system cannot be straight-forwardly applied in the practical networks because of the high expenditure of installing new WSSs.

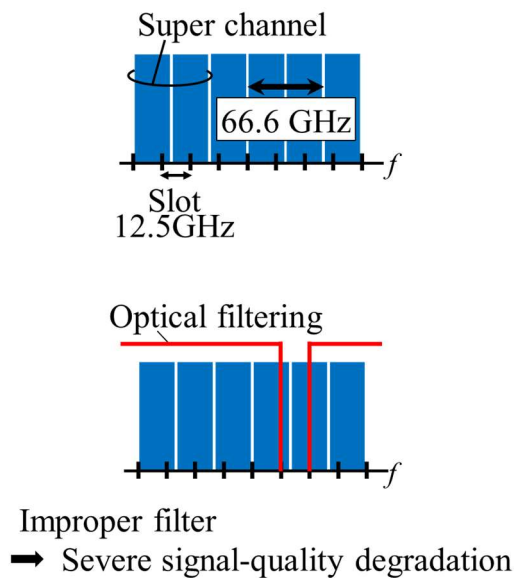


Figure 3.9 The limited WSS-passband resolution.

3.7 Summary

In this chapter, we discussed the trade-off between the spectral-efficiency enhancement and signal-quality degradation in ultra-dense WDM networks. The ultra-dense WDM can potentially enhance spectral efficiency by reducing idle wavelength resources. On the other hand, the obstructions, *i.e.*, spectrum narrowing and mismatch with WSS resolution, hinder the introduction of ultra-dense WDM into a network. The following chapters, Chapter 4, Chapter 5, and Chapter 6, are dedicated for the methods to mitigate or manage the impacts of obstructions.

References

- [1] Optical Internetworking Forum, “Technology options for 400G implementation,” OIF-Tech-Options-400G-01.0 (2015).
- [2] ITU-T, “Spectral grids for WDM applications: DWDM frequency grid,” ITU-T Recommendation G.694.1 (2012).
- [3] G. Bosco, V. Curri, A. Carena, P. Poggiolini, and F. Forghieri, “On the performance of Nyquist-WDM terabit superchannels based on PM-BPSK, PM-QPSK, PM-8QAM or PM-16QAM subcarriers,” *IEEE Journal of Lightwave Technology*, vol. 29, pp. 53-61 (2011).
- [4] S. Kilmurray, T. Fehenberger, P. Bayvel, and Ri Killey, “Comparison of the nonlinear transmission performance of quasi-Nyquist WDM and reduced guard interval OFDM,” *Optica Optics Express*, vol. 20, no. 4, pp. 4198-4205 (2012).
- [5] T. Zami, I. Fernandez de Jauregui Ruiz, B. Lavigne, and A. Ghazisaeidi, “Growing impact of optical filtering in future WDM networks,” in *Optical Fiber Communication Conference (OFC)*, San Diego, USA, paper M1A.6 (2019).
- [6] M. Filer, and S. Tibuleac, “N-degree ROADM architecture comparison: broadcast-and-select versus route-and-select in 120 Gb/s DP-QPSK transmission systems,” in *Optical Fiber Communication Conference (OFC)*, San Diego, USA, paper Th1I.2 (2014).
- [7] C. Pulikkaseril, L. Stewart, M. A. F. Roelens, G. Baxter, S. Poole, and S. Frisken, “Spectral modeling of channel band shapes in wavelength selective switches,” *Optica Optics Express*, vol. 19, no. 9, pp. 8458-8470 (2011).
- [8] K. Okamura, Y. Mori, and H. Hasegawa, “Pre-filtering techniques for spectrum narrowing caused by optical node traversal in ultra-dense WDM networks,” *IEEE Photonics Journal*, vol. 13, no. 2, pp. #7200513 (2021).
- [9] I. F. de J. Ruiz, A. Ghazisaeidi, T. Zami, S. Louis, and B. Lavigne, “An accurate model for system performance analysis of optical fibre networks with in-line filtering,” in *European Conference on Optical communication (ECOC)*, Dublin, Ireland, paper 78 (2019).
- [10] M. S. Faruk and S. J. Savory, “Digital signal processing for coherent transceivers employing multilevel formats”, *IEEE/Optica Journal of Lightwave Technology*, vol. 35, no. 5, pp. 1125-1141 (2017).
- [11] K. Kikuchi, “Fundamentals of coherent optical fiber communications”, *IEEE/Optica Journal of Lightwave Technology*, vol. 34, no. 1, pp. 157-179 (2016).

- [12] Y. Terada, Y. Mori, H. Hasegawa, and K. Sato, "Highly spectral efficient networks based on grouped optical path routing," *Optica Optics Express*, vol. 24, pp. 6213-6228 (2016).
- [13] K. Kayano, S. Yamaoka, Y. Mori, H. Hasegawa, and K. Sato, "Highly dense elastic optical networks enabled by grouped routing with distance-adaptive modulation," *IEEE Photonics Technology Letters*, vol. 31, pp. 295-298 (2019).
- [14] J. M. Fàbrega, M. S. Moreolo, L. Martín, A. C. Piat, E. Riccardi, D. Roccatò, N. Sambo, F. Cugini, L. Potí, S. Yan, E. Hugues-Salas, D. Simeonidou, M. Gunkel, R. Palmer, S. Fedderwitz, D. Rafique, T. Rahman, H. de Waardt, and A. Napoli, "On the filter narrowing issues in elastic optical networks," *IEEE/Optica Journal of Optical Communications and Networking*, vol. 8, no. 7, pp. A23 - A33 (2016).
- [15] F. Paolucci, F. Cugini, F. Fresi, G. Meloni, A. Giorgetti, N. Sambo, L. Potí, A. Castro, L. Velasco, and P. Castoldi, "Superfilter technique in SDN-controlled elastic optical networks [Invited]," *IEEE/Optica Journal of Optical Communications and Networking*, vol. 7, no. 2, pp. A285 – A292 (2015).
- [16] N. Sambo, G. Meloni, F. Paolucci, F. Cugini, M. Secondini, F. Fresi, L. Potí, and P. Castoldi, "Programmable transponder, code and differentiated filter configuration in elastic optical networks," *IEEE/Optica Journal of Lightwave Technology*, vol 32, pp. 2079-2086 (2014).

Chapter 4

Digital signal processing mitigating spectrum narrowing

Since the advent of coherent optical system, various signal impairments such as chromatic dispersion and polarization mode dispersion are compensated by DSP circuits. In this chapter, the ML-based DSP method to mitigate the impact of spectrum narrowing induced in ultra-dense WDM networks is described. The proposed method can adapt to the various channel model by optimizing the ISI-imposing filter shape used for suppressing noise enhancement and decision criteria used for symbol decision.

4.1 Introduction

Ultra-dense WDM systems are expected to realize higher spectral efficiency. In such systems, however, the impact of the spectrum-narrowing effect induced by traversing wavelength-selective switches (WSSs) is critical [1-5]. Since the transfer function of WSSs does not obey the Nyquist criterion, an optical signal suffers from intersymbol interference (ISI) induced by WSS traversals. The ISI can be equalized by linear digital filters in coherent receivers [6, 7]. However, equalization of the WSS-induced ISI degrades the overall signal-to-noise ratio (SNR) as the frequency components attenuated by WSS traversals need to be magnified [2, 8]. In other words, the ISI equalization induces noise enhancement. Sequence estimation such as maximum likelihood sequence estimation (MLSE) can conduct symbol decision in the presence of ISI and thus evade occurrence of noise enhancement [9]. In typical digital coherent receivers, however, ISI is automatically equalized by adaptive filters used for polarization recovery [6, 7]. As a result, sequence estimation is executed while suffering noise enhancement accompanying ISI equalization. To resolve this problem, we need an ISI-imposing filter in front of the sequence estimator [8]. The transfer function of the ISI-imposing filter needs to be determined by the adequate spectrum model including both the noise and filtering characteristics of each optical path.

For a decade, machine learning (ML) technologies have been progressing rapidly. It is now

considered as a viable alternative to realize smart optical networking. ML is being utilized in many applications such as digital signal processing [10-17], fault detection [18], performance monitoring [19, 20], and network resource control [21-23]. ML-based DSP methods are now attractive to enhance the compensation performance for impaired signal [10-12]. The use of ML enables flexible classification for labels and thus offers more accurate symbol decision compared to traditional symbol decision based on the shortest Euclid distance on the constellation map. In this chapter, we report that the NN-based demodulation is effective against the spectrum narrowing caused in ultra-dense WDM networks.

The remainder of this chapter is organized as follows. Section 4.2 describes the conventional demodulation methods such as sequence estimation and ISI-imposing filter. In Section 4.3, we detail the ML-based symbol decision. In Section 4.4, the proposed ML-based demodulation method is described. In Section 4.5, we numerically evaluate its tolerance against the spectrum narrowing in ultra-dense WDM systems. Finally, we conclude this chapter in Section 4.6.

4.2 Conventional demodulation method

4.2.1 Sequence estimation

Sequence estimation can decide symbol labels even with ISI, which potentially avoids noise enhancement. One of the sequence estimation is maximum likelihood sequence estimation (MLSE) [9]. Figure 4.1 shows the schematics of MLSE. In the usual symbol decision method, each symbol label is classified only using the single complex value of the target symbol. In the MLSE, on the other hand, each symbol is classified based on the pattern of received samples. The transmitted symbol is estimated based on the ISI pattern. The length of pattern considering in MLSE is set as the finite memory length, L . The performance of sequence estimation improves as L increases; however, the calculation cost exponentially increases.

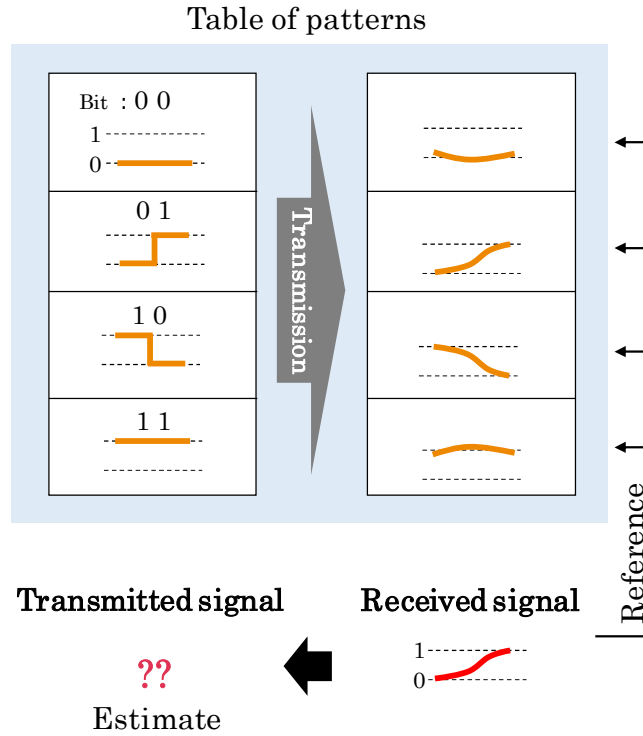


Figure 4.1 An example of maximum likelihood sequence estimation

4.2.2 ISI-imposing filter

In a typical DSP circuit, most of ISI is equalized by adaptive filters. However, the ISI equalization degrades the overall signal-to-noise ratio (SNR) because the frequency components attenuated by WSS filters are emphasized, which is referred to as noise enhancement. The noise enhancement is unavoidable because such equalization process is necessary for polarization recovery. To simultaneously realize polarization recovery and sequence estimation while suppressing noise enhancement, an ISI-imposing filter is necessary in front of the sequence estimator [8]. The ISI-imposing filter needs to be shaped based on spectrum models that include both the ASE noise and filtering characteristics. However, in optical path networks, numerous spectrum models are required because such characteristics of each path depend on combinations of add/express/drop operations of both the target- and adjacent-wavelength signals. In addition, performance deviations in devices such as WSSs, erbium-doped fiber amplifiers (EDFAs), and fiber loss, should be concerned. Moreover, transmission characteristics in dynamic optical path networks are expected to be frequently changed due to path setup and teardown operations. Therefore, we need another approach to mitigating the impact of spectrum narrowing that does not rely on prior channel information.

4.3 Symbol decision based on machine learning

4.3.1 Machine learning for symbol decision

Supervised learning is classified into classification and regression; the difference is whether the output is the probabilities of symbol label or the symbol location symbol location on a complex plane. An ML model based on regression needs the symbol decision process such as the conventional method based on Euclid distance. Since ML can learn a pattern from just the input data, priori system information and heuristic assumptions are unnecessary.

ML-based symbol decision comprises three stages; learning stage, testing stage, and working stage. In the learning stage, training dataset including input vectors and the corresponding symbol labels are prepared based on either computer simulations or transmission experiments. In the testing stage, input vectors are classified using the optimized ML model and the obtained output data are compared with the test labels. In order to confirm the generalization performance, the data used in the testing stage are excluded from the counterpart in the training stage. After feasible ML performance is attained, the process moves to the working stage and symbol decision is conducted. Note that the online learning models can simultaneously perform the learning stage and working stage. However, since the time-varying impairments such as SOP rotation and carrier-phase fluctuations are removed in the polarization and phase recovery processes beforehand, an ML model does not need the online internal-parameter update, which facilitates the implementation for high-symbol-rate systems.

So far, various studies, in which the ML model can learn deterministic signal distortion patterns created by multiple system impairments, have been reported [10-12]. In [12], a neural network (NN) is used for compensating the signal-bandwidth limitation for high-speed optical communication. With a simple ISI model, it has been proven that NN-based demodulation is the functional equivalent to optimum MLSE.

4.3.2 Neural network

An NN is known as an effective and versatile ML model that greatly broadens the applicable area thanks to its ability to compactly express values of numerous states [24-27]. Figure 4.2 shows a unit called neuron used in an NN. A neuron has multiple inputs and a single output; the output value is copied to the neurons on the following layer. In each neuron, the inner potential is calculated using weights and a bias, and the output value is obtained through an activation

4.4 Proposed demodulation method

Figure 4.4 illustrates the concept of our demodulation framework. After chromatic dispersion (CD) compensation, the signal is processed by an adaptive filter that compensates linear impairments such as filter-induced ISI and polarization-related signal distortion. Then, carrier phase and frequency are recovered. Finally, we introduce a bidirectional recurrent neural network (bi-RNN) to alleviate the signal degradation due to spectrum narrowing.

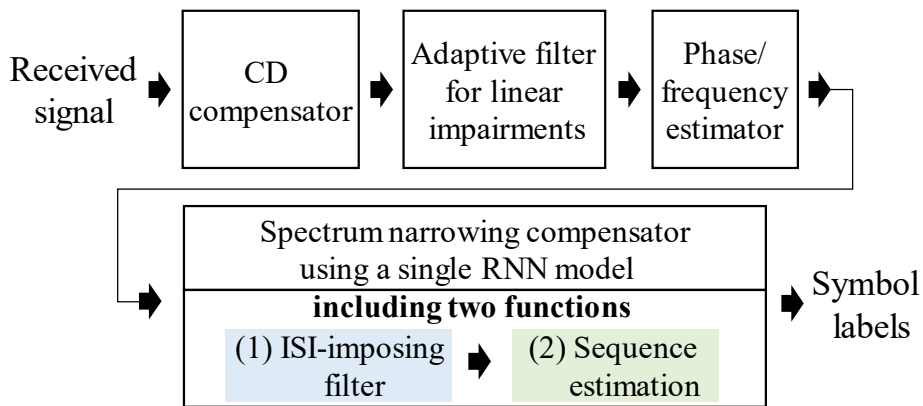


Figure 4.4 Proposed demodulation framework.

Figure 4.5 shows a structure of the bi-RNN model used in our method. The data processed in each RNN cell is fed back onto itself. This recursive connection enables the RNN model to effectively extract the time-dependent pattern. A bi-RNN, which assumes time-series data for both forward- and backward-direction, can consider ISI which spreads in the time domain. In our proposal, the RNN needs to have at least two layers; the needed number of layers are evaluated in the simulation as shown in Figure 4.8. A single RNN can simultaneously function as an ISI-imposing filter and sequence estimator. The bi-RNN model learns the interactive patterns between the ISI and the ASE noise so as to minimize bit-error ratio (BER). Consequently, both functions are simultaneously optimized without using spectrum models. Since NNs and widely used FIR filters have similar structures [29], the proposed demodulation method is expected to offer practical implementation. There are two types of output part; (1) classification, and (2) regression. The classification realizes the simple decision which does not additional symbol decision process. On the other hand, the regression method offers the operation like a FIR filter at the cost of additional symbol decision process, e.g., the conventional symbol decision based on Euclid distance.

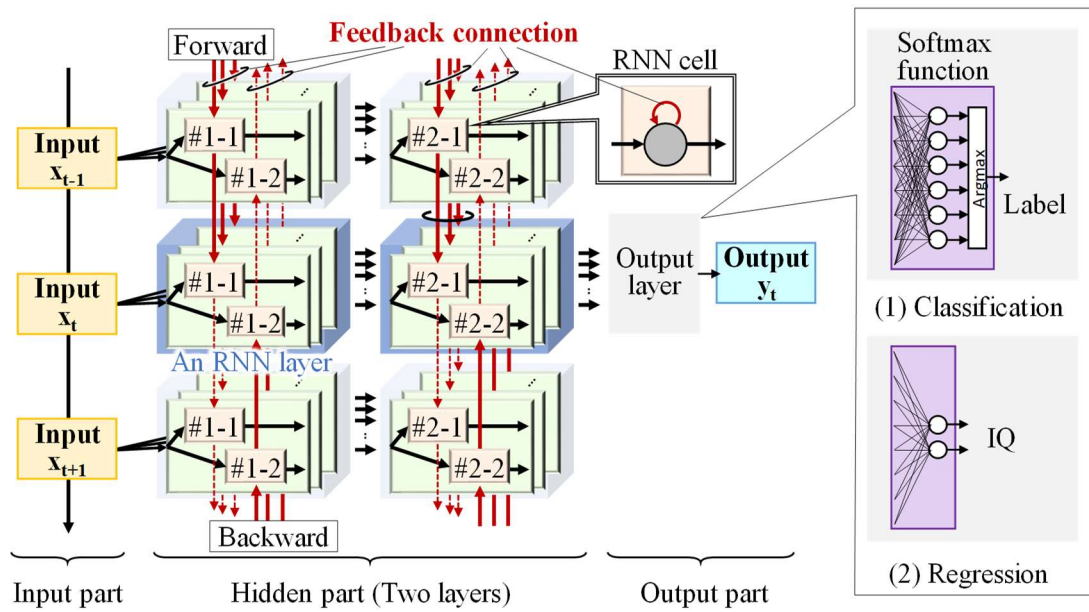


Figure 4.5 Bidirectional RNN model.

The software-defined networking (SDN), which offers the programmability for network applications, will support the creation of training dataset for ML models [30]. To use the proposal in the realistic network, the initial learning stage takes place. The learning stage of each system requires a relatively long training time, which is acceptable as it is a pre-service process. In the working stage, the proposal can adapt to the time-variant effect such as center-frequency fluctuation and passband bandwidth fluctuation of a WSS filter if the online learning is applied using SDN controller. Since the online learning slightly updates the internal parameters of an ML model unless the transmission characteristics change significantly, this process does not need much calculation time. Therefore, the RNN-based DSP supports the realistic transmission systems with a practical calculation cost.

4.5 Simulation

4.5.1 Simulation setup

We performed computer simulations to confirm the effectiveness of the RNN-based demodulation framework. Figure 4.6 depicts the simulation setup. The modulator creates a 32-Gbaud DP-16QAM signal. The spectrum is shaped by a root-raised cosine filter whose roll-off factor is 0.01. The linewidth of the transmitter laser is 100 kHz. The target signal is added to the network via a WSS and combined with two non-target signals whose frequencies are adjacent to that of the

target signal. The channel spacing of the WDM signals is set to 37.5/33.3 GHz to evaluate the spectrum narrowing effect in ultra-dense/quasi-Nyquist WDM networks. The WSS filter is created by convoluting two filter functions [5], where a rectangular function with 37.5-/33.3-GHz bandwidth and a Gaussian function, whose 3-dB bandwidth is parameterized as B_g , are used. The port isolation of the WSS is set to 40 dB. After power compensation with an EDFA, the signals are launched into a 100-km single-mode fiber (SMF). Here, the noise figure of the EDFA is set to 5 dB. We assumed the Kerr effect as fiber nonlinearity, it is characterized by the widely used Manacov model [31]. The loss coefficient, chromatic-dispersion parameter, and nonlinear coefficient of the SMF are, respectively, 0.2 dB/km, 16 ps/nm/km, and 1.5 /W/km. The transmission performance is calculated by the typical split-step Fourier method. We assume widely deployed 8×8-port optical nodes, where the broadcast-and-select (B&S) and route-and-select (R&S) architectures are evaluated [32]. Each B&S node and R&S node have one and two spectrum-narrowing events, respectively. The signal spectrum is narrowed at every WSS transit. After the signal passes through multiple nodes, the target signal is dropped by a splitter in the B&S node structure or by a WSS in the R&S node structure. Next, the target signal is coherently detected by an optical receiver. The linewidth of local oscillator is 100 kHz. In the DSP circuit within the receiver, chromatic dispersion is countered by a non-adaptive filter. Then, the adaptive filter with 64 delayed taps conducts polarization recovery and signal-spectrum reshaping. Then, the carrier phase and frequency offset are estimated. Finally, the signal is recovered by the bi-RNN model. The bi-RNN model comprises three parts; the input part consists of 4 neurons for IQ components of two polarizations; the hidden part comprises several layers based on long-/short-term memory (LSTM) cells [33]; the output part is the classification layer based on the softmax function, where the number of neurons equals the modulation order, or the regression layer based on rectified linear unit (ReLU), where the number of neurons equals 2. The maximum sequence length processed by each RNN cell, k , the number of hidden layers, N_{layer} , and the number of neurons in each hidden layer, N_{neuron} , are parameterized. We adopt the loss function of cross-entropy for classification model and mean least square error (MLSE) for regression model. The optimizer is based on the Adam algorithm [34]. Numerical simulations are conducted using Python 3.6 and Keras whose version is 2.4. The model is trained by using 480,000 symbols and tested by 120,000 symbols. We used the pseudorandom number generator called Mersenne Twister. The BER threshold of forward error correction is set to 0.01.

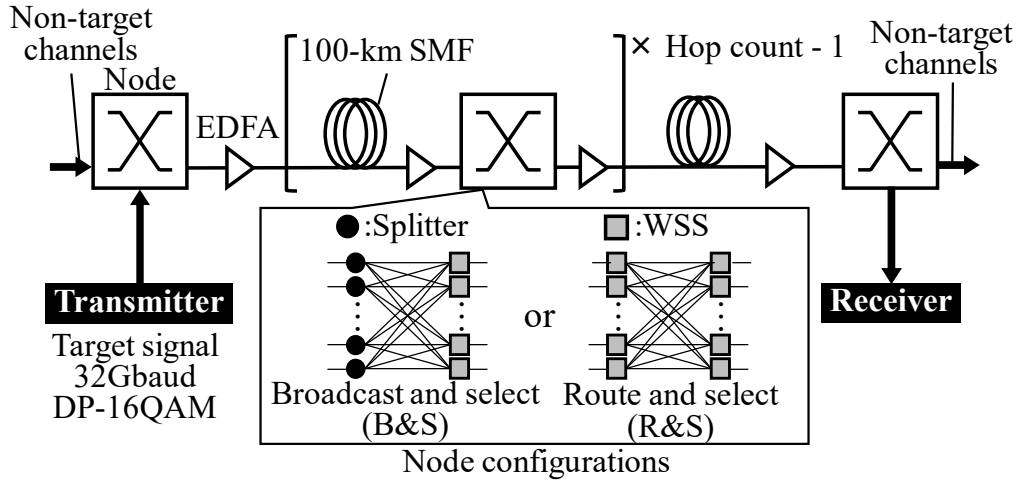


Figure 4.6 Simulation setup.

4.5.2 Simulation result

Figure 4.7 depicts the transition of accuracy of symbol decision in the bi-RNN learning process, where N_{neuron} is 32 and N_{layer} is set to 1 or 2. The transmission distance of 300 km and the node structure of R&S are assumed. The channel spacing of the WDM signals and B_g are set to 37.5 GHz and 5 GHz, respectively. We assume the classification model. We calculate the accuracy from the test dataset every 10 epochs. The accuracy improves as learning progresses. Obviously, the bi-RNN model with two hidden layers outperforms the counterpart with one hidden layer. Figure 4.8 shows a detail comparison of the RNN structures, where N_{neuron} and N_{layer} are parameterized. The RNN model with a single hidden layer yields less improvement than the other RNN models. We do not observe the notable performance differences if $N_{layer} \geq 2$.

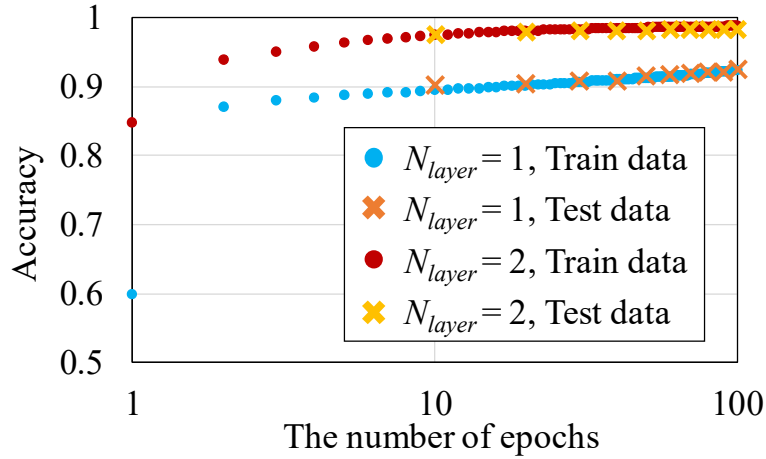


Figure 4.7 The transition of learning accuracy of bi-RNN.

| N_{layer} | N_{neuron} | | | | $\log_{10}(\text{BER})$ |
|-------------|--------------|-------|-------|-------|-------------------------|
| | 8 | 16 | 32 | 64 | |
| 1 | -1.37 | -1.63 | -1.73 | -1.87 | -2.4 -1.3 |
| 2 | -1.97 | -2.23 | -2.24 | -2.28 | |
| 3 | -2.01 | -2.20 | -2.31 | -2.34 | |
| 4 | -2.00 | -2.23 | -2.30 | -2.34 | |
| 4 | -2.00 | -2.23 | -2.30 | -2.34 | |

Figure 4.8 Evaluation of the BER performances of RNN structures.

Next, we investigate the ability of the ISI-imposing filter that is expected to be included in the RNN. We verify the BER performances when test filters are applied prior to the RNN. If the RNN model can realize adequate ISI-imposing filtering, the BER performance should be independent of test filters placed before the RNN. Three Gaussian filters are tested, where the 3-dB bandwidths normalized by the symbol rate are 0.7, 1.0, and 1.3. Here, the transmission distance is 300 km and the node structure is R&S. The channel spacing of the WDM signals of 37.5 GHz and B_g of 5 GHz are assumed. We assume the classification model. Figure 4.9 shows the tolerance to ISI induced by the test filter. We clearly observe that the RNN with two hidden layers can yield constant BER value regardless of test filters. This result implies that the RNN with two or more hidden layers can simultaneously realize an ISI-imposing filter and sequence estimation.

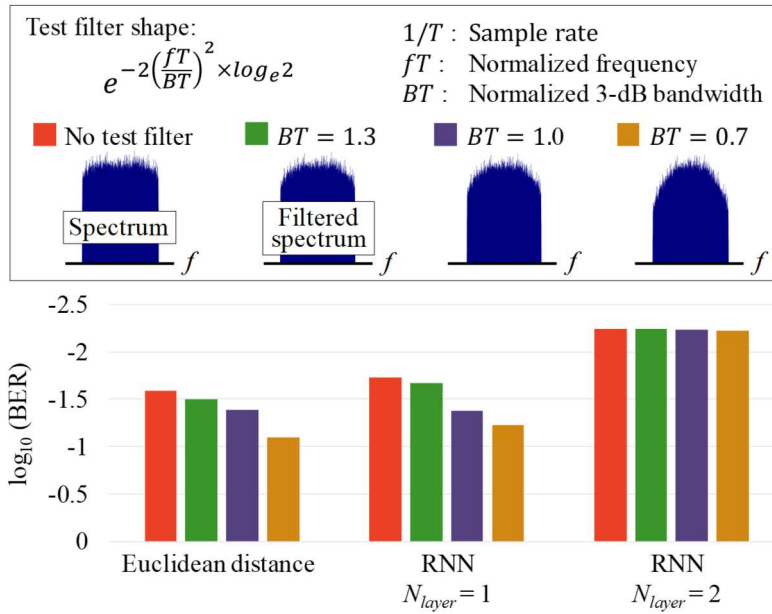


Figure 4.9 Evaluation of the ISI-imposing filter ability

We also evaluate the dependency of the maximum sequence length processed by each RNN cell, k . Figure 4.10 depicts BER versus hop count, where the value k is parameterized. N_{layer} and N_{neuron} are set to 2 and 32, respectively. When $k = 4$, the RNN performance in the transmission of 200 km or 300 km is low. On the other hand, similar trends are observed among the RNN whose k equals to or more than 8.

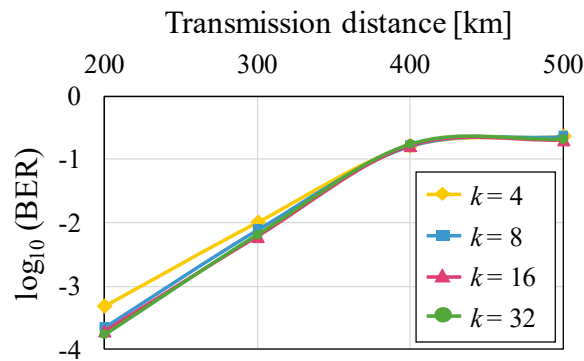


Figure 4.10 The time-sequence dependency of bi-RNN performance.

We confirm the performance of RNN model based on regression. Figure 4.11 shows the constellation map after processing the regression-based RNN model. The transmission distance is 300 km and the node structure is B&S. The channel spacing of the WDM signals of 37.5 GHz is assumed. The ML model learns for 1,000 epochs. The same color is assigned for the samples

whose labels defined in a transmitter are the same. We can observe that the samples spreading like Gaussian noise converge using information containing time-dependent patterns and geographical patterns. We also observe that the outer samples are still spread compared to the inner samples.



Figure 4.11 A constellation map after RNN model based on regression.

Next, we compare two output types, classification and regression. Figure 4.12 shows BER as a function of transmission distance and hop count in an ultra-dense WDM network. We assume the use of B&S nodes. The typical symbol decision based on the Euclidean distance is also evaluated as a reference. The channel spacing of the WDM signals of 37.5 GHz and B_g of 7 GHz are assumed. We confirm that both classification-/regression-based RNN model elongates the transmission distance compared to the conventional method based on Euclid distance. In this case, the regression-based RNN model overcomes the classification-based RNN model. However, since the expression capability is almost irrelevant to the output-layer type, we expect that the performances of both RNN models could be the same by tuning the hyper-parameters.

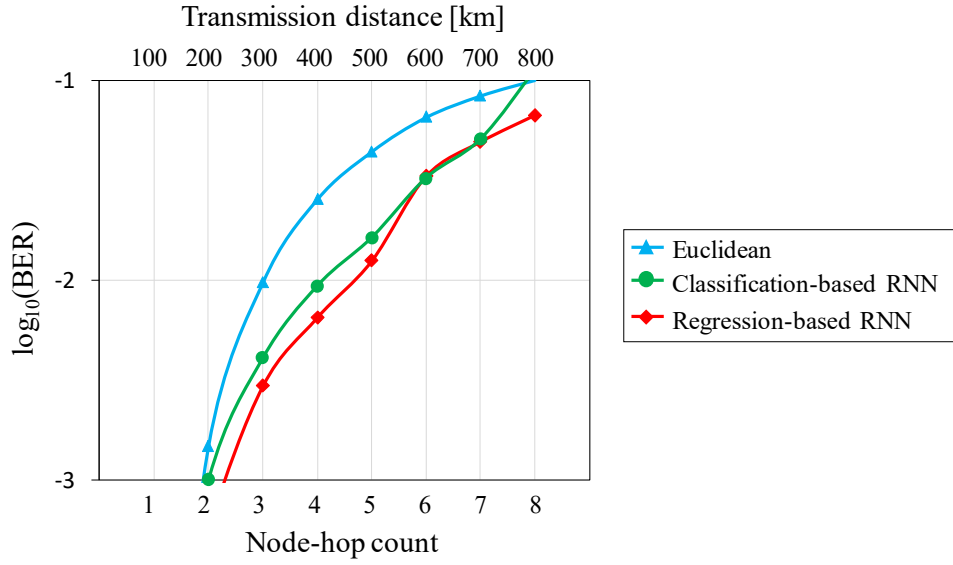


Figure 4.12 Demodulation performances of classification-/regression-based RNN.

Finally, we verify the effectiveness of our RNN-based demodulation framework. The typical symbol decision based on the Euclidean distance is also evaluated as a reference. The RNN parameters of k , N_{layer} , and N_{neuron} are set to 32, 2, and 32, respectively. Both the R&S node and the B&S node are examined. We assume B_g of 7 GHz. Figure 4.13 and Figure 4.14 show BER as a function of transmission distance and hop count in an ultra-dense WDM network and quasi-Nyquist WDM network. We observe that the maximum transmissible reach is extended in both cases compared to the reference method. Due to the instability of the adaptive FIR filters, the performance in the system using R&S nodes is steeply degraded.

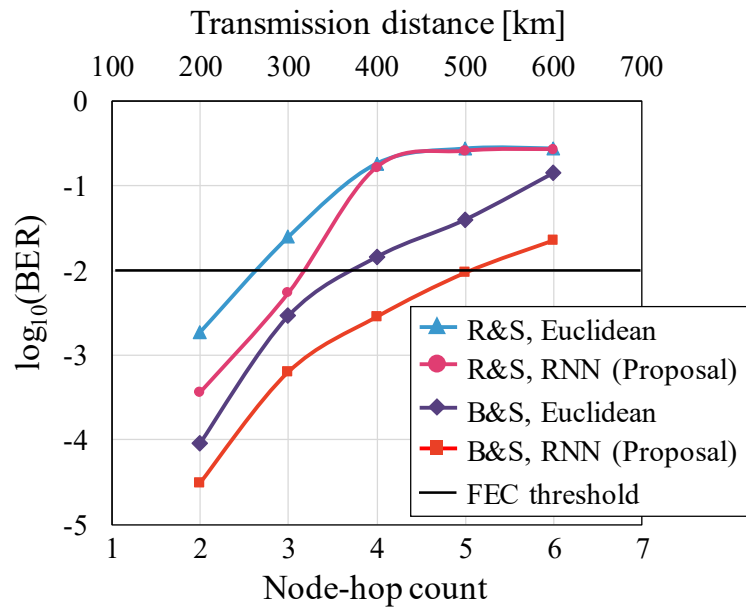


Figure 4.13 BER vs. transmission distance in ultra-dense WDM network.

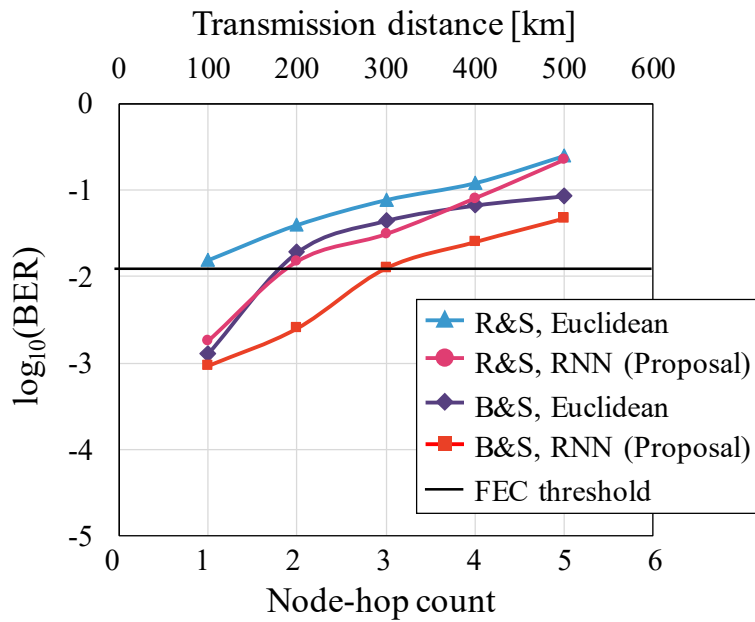


Figure 4.14 BER vs. transmission distance in quasi-Nyquist WDM network.

4.6 Conclusion

In this chapter, we introduced and evaluated an RNN-based demodulation method that counters the spectrum narrowing induced by the traversal of optical nodes in ultra-dense WDM networks. Extensive simulations proved that our proposed method could successfully extend the transmissible range compared with the typical symbol decision method. The increments in the maximum hop count are up to 2 in ultra-dense WDM networks. In addition, we verified the two functions of the proposed RNN-based DSP method with at least two hidden layers: ISI-imposing filter and sequence estimation. By interactively optimizing both ISI-imposing filter shape and sequence-estimation patterns as a single model, our proposal can construct an effective RNN without necessitating spectrum models of optical paths; this adaptability well suits future dynamic optical path networks. Note that the proposal can adapt to the time-variant effect such as center-frequency fluctuation and passband bandwidth fluctuation of a WSS filter if the online learning is applied. Although the robustness against the spectrum narrowing has been enhanced by the RNN-based demodulation method, the impact of spectrum narrowing cannot be perfectly eliminated. The next chapter presents how to design a network robust for the spectrum narrowing.

References

- [1] G. Bosco, V. Curri, A. Carena, P. Poggiolini, and F. Forghieri, "On the performance of Nyquist-WDM terabit superchannels based on PM-BPSK, PM-QPSK, PM-8QAM or PM-16QAM subcarriers," *IEEE Journal of Lightwave Technology*, vol. 29, pp. 53-61 (2011).
- [2] K. Okamura, Y. Mori, and H. Hasegawa, "Pre-filtering techniques for spectrum narrowing caused by optical node traversal in ultra-dense WDM networks," *IEEE Photonics Journal*, vol. 13, no. 2, pp. #7200513 (2021).
- [3] T. Zami, I. Fernandez de Jauregui Ruiz, B. Lavigne, and A. Ghazisaeidi, "Growing impact of optical filtering in future WDM networks," in *Optical Fiber Communication Conference (OFC)*, San Diego, USA, paper M1A.6 (2019).
- [4] I. F. de J. Ruiz, A. Ghazisaeidi, T. Zami, S. Louis, and B. Lavigne, "An accurate model for system performance analysis of optical fibre networks with in-line filtering", in *European Conference on Optical communication (ECOC)*, Dublin, Ireland, paper 78 (2019).
- [5] C. Pulikkaseril, L. Stewart, M. A. F. Roelens, G. Baxter, S. Poole, and S. Frisken, "Spectral modeling of channel band shapes in wavelength selective switches," *Optica Optics Express*, vol. 19, no. 9, pp. 8458-8470 (2011).

- [6] M. S. Faruk and S. J. Savory, "Digital signal processing for coherent transceivers employing multilevel formats", *IEEE/Optica Journal of Lightwave Technology*, vol. 35, no. 5, pp. 1125-1141 (2017).
- [7] K. Kikuchi, "Fundamentals of coherent optical fiber communications", *IEEE/Optica Journal of Lightwave Technology*, vol. 34, no. 1, pp. 157-179 (2016).
- [8] K. Horikoshi, T. Kobayashi, S. Yamanaka, E. Yamazaki, A. Sano, E. Yoshida, and Y. Miyamoto, "Spectrum-narrowing tolerant 171-Gbit/s PDM-16QAM transmission over 1,200 km using maximum likelihood sequence estimation," in *European Conference on Optical communication (ECOC)*, Geneva, Switzerland, paper We.10.P1.73 (2011).
- [9] J. G. Proakis and M. Salehi, "Trellis and graph based codes", in *Digital Communications Fifth Edition*, McGraw-Hill, New York, USA, pp. 510-516 (2008).
- [10] M. Schaedler, F. Pittalà, G. Böcherer, C. Bluemm, M. Kuschnerov, and S. Pachnicke, "Recurrent neural network soft-demapping for nonlinear ISI in 800Gbit/s DWDM coherent optical transmissions," *IEEE/Optica Journal of Lightwave Technology*, vol. 39, no. 16, pp. 5278-5286 (2021).
- [11] S. Deligiannidis, C. Mesaridakis, and A. Bogris, "Performance and complexity analysis of bidirectional recurrent neural network models vs. Volterra nonlinear equalizers in digital coherent systems," *IEEE/Optica Journal of Lightwave Technology*, vol. 39, no. 18, pp. 5791-5798 (2021).
- [12] S. C. K. Kalla, C. Gagné, M. Zeng, and L. A. Rusch, "Recurrent neural networks achieving MLSE performance for optical channel equalization," *Optica Optics Express*, vol. 29, no. 9, pp. 13033-13047 (2021).
- [13] M. Li, S. Yu, J. Yang, Z. Chen, Y. Han, and W. Gu, "Nonparameter nonlinear phase noise mitigation by using M-ary support vector machine for coherent optical systems," *IEEE Photonics Journal*, vol. 5, no. 6, paper. 7800312 (2013).
- [14] J. Zhang, W. Chen, M. Gao, and G. Shen, "K-means-clustering-based fiber nonlinearity equalization techniques for 64-QAM coherent optical communication system," *Optica Optics Express*, vol. 25, no. 22, pp. 27570-27580 (2017).
- [15] J. Zhang, M. Gao, W. Chen, and G. Shen, "Non-data-aided k-nearest neighbors technique for optical fiber nonlinearity mitigation," *IEEE/Optica Journal of Lightwave Technology*, vol. 36, no. 17, pp. 3564-3572 (2018).
- [16] J. Zhang, W. Chen, M. Gao, Y. Ma, Y. Zhao, W. Chen, and G. Shen, "Intelligent adaptive coherent optical receiver based on convolutional neural network and clustering algorithm," *Optica Optics Express*, vol. 26, no. 14, pp. 18684-18698 (2018).

- [17] D. Wang, M. Zhang, M. Fu, Z. Cai, Z. Li, H. Han, Y. Cui, and B. Luo, "Nonlinearity mitigation using a machine learning detector based on k-nearest neighbors," *IEEE Photonics Technology Letters*, vol. 28, no. 19, pp. 2102-2105 (2016).
- [18] D. Rafique, T. Szyrkowiec, H. Griebner, A. Autenrieth, and J. -P. Elbers, "Cognitive assurance architecture for optical network fault management," *IEEE/Optica Journal of Lightwave Technology*, vol. 36, no. 7, pp. 1443-1450 (2018).
- [19] J. Thrane, J. Wass, M. Piels, J. C. M. Diniz, R. Jones, and D. Zibar, "Machine learning techniques for optical performance monitoring from directly detected PDM-QAM signals," *IEEE/Optica Journal of Lightwave Technology*, vol. 35, no. 4, pp. 868-875 (2017).
- [20] R. M. Morais and J. Pedro, "Machine learning models for estimating quality of transmission in DWDM," *IEEE/Optica Journal of Optical Communications and Networking*, vol. 10, no. 10, pp. D84-D99 (2018).
- [21] W. Mo, C. L. Gutterman, Y. Li, S. Zhu, G. Zussman, and D. C. Kilper, "Deep-neural-network-based wavelength selection and switching in ROADM systems," *IEEE/Optica Journal of Optical Communications and Networking*, vol. 10, no. 10, pp. D1-D11 (2018).
- [22] S. K. Singh and A. Jukan, "Machine-learning-based prediction for resource (re)allocation in optical data center networks," *IEEE/Optica Journal of Optical Communications and Networking*, vol. 10, no. 10, pp. D12-D28 (2018).
- [23] R. Shiraki, Y. Mori, H. Hasegawa, and K. Sato, "Dynamically controlled flexible-grid networks based on semi-flexible spectrum assignment and network-state-value evaluation," in *Optical Fiber Communication Conference (OFC)*, San Diego, USA, paper M1B.4 (2020).
- [24] V. Bajaj, F. Buchali, M. Chagnon, S. Wahls, and V. Aref, "Single-channel 1.61 Tb/s optical coherent transmission enabled by neural network-based digital pre-distortion," in *European Conference on Optical Communications (ECOC)*, Brussels, Belgium, paper Tu1D-5 (2020).
- [25] M. Schaedler, S. Calabrò, F. Pittalà, G. Böcherer, M. Kuschnerov, C. Bluemm, and S. Pachnicke, "Neural network assisted geometric shaping for 800Gbit/s and 1Tbit/s optical transmission," in *Optical Fiber Communication (OFC) Conference*, San Diego, USA, paper M1G.1 (2020).
- [26] M. Schaedler, F. Pittalà, G. Böcherer, C. Bluemm, M. Kuschnerov, and S. Pachnicke, "Recurrent neural network soft-demapping for nonlinear ISI in 800gbit/s DWDM coherent optical transmissions," in *European Conference on Optical Communications (ECOC)*, Brussels, Belgium, paper We1D-1 (2020).
- [27] O. Kotlyar, M. Pankratova, M. Kamalian-Kopae, A. Vasylchenkova, J. E. Prilepsky, and S. K. Turitsyn, "Combining nonlinear Fourier transform and neural network-based processing in optical communications," *Optica Optics letters*, vol. 45, no. 13, pp. 3462-3465 (2020).

- [28] M. Anthony and P. L. Bartlett, “Neural network learning: theoretical foundations”, Cambridge Press (1999).
- [29] Z. Zhai H. Jiang, M. Fu, L. Liu, L. Yi, W. Hu, and Q. Zhuge, “An interpretable mapping from a communication system to a neural network for optimal transceiver-joint equalization,” *IEEE/Optica Journal of Lightwave Technology*, vol. 39, no. 17, pp. 5449-5458 (2021).
- [30] W. Xia, Y. Wen, C. H. Foh, D. Niyato, and H. Xie, “A survey on software-defined networking,” *IEEE Communications Surveys and Tutorials*, vol. 17, no. 1, pp. 27-51 (2015).
- [31] K. Kikuchi, “Analyses of wavelength- and polarization-division multiplexed transmission characteristics of optical quadrature-amplitude-modulation signals,” *Optica Optics Express*, vol. 19, no. 19, pp. 17985-17995 (2011).
- [32] S. L. Woodward, M. D. Feuler, and P. Palacharla, “ROADM-node architectures for reconfigurable photonic networks”, in *Optical Fiber Telecommunications VIB*, Academic Press, ch. 15, pp. 683-707 (2013).
- [33] Z. Huang, W. Xu, and K. Yu, “Bidirectional LSTM-CRF models for sequence tagging,” *arXiv preprint arXiv:1508.01991* (2015).
- [34] S. J. Reddi, S. Kale, and S. Kumar, “On the convergence of Adam and beyond,” in *International Conference on Learning Representations (ICLR)*, Vancouver, Canada (2018).

Chapter 5

Design for ultra-dense WDM networks

Since network components cannot be easily installed or changed, we need to optimize a network considering the various factors such as current/future traffic-demand distribution, terrestrial conditions, and so on. In the ultra-dense WDM networks, since the impact of spectrum narrowing cannot be perfectly eliminated, a network robust for the spectrum narrowing is desired. In this chapter, we focus on how to design the network that can easily control the impact of spectrum narrowing.

5.1 Introduction

The amount of Internet traffic has continued to increase steeply worldwide due to the introduction of 5G services and the connection of geographically dispersed data centers. Owing to the cost-sensitivity of optical path networks, it is essential to enhance network capacity while suppressing the cost increase. So far, the network capacity has been enhanced by the introduction of higher-order modulation formats and denser wavelength-division multiplexing (WDM). As the feasible modulation order reaches the theoretical limit [1], the vacant spectral resources set between WDM signals, referred to as guardbands, must be minimized to improve the network capacity in a cost-effective manner [2]. On the other hand, such ultra-dense WDM systems suffer from the spectrum narrowing induced by the non-rectangular passbands of wavelength-selective switches (WSSs) used as a wavelength cross-connect (WXC) in the optical node [3, 4]. Since the impact of spectrum narrowing accumulates as the optical signal traverses more nodes, the transparent transmission distance is severely shortened. In this chapter, the network design where the impact of spectrum narrowing effect can easily be suppressed and controlled is reported.

The remainder of this chapter is organized as follows. Section 5.2 overviews the previous scheme of coarsely granular routing. In Section 5.3, the proposed network design and control scheme enabling effective network-resource management are discussed. Section 5.4 examines the spectral efficiency of our proposal through computer simulations. Finally, this chapter is concluded in Section 5.5.

5.2 Coarsely granular routing

To alleviate the impact of spectrum narrowing, coarsely granular express routing was proposed [5-8]. In [7, 8], the super-filter scheme, which aggregates several independent channels within the same passband, is proposed. Grouped routing (GR) networks effectively enhance the spectral efficiency by adopting not only the super-filter scheme but also impairment-aware routing. In this scheme, the available spectrum range, *e.g.*, C-band, is divided into multiple wavebands called grouped routing entity (GREs), and relatively broad guardbands are inserted only between neighboring GREs. Since denser channel alignment is possible within each GRE, the spectral efficiency can be enhanced compared to conventional networks. An extreme case for the GR network is a fiber-granular routing network with wavelength-granular add/drop; in other words, the number of paths in a GRE is equal to that in a fiber. In such a network, fiber cross-connects (FXCs) will be beneficial to handle the enormous traffic volume cost-efficiently [9, 10]. Another related scheme is the spatial-channel network (SCN) [11, 12], where FXCs and spatial-channel cross-connects (SXC) are used. This solution supports the space-division-multiplexing (SDM) signals and can reduce node loss and mitigate spectrum narrowing as well.

Since the use of GR networks degrades flexibility in routing and wavelength assignment (RWA), it penalizes the path accommodation efficiency. This penalty can be relaxed using a sophisticated algorithm in green-field design scenarios, which allows fully flexible optimization of fiber installations and selection of route and wavelength for optical paths. It has been verified that the deterioration in path-accommodation efficiency can also be mitigated for the fiber-granular routing case [9]. On the other hand, in dynamic path-operation scenarios, existing paths often prohibit the reconfiguration needed for GRE. For example, a GRE cannot be released if it is carrying even a path. This inflexibility makes responding to path distribution changes difficult.

5.3 Filter-less drop operation

Since only paths adjacent in the frequency domain cause spectrum narrowing, the impact of spectrum narrowing can be controlled by considering adjacent-path operations at nodes. The filter-less signal drop at nodes can relax the effect of spectrum narrowing [13-16]. At the broadcast-and-select (B&S) WXC-based node or FXC-based node, the signals to be dropped are sent to the drop portion by using a splitter and detected by coherent receivers. Here, the dropped signal residual in the express port should not be terminated unless another signal using the same wavelength is newly added, as shown in Figure 5.1.

Note that the filter-less drop operation is impossible when we adopt WSSs at the input side of the

node. For example, the R&S node architecture cannot exploit this benefit because the drop operation is performed by a WSS [17]. As for the R&C node architecture, although a similar approach, i.e., filter-less add, could be applied, the resulting noise would severely degrade the signal quality; thus, applying the scheme to R&C nodes is impractical. The impact of crosstalk is more serious in B&S nodes than in R&S nodes. Therefore, we need to consider the tradeoff between spectrum narrowing and crosstalk. For example, a reference reported that the B&S node is preferable if the port count is less than 9 and the channel configuration is 120-Gbps DP-QPSK signals with 50-GHz spacing [18].

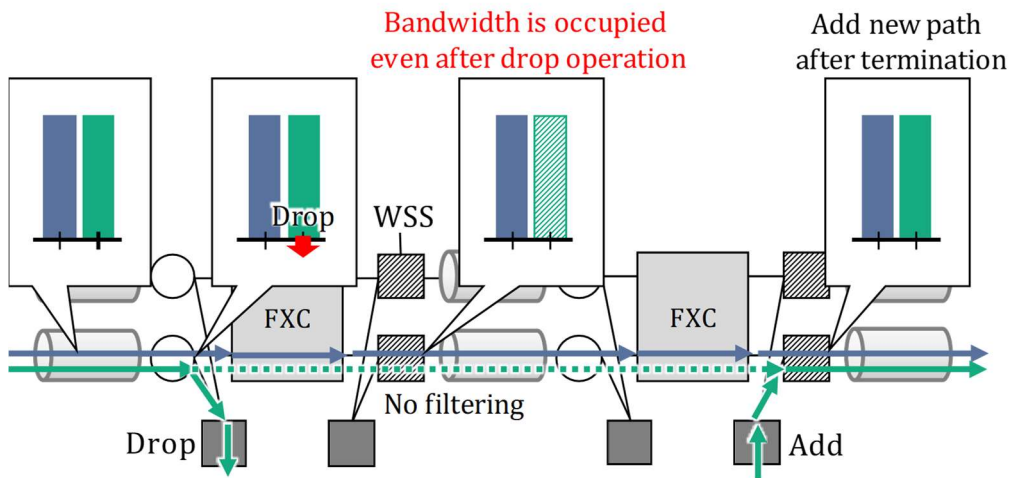


Figure 5.1 Filter-less drop.

5.4 Design scheme of ultra-dense WDM networks

5.4.1 Concept

To realize the ultra-dense WDM network, the proposed network architecture assumes that nodes have fiber-granular express routing and wavelength-granular add/drop. Figure 5.2 shows the fiber-granular routing scheme based on overlaid sub-networks. A sub-network consists of several fibers, where each link on a topology has at most one fiber and there is no branching of routes; as a result, it forms line- or ring-shaped topology. The physical network is shaped by stacking sub-networks. In other words, sub-networks can be seen as the physical network divided for express routing. Since optical paths are set up on a sub-network basis, spectrum narrowing induced by adjacent-path “express” operations are eliminated. Furthermore, since the assuming FXC-based node architecture has a broadcast-and-select structure, we apply filter-less drop operation, which results in suppressing the spectrum narrowing induced by adjacent-path “drop” operations. Consequently, the spectrum narrowing is triggered only by adjacent-path “add” operation, as shown in Figure 5.3. Here, the impairment of the added signal can be compensated by pre-equalization using an inverse optical filter against the WSS operation. On the other hand, the spectrum narrowing shown by the yellow balloon cannot be compensated since optical filtering at the express node impairs signal quality by interacting with amplified spontaneous emission (ASE) noise. Note that our proposal can still be applied to nodes with the route-and-select structure as we can manage the network so that the number of spectrum-narrowing events does not exceed the limit; however, RWA is restricted more severely by spectrum-narrowing events triggered by adjacent-path “add/drop” operations.

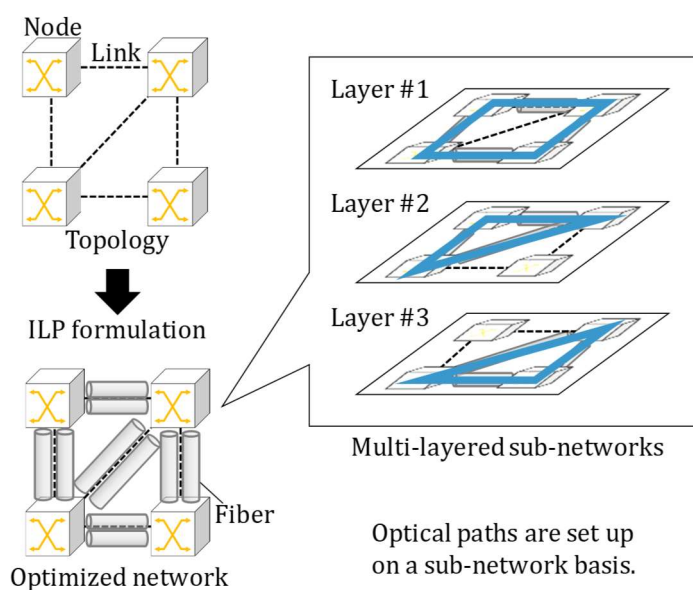


Figure 5.2 Proposed sub-network-based network design scheme

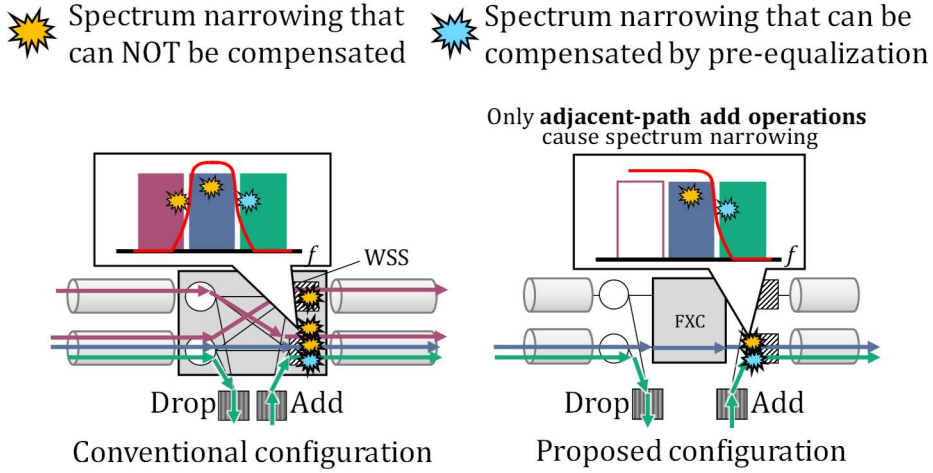


Figure 5.3 Comparison of spectrum-narrowing occurrences.

5.4.2 Network design algorithm

We propose an initial design scheme for constructing line-/ring-shaped sub-networks. In the proposed scheme, a set of sub-networks that can accommodate the given path demands is constructed so that the number of necessary fibers is minimized. The network, which consists of the minimum number of fibers, is modeled with an integer linear programming (ILP) formulation defined on a set of sub-networks. Each sub-network is formed as a line-/ring-shaped network. In network control phase, the paths are dynamically set up and torn down on the sub-networks. The spectrum-narrowing mitigation is mainly realized by selecting appropriate route pairs and wavelength.

To optimize the fiber arrangement, the following ILP formulation (Eqs. (1) - (8)) is adopted. All the variables and parameters are defined in Table 2. The conditions are made from the information of topology including the set of nodes, N , the set of links, L , the maximum number of wavelengths per fiber, W , and the traffic intensity between each node pair, $T_{(s,d)}$. Then, the conditions are input to the ILP solver. Each element of $T_{(s,d)}$ for formulating ILP is an integer variable. This formulation aims to minimize the fiber number in the given network (Eq. (1)). Eqs. (2) - (8) cover the conditions of the network. The first five constraints (Eqs. (2) - (6)) are about flow conservation. Eqs. (2) and (3) define the number of traffic demands at each node. Eq. (4) shows the fiber capacity in each link. Eq. (5) signifies the relationship between the amount of traffic-flow added to node s and that of the flow going through the link around s . Eq. (6) is like Eq. (5), but for dropped flows. To distinguish the traffic in terms of the source node, parameters for dropped

traffic need the source node's information. The last two constraints impose ring or line shapes. Eq. (7) restricts the bidirectional fiber in each link. Eq. (8) forbids the branching of fibers in each sub-network. As a result, each sub-network only has a line-/ring-shaped fiber series and can eliminate the spectrum narrowing caused by express routing. After solving the ILP, the values of $f(\cdot, \cdot, \cdot)$ give a set of sub-networks as outputs. As a network is built from a scratch, long calculation times are acceptable. Since the effectiveness of the proposal relies on the fiber arrangement, the optimal fiber arrangement is pursued even though it incurs much longer calculation times than heuristic methods.

Table 5.1 Variables and parameters for ILP-based network design scheme.

| Notation | Definition |
|---------------------|---|
| $f_{(k,l_s,l_d)}$ | A binary variable which stands for # of fibers from l_s to l_d on k -th sub-network. |
| $a_{(k,n)}$ | An integer-valued variable that stands for # of paths added at node n to k -th sub-network. |
| $d_{(k,s,n)}$ | An integer-valued variable that stands for # of paths added at s and at n to k -th sub-network. |
| $t_{(k,s,l_s,l_d)}$ | An integer-valued variable that stands for # of paths added to k -th sub-network at s and going through from l_s to l_d . |
| $T_{(s,d)}$ | An integer that stands for # of paths to be established from s to d . |
| L | The set of all links in the given topology. |
| N | The set of all nodes in the given topology. |
| K | The set of all sub-networks. |
| W | The # of wavelengths per fiber. |

Minimize:

$$\sum_{k \in K} \sum_{l_s \in N} \sum_{l_d \in N} f_{(k,l_s,l_d)} \quad (1)$$

Subject to:

$$\sum_{k \in K} a_{(k,s)} - \sum_{d \in N} T_{(s,d)} = 0 \quad \text{for all } s \in N \quad (2)$$

$$\sum_{k \in K} d_{(k,s,d)} - T_{(s,d)} = 0 \quad \text{for all } s, d \in N \quad (3)$$

$$\sum_{s \in N} t_{(k,s,l_s,l_d)} - f_{(k,l_s,l_d)} * W \leq 0 \quad \text{for all } l_s, l_d \in N \text{ and } k \in K \quad (4)$$

$$a_{(k,s)} - \sum_{n \in N} t_{(k,s,s,n)} = 0 \quad \text{for all } s \in N \text{ and } k \in K \quad (5)$$

$$d_{(k,s,d)} + \sum_{l_d \in N} t_{(k,s,d,l_d)} - \sum_{l_s \in N} t_{(k,s,l_s,d)} = 0 \quad \text{for all } s, d \in N \text{ and } k \in K \quad (6)$$

$$f_{(k,l_s,l_d)} + f_{(k,l_d,l_s)} \leq 1 \quad \text{for all } l_s, l_d \in N \text{ and } k \in K \quad (7)$$

$$\sum_{l_d \in N} f_{(k,n,l_d)} + \sum_{l_s \in N} f_{(k,l_s,n)} \leq 2 \quad \text{for all } n \in N \text{ and } k \in K \quad (8)$$

The above ILP is formulated to minimize the number of fibers based on the number of paths to be virtually established between each node pair; this information is used only for green-field design and these paths need not be established in practice. When introducing the proposed architecture to existing networks, we must identify a sub-network set that does not demand changes to the existing fiber deployment. To find a feasible set of sub-networks, we introduce the following conditions

$$\sum_{k \in K} f_{(k,l_s,l_d)} \leq f_{exist(k,l_s,l_d)} \quad \text{for all } l_s, l_d \in N, \quad (9)$$

where f_{exist} stands for the number of already deployed fibers on each link. We can define

another variable to find a set of sub-networks that provides robust scale in terms of path numbers. It can be summarized as follows. Let $\alpha(\geq 1)$ be a scaling parameter. Verify whether the ILP with Eq.(9) is still satisfied if we let $T_{(s,d)} := \lceil \alpha T_{(s,d)} \rceil$. If satisfied, then increase α ; otherwise, decrease α . Repeat this procedure to find an approximation of the highest value of α . Output the set of sub-networks that corresponds to the approximation.

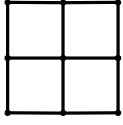
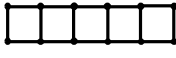
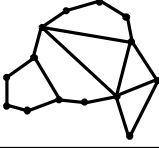
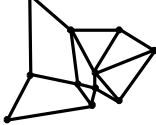
Solving the ILP becomes complicated with increase in the number of nodes since the number of parameters optimized by ILP, *i.e.*, $f_{(k,l_s,l_d)}$, $a_{(k,n)}$, $d_{(k,s,n)}$, and $t_{(k,s,l_s,l_d)}$ increases. As a result, the calculation time becomes longer. The effectiveness of the proposal mostly relies on the fiber arrangement described in this section. We believe that we have to pursue the optimal fiber arrangement given by ILP even though this incurs much longer calculation times than heuristics. By using the heuristics method as shown in [19], the calculation cost reduces in return for the slight performance deterioration.

5.5 Simulations

5.5.1 Simulation setup

The transmission in the 4.8 THz bandwidth range, *i.e.*, extended C-band, is assumed. We examined several networks: a 3×3 regular-mesh network, 2×6 regular-mesh network, US-metro Verizon network [20], and Kanto network [21], summarized in Table 5.2. Each path comprises a 100-Gbps 32-Gbaud DP-QPSK signal. The maximum number of paths accommodated per fiber, W , is 96 (50-GHz spacing) or 128 (37.5-GHz spacing) for the conventional DWDM network and the ultra-dense WDM network, respectively. In ultra-dense WDM networks, the allowable number of spectrum-narrowing events induced by adjacent-path add operation, N_s , is set to 1 considering adequate transmission distances.

Table 5.2 Tested physical topologies and their characteristics.

| | | | | |
|------------------------------|---|---|--|---|
| |  |  |  |  |
| Network topology | (a) 3×3 regular mesh network | (b) 2×6 regular mesh network | (c) Verizon network | (d) Kanto network |
| The number of nodes | 9 | 12 | 14 | 11 |
| The number of links | 24 | 32 | 38 | 36 |
| Max. node degree | 4 | 3 | 5 | 5 |
| Average node degree | 2.67 | 2.67 | 2.71 | 3.27 |
| Max. number of shortest hops | 4 | 6 | 5 | 4 |

5.5.2 Simulation result

The traffic intensity is represented as the number of wavelength-path demands between each node pair, D_{static} . We tested the three network schemes summarized in Table 5.3. Scheme A is the conventional DWDM system. Scheme B is the ultra-dense WDM system with wavelength-granular express routing. Scheme C is the proposed ultra-dense WDM system with fiber-granular express routing and wavelength-granular add/drop. In Scheme B, assigned wavelength for each traffic demand is selected so as not to exceed N_s .

Table 5.3 Network configurations.

| | Scheme A (Conventional) | Scheme B | Scheme C (Proposed) |
|-----------------------------|----------------------------|----------|------------------------|
| # of wavelengths / fiber | 96 | 128 | 128 |
| Add/drop granularity | Path | Path | Path |
| Express routing granularity | Path | Path | Fiber |

Figure 5.4 shows an example of the fiber arrangement yielded by ILP-formulation (Scheme C) for the Kanto network with $D_{static} = 16$ and $W = 128$. Directional optical fibers are depicted as red arrows. All the sub-networks consist of ring-shaped fiber arrangements in this case. While line-shaped sub-networks are possible in theory, all sub-networks found throughout the

simulations were ring-shaped.

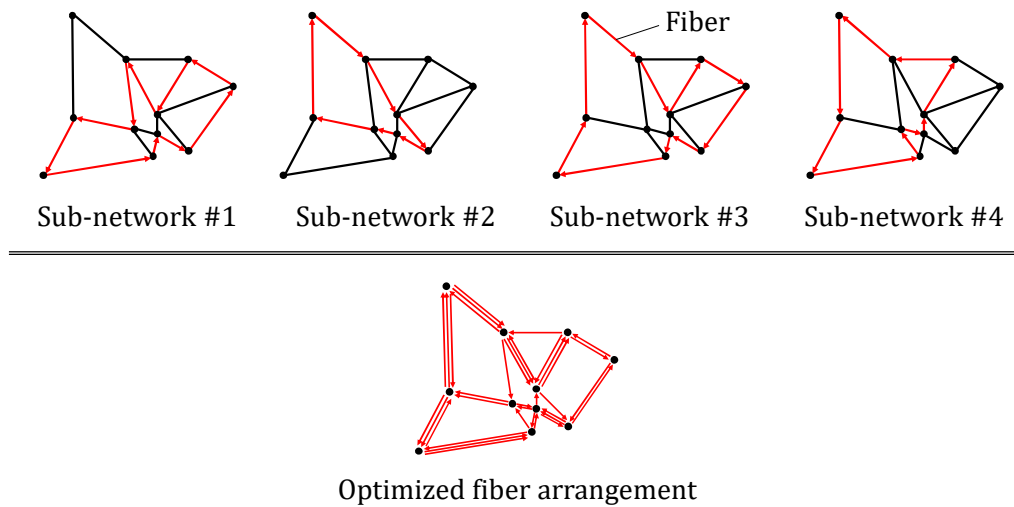


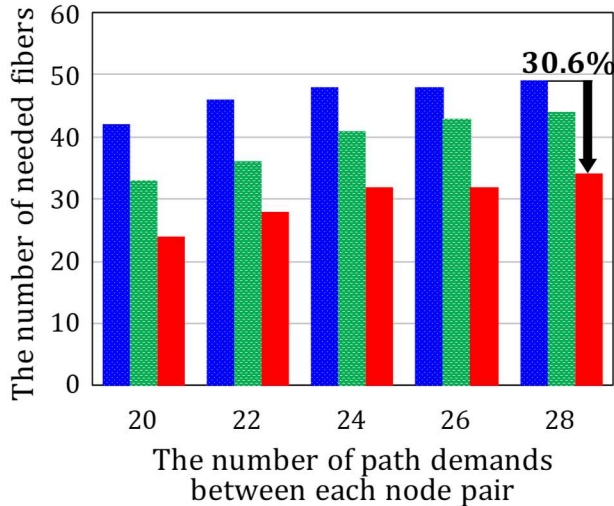
Figure 5.4 An example of sub-networks.

Figure 5.5 shows the numbers of optical fibers needed by the three schemes for the four tested topologies. The proposal, i.e., Scheme C, needs fewer fibers than Schemes A and B. Since the parameter space optimized by ILP expands with the node degree, it is difficult to obtain the sub-optimal fiber arrangement; consequently, our proposal attains less improvement in the Verizon and Kanto networks whose node degree is relatively high. On the other hand, our proposal offers better performance in the 3×3 regular mesh network and the 2×6 regular mesh network with small node degree; the number of fibers required is reduced by up to 31.7%. The reduction in fiber number induced by the proposal approaches 33.3% as the number of path demands increases.

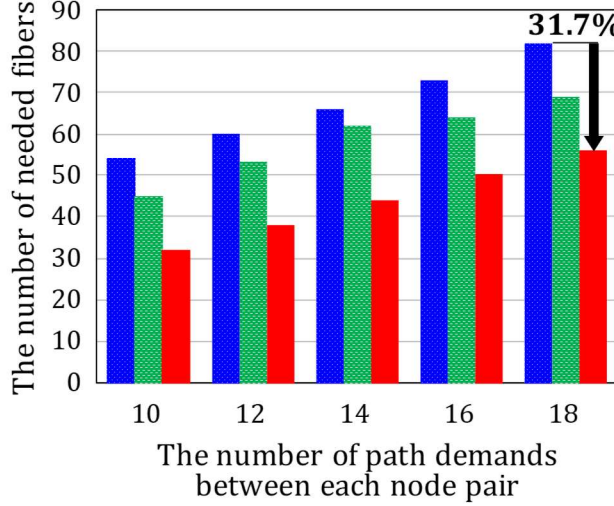
The calculation cost for ILP significantly increases as network size and the number of layers formulated are expanded; more layers are necessary for larger traffic. As the network is built from a scratch in Phase I, the acceptable calculation time is long. The calculation time taken by the ILP solver of CPLEX running on a 16-core/3.4GHz Intel Xeon E5 server was about 10 hours for a 5-layer graph for all topologies examined. It could be much quicker if we allow the termination of the calculation when the duality gap becomes sufficiently small, e.g., the calculation time reduces to 8 hours if the duality gap of 20% is allowed.

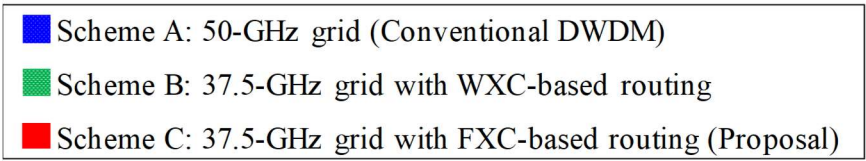
- Scheme A: 50-GHz grid (Conventional DWDM)
- Scheme B: 37.5-GHz grid with WXC-based routing
- Scheme C: 37.5-GHz grid with FXC-based routing (Proposal)

3×3 regular-mesh network

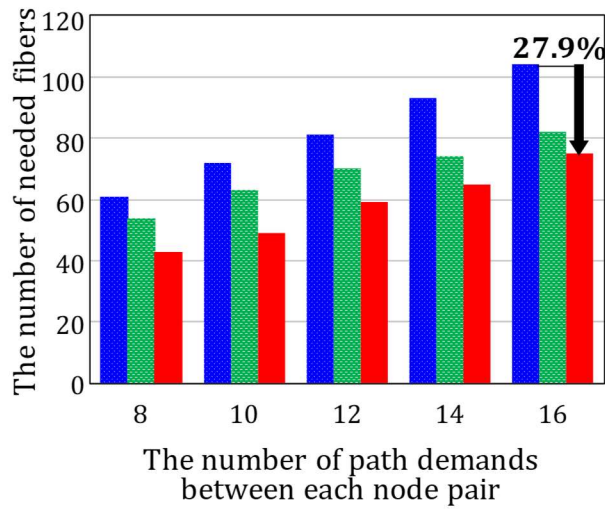


2×6 regular-mesh network





US-metro Verizon network



Kanto network

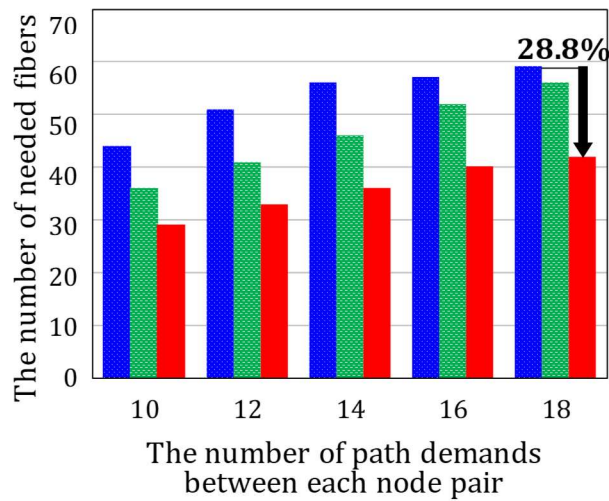


Figure 5.5 Variations of the number of fibers.

5.6 Conclusion

In this chapter, we proposed a design scheme for networks that adopt fiber-granular express routing and wavelength-granular add/drop operations for achieving ultimately dense channel arrangements. The severe spectrum narrowing triggered by the high channel density is mitigated by fiber-granular routing using a tailor-made ILP-based network design scheme and a spectrum-narrowing-aware dynamic path operation method. As a result, ultra-dense WDM networks can be realized by using WXC-based nodes or cost-efficient FXC-based nodes. We can take advantage of filter-less drop provided these nodes have the broad-cast-select structure. However, even for a network based on the route-and-select structure, we can manage the network so that the number of spectrum-narrowing events does not exceed the limit. Hence, the combination of ultra-dense WDM and fiber-granular express routing can be applied to route-and-select nodes if the routing inflexibility caused by omitting the filter-less drop function is marginal. To exploit the benefit of proposed network design, the sophisticated network control that effectively manage the spectrum narrowing is needed. In the next chapter, we described how to control optical paths and networks.

References

- [1] R.-J. Essiambre, G. Kramer, P.-J. Winzer, G.-J. Foschini, and B.-Goebel, "Capacity limits of optical fiber networks," *IEEE/Optica Journal of Lightwave Technology*, vol. 28, pp. 662-701 (2010).
- [2] G. Bosco, V. Curri, A. Carena, P. Poggiolini, and F. Forghieri, "On the performance of Nyquist-WDM terabit superchannels based on PM-BPSK, PM-QPSK, PM-8QAM or PM-16QAM subcarriers," *IEEE Journal of Lightwave Technology*, vol. 29, pp. 53-61 (2011).
- [3] T. Zami, I.-F.-J Ruiz, B. Lavigne, A. Ghazisaeidi, and B. Lavigne, "Growing impact of optical filtering in future WDM networks," in *Optical Fiber Communication Conference (OFC)*, San Diego, USA, paper M1A.6 (2019).
- [4] L. Gifre, F. Paolucci, A. Aguado, R. Casellas, A. Castro, F. Cugini, P. Castoldi, L. Velasco, and V. Lopez, "Experimental assessment of in-operation spectrum defragmentation," *Springer Photonic Network Communications*, vol. 27, pp. 128-140 (2014).
- [5] Y. Terada, Y. Mori, H. Hasegawa, and K. Sato, "Highly spectral efficient networks based on grouped optical path routing," *Optica Optics Express*, vol. 24, pp. 6213-6228 (2016).

- [6] K. Kayano, S. Yamaoka, Y. Mori, H. Hasegawa, and K. Sato, "Highly dense elastic optical networks enabled by grouped routing with distance-adaptive modulation," *IEEE Photonics Technology Letters*, vol. 31, pp. 295-298 (2019).
- [7] J. M. Fàbrega, M. S. Moreolo, L. Martín, A. C. Piat, E. Riccardi, D. Roccató, N. Sambo, F. Cugini, L. Potí, S. Yan, E. Hugues-Salas, D. Simeonidou, M. Gunkel, R. Palmer, S. Fedderwitz, D. Rafique, T. Rahman, H. de Waardt, and A. Napoli, "On the filter narrowing issues in elastic optical networks," *IEEE/Optica Journal of Optical Communications and Networking*, vol. 8, no. 7, pp. A23 - A33 (2016).
- [8] F. Paolucci, F. Cugini, F. Fresi, G. Meloni, A. Giorgetti, N. Sambo, L. Potí, A. Castro, L. Velasco, and P. Castoldi, "Superfilter technique in SDN-controlled elastic optical networks [Invited]," *IEEE/Optica Journal of Optical Communications and Networking*, vol. 7, no. 2, pp. A285 – A292 (2015).
- [9] M. Ganbold, T. Yasuda, Y. Mori, H. Hasegawa, F. Inuzuka, A. Hirano, and K. Sato, "Assessment of optical node architectures for building next generation large bandwidth networks," *IEICE Transactions on Communications*, E103-B, pp. 679-689 (2020).
- [10] K. Anazawa, T. Mano, T. Inoue, A. Taniguchi, and K. Mizuno, "Reconfigurable transport networks to accommodate much more traffic demand," in *International Conference on Information Networking*, paper 361-366 (2021).
- [11] M. Jinno, "Spatial channel network (SCN): opportunities and challenges of introducing spatial bypass toward the massive SDM era," *IEEE/Optica Journal of Optical Communications and Networking*, vol. 11, pp.1-14 (2019).
- [12] M. Jinno, T. Kodama, and T. Ishikawa, "Principle, design, and prototyping of core selective switch using free-space optics for spatial channel network," *IEEE/Optica Journal of Lightwave Technology*, vol. 38, pp. 4895-4905 (2020).
- [13] C. Tremblay, F. Gagnon, B. Chatelain, E. Bernier, and M.-P. Bélanger, "Filterless optical networks: a unique and novel passive WAN network Solution," in *Optoelectronics and Communications Conference/International Conference on Integrated Optics and Optical Fiber Communication*, paper 466-467 (2007).
- [14] O. Ayoub, S. Shehata, F. Musumeci, and M. Tornatore, "Filterless and semi-filterless solutions in a metro-HAUL network architecture," in *International Conference on Transparent Optical Networks*, paper 1-4 (2018).
- [15] É. Archambault, D. O'Brien, C. Tremblay, F. Gagnon, M.-P. Bélanger, and É. Bernier, "Design and simulation of filterless optical networks: problem definition and performance evaluation," *IEEE/Optica Journal of Optical Communications and Networking*, vol. 2, pp. 496 - 501 (2010).

- [16] L. Askari, O. Ayoub, F. Musumeci, and M. Tornatore, "On dynamic service chaining in filterless optical metro-aggregation networks," *IEEE Access* 8, pp. 222233 – 222241 (2020).
- [17] S.-L. Woodward, M.-D. Feuer, and P. Palacharla, "ROADM-node architectures for reconfigurable photonic networks," *Optical Fiber Telecommunications*, I.-P. Kaminow, T.-Li, and A.-E. Willner, 6th ed. Waltham, MA, USA: Academic, Ch. 15, Sec. 2, pp. 686–696 (2013).
- [18] M. Filer, and S. Tibuleac, "N-degree ROADM architecture comparison: broadcast-and-select versus route-and-select in 120 Gb/s DP-QPSK transmission systems," in *Optical Fiber Communication Conference (OFC)*, San Diego, USA, paper Th1I.2 (2014).
- [19] T. Matsuo, R. Shiraki, Y. Mori, and H. Hasegawa, "Design and dynamic control of fiber-granular routing networks with next-generation optical paths," in *Optical Fiber Communication Conference and Exposition (OFC)*, San Diego, USA, paper W3F.6 (2022).
- [20] R. Hashimoto, S. Yamaoka, Y. Mori, H. Hasegawa, and K. Sato, "First demonstration of subsystem-modular optical cross-connect using single-module 6×6 wavelength-selective switch," *IEEE/Optica Journal of Lightwave Technology*, vol. 36, pp. 1435-1442 (2018).
- [21] Y. Hirota, "[Invited Talk] A study on Japan photonic network model and spatial division multiplexed elastic optical networks," *IEICE Technical Report*, pp. PN2019-29 (2019).

Chapter 6

Control in ultra-dense WDM networks

After network deployment, optical paths are established in response to the path setup/teardown requests. To enjoy the benefit of network design suitable for ultra-dense WDM networks, we need to develop a network-resource assignment method that effectively controls the impact of spectrum narrowing. In this chapter, we described the proposed wavelength assignment method aware of spectrum narrowing for ring topology widely used in metro-regional networks. Furthermore, we offer the path control method enabling the use of grid-less WDM, i.e., quasi-Nyquist WDM, without changing the currently deployed wavelength-routing devices.

6.1 Introduction

In optical path networks, wavelength-selective switches (WSSs) process wavelength-division-multiplexed (WDM) signals without power-consuming optical-to-electrical and electrical-to-optical conversion. Due to the rise of subscription-based streaming services and cloud-computing services, the amount of Internet traffic is exponentially increasing [1]. To cost-effectively accommodate the large amounts of expected traffic, the network capacity needs to be increased by enhancing the spectral efficiency without replacing currently deployed hardware. Setting smaller guardbands between WDM signals results in higher spectral efficiency. In such networks, however, the signal spectrum is narrowed with each WSS traversal [2-4]. Furthermore, the spectrum-narrowing effect is emphasized as the number of WSS traversals increases. Since the signal-to-noise ratio (SNR) is degraded by spectrum narrowing, employing smaller guardbands shortens the signal transmission reach.

Quasi-Nyquist WDM can minimize the idle wavelength resources in a feasible way and thus offers high spectral efficiency provided that a transmitter and receiver are connected in a point-to-point manner [5,6]. In optical path networks, however, quasi-Nyquist WDM signals suffer from severe spectrum narrowing. Furthermore, the bandwidth assigned for each quasi-Nyquist WDM signal does not match the WSS bandwidth resolution; hence, the signals cannot be processed on a path basis. Although finely tunable WSSs are available [7], installing them in networks or replacing existing ones would be impractical due to the general fact that finely tunable

WSSs are much more costly than coarsely tunable ones. The currently deployed WSSs will continue to be used for a long time since mean time between WSS failures is over 20 years [8]. In this chapter, we show that highly dense WDM networks can be realized without relying upon state-of-the-art hardware. We assume a ring topology commonly utilized in metro-regional networks in this chapter. The proposed network-control scheme can be applied to mesh networks by using the network-design scheme described in Chapter 5. In other words, the routing and wavelength assignment problem in a mesh network is reduced to wavelength assignment on ring-shaped sub-networks.

The remainder of this chapter is organized as follows. In Section 6.2, our proposed quasi-Nyquist WDM network architecture is presented. Section 6.3 evaluates its spectral efficiency through intensive computer simulations. In Section 6.4, the feasibility of the quasi-Nyquist WDM network is experimentally proven. Finally, this chapter is concluded in Section 6.5.

6.2 Proposed path control scheme for ultra-dense WDM networks

6.2.1 Path bundling

To process quasi-Nyquist WDM signals under the restriction of limited WSS-passband resolution, multiple paths are bundled and filtered as a bundle. The concept is shown in Figure 6.1, where the 33.3-GHz and 66.6-GHz channel intervals depicted are just examples. Multiple channels are bundled so as to match the aggregated bandwidth with the WSS-passband resolution. For example, three 32-Gbaud/100-Gbps DP-QPSK signals aligned with 33.3-GHz spacing are bundled into a 100-GHz bandwidth, which is a multiple of 12.5 GHz. Bundled paths need to share the same sequence of optical fibers until the bundle is physically terminated by a WSS because paths once bundled cannot be separated by WSSs. On the other hand, with path bundling, quasi-Nyquist WDM signals can be processed with widely deployed WSS hardware. Thus, we can optically process quasi-Nyquist WDM signals though the selectable routes and wavelengths in the path-setup process are restricted due to path bundling. This scheme differs from the super-channel technique. A bundle may have vacant wavelengths whereas a super channel does not. In this scheme, multiple super channels can be bundled, *e.g.*, three 32-Gbaud/400-Gbps dual-carrier DP-16QAM signals can be bundled into a 200-GHz bandwidth, which is a multiple of 12.5 GHz. Note that the frequency resolution of practical lasers is fine enough for quasi-Nyquist WDM systems; lasers with 1-MHz tuning capability are recommended by OIF for the integrable tunable laser assembly [8].

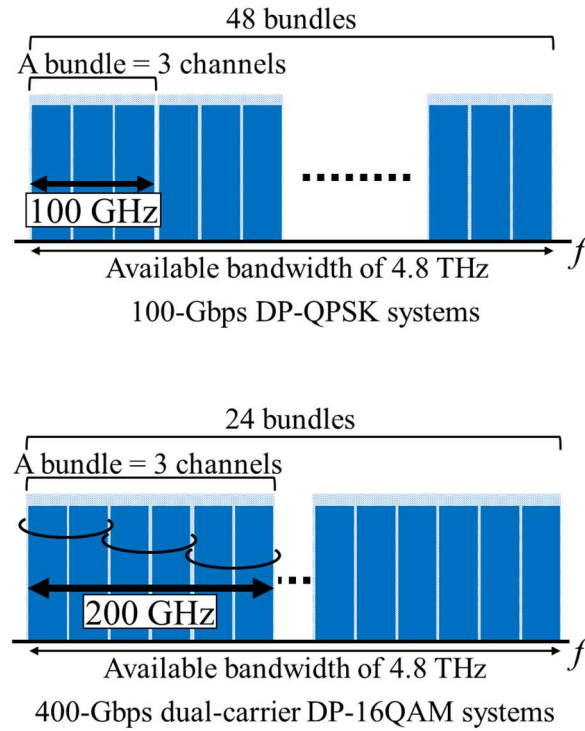


Figure 6.1 Bundling of multiple paths.

6.2.2 Wavelength assignment aware of signal-spectrum narrowing

To mitigate the impact of spectrum narrowing, we introduce a wavelength-assignment scheme that is aware of the number of spectrum-narrowing events. Since spectrum narrowing degrades signal quality as the optical path traverses each WSS, we need to control the number of spectrum-narrowing events so as not to exceed the prescribed limit. The limit is determined by the transmission characteristics, *e.g.*, transmission distance, modulation format, and WSS attenuation slope.

6.2.3 Filter-less drop operation for path bundling

As described in Section 5.3, the filter-less signal drop is beneficial for the spectrum narrowing imposing the restriction in terms of wavelength assignment to optical paths. Besides, the scheme is also effective for the bundled-path wavelength assignment shown in Section 6.2.1. The signals to be dropped are sent to the drop portion by using a splitter and detected by coherent receivers.

Here, an arbitrary wavelength signal can be extracted by a combination of coherent detection, analog filtering, and digital filtering [9]. Since the drop operation does not necessitate optical filtering, the signal can be dropped with the path granularity irrespective of the WSS-passband resolution. Consequently, paths having different destination nodes can be bundled, and the restriction imposed by path bundling is relaxed. Here, the dropped signal residual in the express port should not be terminated unless another signal is newly added to the same wavelength; the spectrum narrowing is then induced only by the adjacent-path “add” operation, and as a result the restriction due to the spectrum narrowing can also be alleviated.

6.2.4 Wavelength-assignment algorithm

Figure 6.2 shows a flowchart of the proposed wavelength-assignment algorithm for quasi-Nyquist WDM networks using widely deployed WSSs. We assume the use of B&S nodes but applying the proposed concept to the network using R&S nodes is straightforward. The procedure is detailed below;

- Step 0. Initialize parameters and load traffic demands.
 - Set the limit number of spectrum-narrowing events.
 - Set the initial target frequency slot number to 1.
 - Set the initial target fiber number to 1.
 - Load a set of traffic demands.
- Step 1. Bundle optical paths.
 - Bundle optical paths in the following priority.
 - Optical paths having the same source and destination nodes.
 - Optical paths having the same source node.
- Step 2. Make a priority list.
 - Make a list that defines the order of assigning bundles as follows.
 - A bundle that shares the same source and destination nodes with the already-assigned adjacent-frequency bundle.
 - A bundle that shares the same source node and more nodes with the already-assigned adjacent-frequency bundle.
 - A bundle that shares more nodes with the already-assigned adjacent-frequency bundle.
- Step 3. Find a valid bundle.
 - Assign the bundle tentatively in accordance with the priority list and count the number of spectrum-narrowing events of paths in all bundles involved.
 - Iterate the above procedure until a valid bundle is found. The number of spectrum-

narrowing events must be less than or equal to the limit number defined in Step 0.

Step 4. Does a valid bundle exist?

Decide whether a valid bundle exists.

Step 4.5. Increase the target frequency slot number or fiber number.

Increase the target frequency slot number. If the frequency number is invalid, increase the target fiber number and set the target frequency slot number to 1. If the fiber number is invalid, install new fibers.

Step 5. Assign the bundle.

Assign the bundle definitively to the given frequency slot and fiber.

Step 6. Does an unassigned bundle exist?

Decide whether an unassigned bundle exists.

In Step 0, the limit number of spectrum-narrowing events is determined by transmission simulations or experiments. Step 1 allows currently deployed WSSs to process quasi-Nyquist WDM signals; signals in a bundle are free from intra-bundle spectrum narrowing. Step 2, Step 3, and Step 4 jointly suppress the number of inter-bundle spectrum-narrowing events. Step 6 detects whether all of the traffic demands have been successfully accommodated in the network or not.

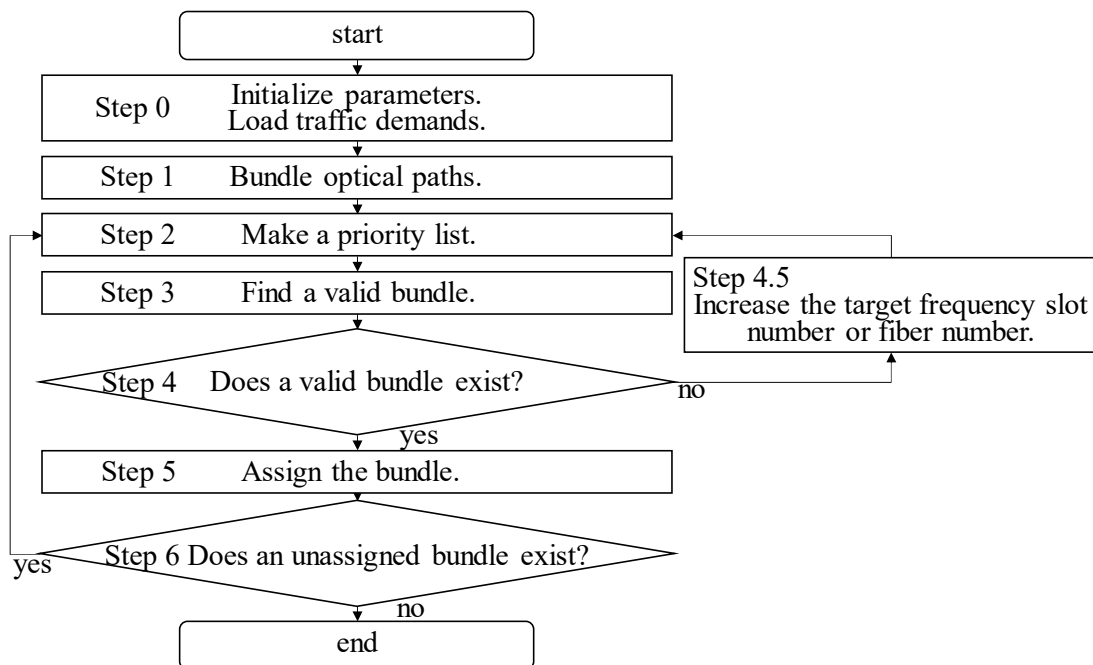


Figure 6.2 Flowchart of the proposed wavelength-assignment algorithm.

6.3 Simulations

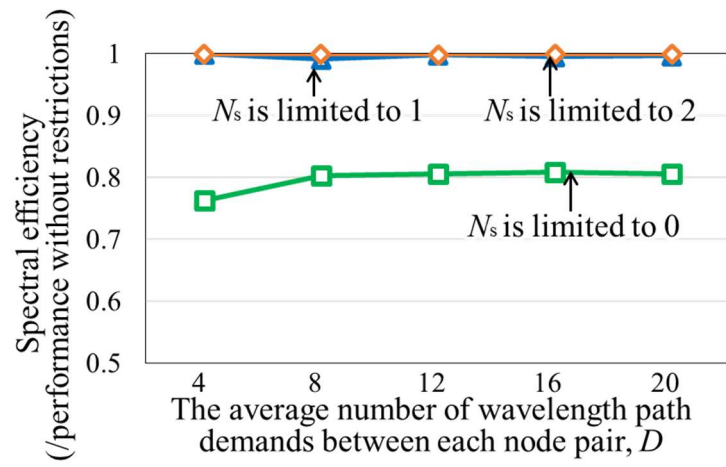
To evaluate the spectral efficiency of quasi-Nyquist WDM networks, we execute computer simulations of network design scenarios; networks are built from scratch to accommodate the given traffic-demand set (i.e. traffic matrix) with the minimum number of fibers. Then, the resulting improvement in spectral efficiency is evaluated. The physical topology tested is an 18-node ring network. Each link comprises 100-km single-core single-mode fiber/s, which is consistent with the experimental assessments in Section 6.4. The frequency bandwidth of a fiber is 4.8 THz. All optical channels are assumed to be 32-Gbaud/400-Gbps dual-carrier DP-16QAM signals and path demands are given in this channel granularity through traffic/service aggregation in the electrical layer. The average number of path demands between each node pair, D_{static} , is changed from 4 to 20. A set of path demands are created based on the given traffic matrix that defines the number of traffic demands between each node pair. Two traffic-distribution patterns are examined. One is that the traffic demands are uniformly distributed. The other is that the traffic demands are distributed non-uniformly and one selected node has 5 times traffic larger than the other nodes. In both cases, the total number of traffic demands is same when the average number of traffic demands between each node pair is same. For example, the average number of fibers of each link is around 7 when D_{static} is 12. The maximum number of spectrum-narrowing events triggered by adjacent paths, N_s , is controlled. Table 6.1 compares the networking schemes examined. Scheme A corresponds to typical networks in which sufficient guardbands are inserted and thus the impact of spectrum narrowing is negligible. Scheme B enables denser WDM than Scheme A. Scheme C is quasi-Nyquist WDM system attaining the highest spectral efficiency in return for the wavelength-assignment restrictions due to the signal-spectrum narrowing and the WSS-passband resolution.

Table 6.1 Comparison of networking schemes.

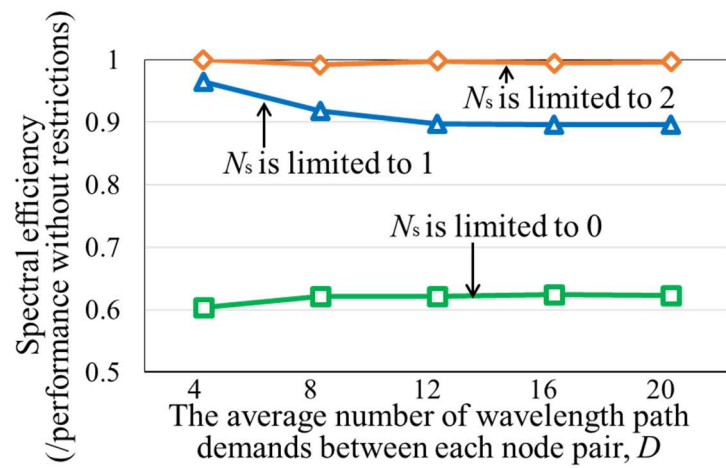
| Configurations | Scheme A (Typical network) | Scheme B | Scheme C (Proposed network) |
|---|-------------------------------|----------|-------------------------------------|
| Assigned bandwidth for 400-Gbps signals | 87.5 GHz | 75 GHz | 66.6 GHz |
| Channel bandwidth and WSS-passband resolution | Matched | Matched | Mismatched (3 paths are bundled) |
| Impact of spectrum narrowing | Negligible | Severe | Extremely severe |

First, we analyze wavelength-assignment inflexibility in quasi-Nyquist WDM networks by means

of spectral efficiency. The baseline is the spectral efficiency obtained with the ideal WSSs that have rectangular passbands and full frequency-setting flexibility. Figure 6.3 shows the spectral-efficiency penalty induced by limiting the number of spectrum-narrowing events, N_s , where we assume that spectrum narrowing is triggered (a) by adjacent-path add operation, *i.e.*, B&S nodes and (b) by adjacent-path add-drop operation, *i.e.*, R&S nodes. If N_s is limited to 2, the penalty is marginal in both cases; it is less than 0.2% when D is 20. When N_s is limited to 1, the impact of spectrum narrowing can be suppressed in the case of (a); in contrast, the penalty is over 10% if condition (b) is applied. In this way, thanks to the use of our impairment-aware wavelength assignment, the restriction caused by spectrum narrowing can be mitigated without any notable penalty in spectral efficiency even if the allowable number of spectrum-narrowing events is just 1 for the network using B&S nodes. If no adjacent filtering operation is permitted, the penalty is excessive in both cases and our method is of no avail.



(a) By the adjacent-path add operation



(b) By the adjacent-path add-drop operation

Figure 6.3 Spectral-efficiency degradation due to spectrum narrowing.

Figure 6.4 shows the spectral-efficiency penalty due to path bundling when the add/drop operation is performed (a) on a bundle/path basis i.e. B&S nodes and (b) on a bundle/bundle basis i.e. R&S nodes. In both cases, the penalty decreases as the number of traffic demands increases because path bundling is facilitated by increasing the number of traffic demands between node pairs. When D is 20, the penalty is less than 0.7% in case of (a); however, applying (b) results in a penalty of 4.7%.

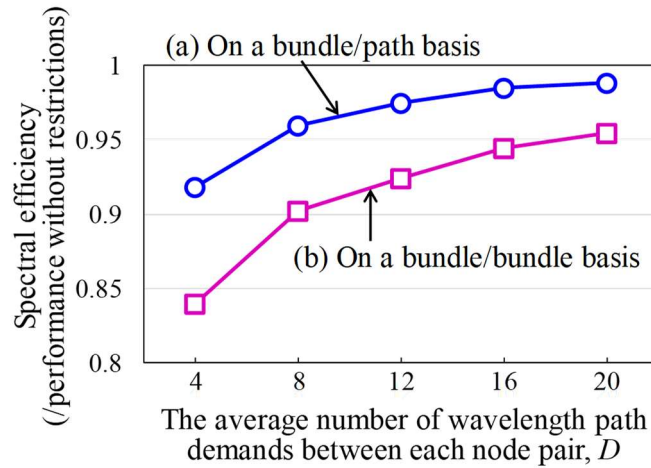
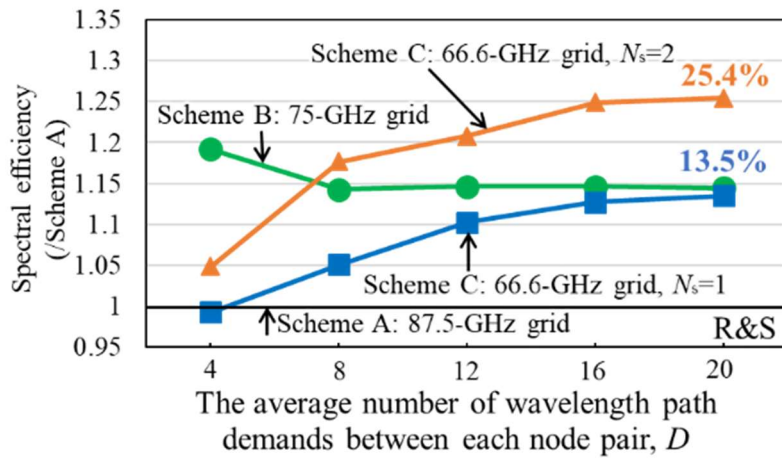
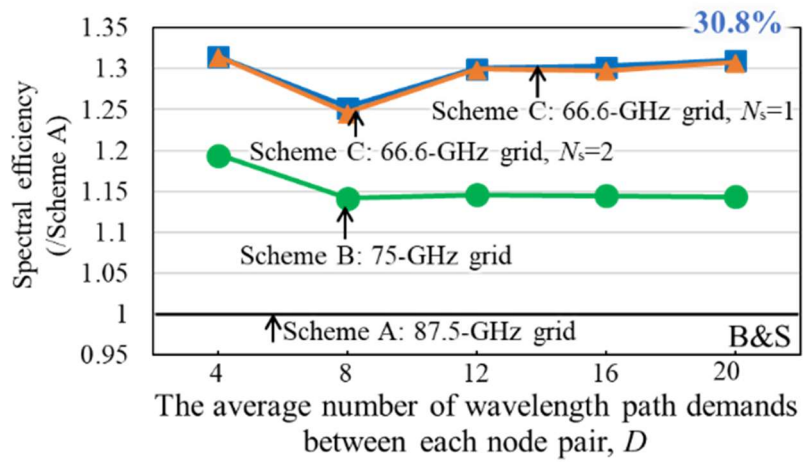


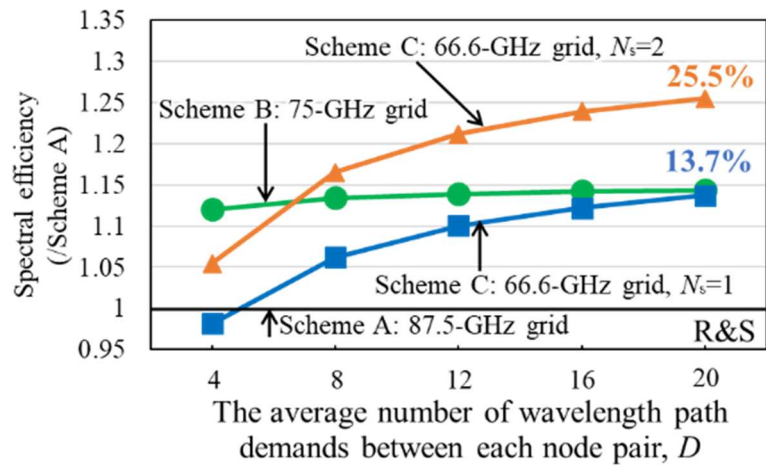
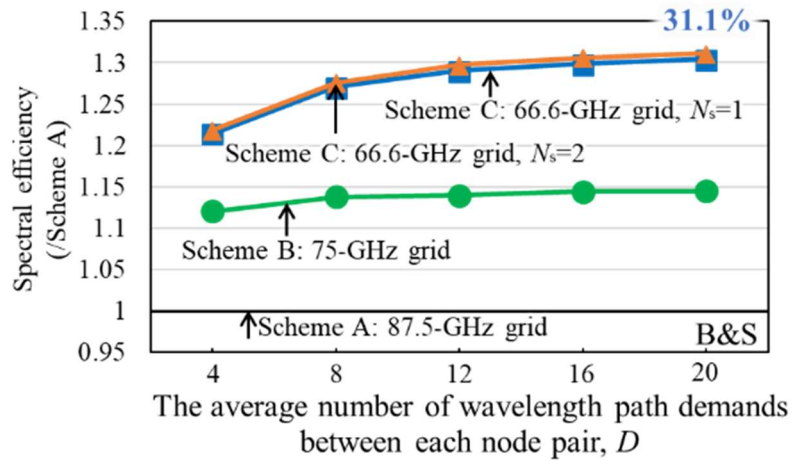
Figure 6.4 Spectral-efficiency degradation due to path bundling.

Finally, we evaluate the improvement in the spectral efficiency of quasi-Nyquist WDM networks. Figure 6.5 and Figure 6.6 plot the spectral efficiency where the results are normalized by the counterparts of Scheme A shown in Table 6.1. The B&S node architecture outperforms the R&S node architecture for the same N_s . In the uniform-traffic scenario, when B&S nodes are utilized and $N_s = 0$, the improvement in spectral efficiency is 4.8% compared to Scheme A. In this case, Scheme C is not spectrally efficient compared to Scheme B whose spectral-efficiency improvement is 14.2%. Furthermore, Scheme C always yields shorter transmission distances than Scheme B due to its worse spectrum narrowing and larger cross-phase modulation. A similar argument is valid when R&S nodes are utilized and $N_s \leq 1$. Consequently, Scheme C requires N_s to be larger than or equal to 1 for B&S-node-based networks and 2 for R&S-node-based networks so as to attain high spectral efficiency. When $D = 20$, the improvement in the B&S node network is 30.8% with $N_s = 1$; in the R&S node network, an improvement of 25.3% is observed if $N_s = 2$. We also observe the similar results for the centralized traffic distribution; the improvement in the B&S node network is 30.1% with $N_s = 1$ and that in the R&S node network is 25.4% if $N_s = 2$. In this way, the traffic distribution has virtually no impact on spectral efficiency in the large-traffic situations.



Traffic distribution is uniform

Figure 6.5 Spectral efficiency as a function of traffic intensity, where the traffic distribution is uniform.



Traffic distribution is centralized at one node

Figure 6.6 Spectral efficiency as a function of traffic intensity, where the traffic distribution is centralized.

6.4 Transmission experiments

We conducted transmission experiments to confirm the feasibility of the proposed network architecture. The experimental configuration is depicted in Figure 6.7. The 4.8-THz bandwidth between 191.32500 THz and 196.12500 THz was fully utilized. At the transmitter side, six continuous waves (CWs) consecutively aligned in the frequency domain were generated by six independent tunable lasers (TLs). The frequencies were set at 193.54167-193.70833 THz with 33.3-GHz spacing. To create three 32-Gbaud/400-Gbps dual-carrier DP-16QAM signals, the CWs were modulated by a lithium-niobate IQ modulator (IQM) driven by a two-channel arbitrary-waveform generator (AWG) with eight-bit resolution; the electrical-signal spectrum was formed by a root-raised cosine filter with a roll-off factor of 0.01. Then, polarization-division multiplexing (PDM) was emulated by a polarization-beam splitter (PBS), 10-ns delay fiber, and polarization-beam combiner (PBC). On the other hand, 48 CWs aligned with 100-GHz spacing were generated from 48 TLs and combined in an optical coupler. CW intensity was modulated by a lithium-niobate intensity modulator (IM) driven by a 33.3-GHz cosine wave generated from a synthesizer; the IM bias was set to yield the carrier-residual condition. This yielded 144 CWs aligned with 33.3-GHz spacing. Next, 72-channel 400-Gbps dual-carrier DP-16QAM signals were created by an IQM and a PDM emulator. The target bundle consisting of three 400-Gbps dual-carrier DP-16QAM signals was added to the network by a WSS and multiplexed with the other wavelength signals, where the non-target signals having the same frequency with the added bundle were terminated by the WSS. The resulting 72-channel 400-Gbps dual-carrier DP-16QAM signals were aligned with 66.6-GHz spacing over the 4.8-THz bandwidth. After passing through an erbium-doped fiber amplifier (EDFA), the signals entered the link consisting of a 100-km standard single-mode fiber (SMF). The loss coefficient, dispersion parameter, and nonlinearity coefficient of the SMF were 0.18 dB/km, 16.5 ps/nm/km, and 1.5 /W/km, respectively. The noise figure of the EDFA was around 5 dB. The signals were amplified by an EDFA and delivered to the next node. Each node comprised a 1×9 splitter and 9×1 WSS in the B&S arrangement or a 1×9 WSS and 9×1 WSS in the R&S arrangement. The loss of each node was around 18 dB for the B&S architecture and 17 dB for the R&S architecture. The bandwidth resolution of the WSS was 12.5 GHz. After passing through two nodes, the signals were inserted into a recirculating fiber loop that comprised two synchronous loop-controlling switches (SW), a 2×2 splitter, a 100-km SMF, an EDFA, and a node. Here, the excess loss of 3.5 dB due to the loop-controlling switch and the 2×2 splitter was pre-compensated by the preceding EDFA so as to avoid excess signal-to-noise ratio (SNR) degradation. After multiple loops, the target signal was dropped and detected by a digital coherent receiver; here, the signal on 193.70833 THz was evaluated because both cross-phase modulation and spectrum narrowing were worst at this frequency. The detected signal was sampled at 50 Gsample/s by a four-channel analog-to-digital converter with eight-bit

resolution. The digitized data was processed by a digital-signal-processing (DSP) circuit. The DSP circuit performs chromatic dispersion compensation, polarization division demultiplexing, phase and frequency estimation, and symbol decoding [10]. The clock recovery was performed based on adaptive filtering [11]. In our scheme, spectrum narrowing is induced at only one side of each signal spectrum because of path bundling and hence the clock can be extracted even if the single-side filtering is too tight. The target bit-error ratio (BER) was 2.7×10^{-2} as we assumed the use of forward error correction (FEC) [12]. The maximum number of spectrum-narrowing events triggered by adjacent paths, N_s , was controlled as follows. If the given WSS imposes spectrum narrowing on the target signal, we set the passband of WSS port #1 to 200 GHz and that of WSS port #2 to residual 4,600 GHz. Port #1 was used for the target bundle while port #2 was used for the non-target bundles. The 200-GHz passband causes spectrum narrowing at the edge channels of the target bundle. Here, the symbol timing skew between port #1 and port #2 was shifted with each WSS traversal. If the given WSS does not impose spectrum narrowing on the target signal, we set the passband of WSS port #1 to 4,800 GHz and no passband is assigned to the other WSS ports. Considering the worst case, spectrum narrowing was caused at the node/s closest to the source node when N_s was limited.

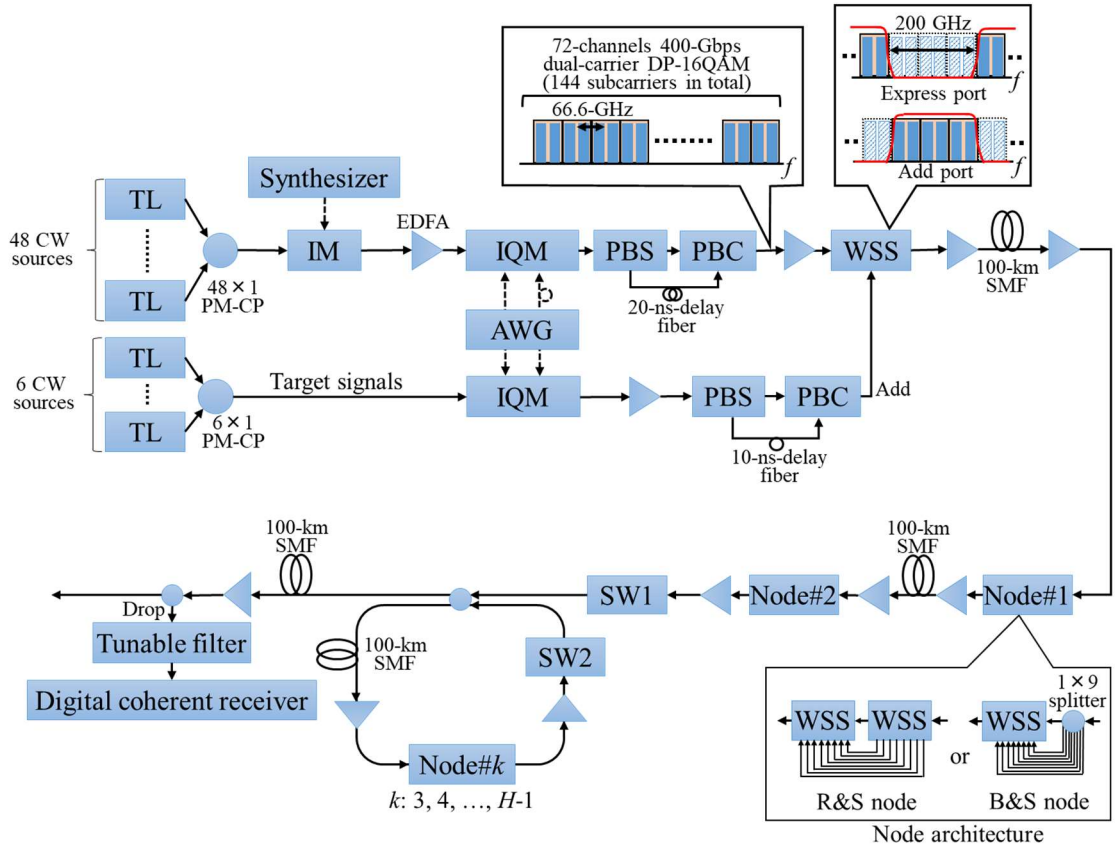


Figure 6.7 Experimental setup.

Figure 6.8 plots the BER characteristics as a function of transmission distance measured for each node architecture. The maximum transmittable distances are summarized in Table 6.2. Note that spectrum narrowing could occur at each traversed node, *i.e.*, the possible N_s is equal to $H - 1$ for the B&S nodes and $2(H - 1)$ for the R&S nodes, where H is the hop count. In addition, B&S node networks suffer from spectrum narrowing at the source node whereas R&S node networks suffer at the source and destination nodes. Without limiting N_s , the transmission distance is severely bounded since the signals are impaired with each WSS traversal. The transmission distances with B&S nodes and R&S nodes were 400 km and 200 km, respectively. The use of small N_s suppresses the signal degradation induced by the spectrum narrowing and extends the maximum transmission distance. When N_s is 2/1/0, the transmission distances in B&S node networks are 600/900/900 km whereas those in R&S node networks are 500/900/1000 km. In both cases, N_s needs to be less than or equal to 1 for the longest path for the network examined in Section 3.4. Note that in general the required N_s depends on transmission characteristics such as transmission distance and hop count of each path. Here, the simulation results show that the improvements in spectral efficiency reach 30.8% for the B&S node network

and 13.4% for the R&S node network when $N_s = 1$. Thus, the network using R&S nodes cannot enjoy the benefits of quasi-Nyquist WDM. The B&S node networks in conjunction with our restriction-aware wavelength-assignment algorithm can realize truly efficient quasi-Nyquist WDM networks without replacing currently deployed WSSs. The obtained spectral-efficiency improvement, 30.8%, is quite close to the theoretical limit of 31.3%.

It should be noted that the allowable number of spectrum-narrowing events can be increased and the number of channels to be bundled would be changed if WSSs with finer frequency resolution and better filtering characteristic become cost-effective in the future. These attributes also facilitate the realization of quasi-Nyquist WDM networks.

Table 6.2 Transmittable distance for 400-Gbps signals

| Node architecture | The maximum number of spectrum-narrowing events, N_s | | | |
|-------------------|--|--------|--------|----------|
| | The maximum value | 2 | 1 | 0 |
| B&S | 400 km | 600 km | 900 km | 900 km |
| R&S | 200 km | 500 km | 900 km | 1,000 km |

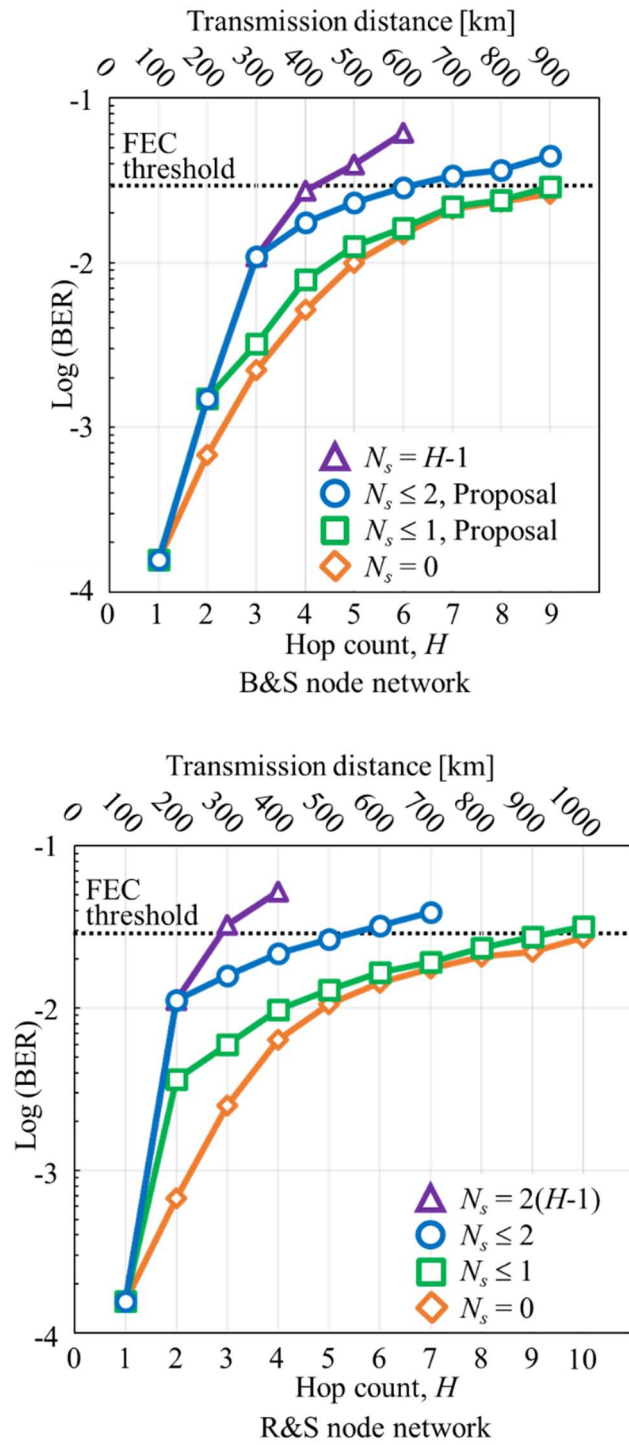


Figure 6.8 BER characteristics for 400-Gbps signals.

6.5 Conclusion

In this chapter, a highly efficient quasi-Nyquist WDM network architecture that allows us to utilize widely deployed WSSs is demonstrated. The proposed wavelength-assignment algorithm can suppress the impact of restrictions imposed by the limited bandwidth granularity of WSS passbands and the significant spectrum narrowing occasioned by WSS traversal. Intensive network analyses based on computer simulations showed that our network architecture improves the spectral efficiency of 32-Gbaud/400-Gbps DP-16QAM networks by 30.8%. To confirm the feasibility of the proposed architecture, we conducted transmission experiments on 72-channel 400-Gbps dual-carrier DP-16QAM signals aligned with 66.6-GHz spacing in the full C-band. The fiber capacity reached 28.8 Tbps even after 900-km transmission and 9 node hops. Note that our proposed scheme can be applied to core mesh networks by using DP-QPSK signals, as they are much more tolerant of transmission impairments.

References

- [1] Cisco Visual Networking Index (VNI) White paper, “Forecast and methodology, 2017–2022,” (2019).
- [2] T. Zami, I. F. de J. Ruiz, B. Lavigne, and A. Ghazisaeidi, “Growing impact of optical filtering in future WDM networks,” in Optical Fiber Communication Conference (OFC), San Diego, USA, paper M1A.6 (2019).
- [3] M. Filer, and S. Tibuleac, “N-degree ROADM architecture comparison: broadcast-and-select versus route-and-select in 120 Gb/s DP-QPSK transmission systems,” in Optical Fiber Communication Conference (OFC), San Diego, paper Th1I.2 (2014).
- [4] C. Pulikkaseril, L. Stewart, M. A. F. Roelens, G. Baxter, S. Poole, and S. Frisken, “Spectral modeling of channel band shapes in wavelength selective switches,” *Optica Optics Express*, vol. 19, no. 9, pp. 8458-8470 (2011).
- [5] S. Kilmurray, T. Fehenberger, P. Bayvel, and Ri Killey, “Comparison of the nonlinear transmission performance of quasi-Nyquist WDM and reduced guard interval OFDM,” *Optica Optics Express*, vol. 20, no. 4, pp. 4198-4205 (2012).
- [6] G. Bosco, V. Curri, A. Carena, P. Poggiolini, and F. Forghieri, “On the performance of Nyquist-WDM terabit superchannels based on PM-BPSK, PM-QPSK, PM-8QAM or PM-16QAM subcarriers,” *IEEE Journal of Lightwave Technology*, vol. 29, pp. 53-61 (2011).

- [7] D. Sinefeld, S. Shalva Ben-Ezra, and D. M. Marom, "Nyquist-WDM filter shaping with a high-resolution colorless photonic spectral processor," *Optica Optics Letters*, vol. 38, no. 17, pp. 3268-3271 (2013).
- [8] Optical Internetworking Forum, "Technology options for 400G implementation," OIF-Tech-Options-400G-01.0 (2015).
- [9] K. Kikuchi, "Fundamentals of coherent optical fiber communications," *IEEE/Optica Journal of Lightwave Technology*, vol. 34, no. 1, pp. 157-179 (2016).
- [10] Y. Mori, C. Zhang, and K. Kikuchi, "Novel configuration of finite-impulse-response filters tolerant to carrier-phase fluctuations in digital coherent optical receivers for higher-order quadrature amplitude modulation signals," *Optica Optics Express*, vol. 20, no. 24, pp. 26236-26251 (2012).
- [11] K. Kikuchi, "Clock recovering characteristics of adaptive finite-impulse-response filters in digital coherent optical receivers," *Optica Optics Express*, vol. 19, no. 6, pp. 5611-5619 (2011).
- [12] D. Chang, F. Yu, Z. Xiao, N. Stojanovic, F. Hauske, Y. Cai, C. Xie, L. Li, X. Xu, and Q. Xiong, "LDPC convolutional codes using layered decoding algorithm for high speed coherent optical transmission," in *Optical Fiber Communication Conference (OFC)*, Los Angeles, USA, paper OW1H.4 (2012).

Chapter 7

Integration

In Chapter 4, 5, and 6, we have proposed three technologies realizing the ultra-dense WDM networks. In this chapter, we discuss and evaluate the integration system of three technologies. Since each technology does not hinder the performance of other technologies, the extremely high spectral efficiency can be obtained by collaborating all technologies. In Section 7.1, the RNN-based demodulation framework assuming impairment-aware path control is discussed. Section 7.2 describes the proposed network design. In Section 7.3, we evaluate the dynamic path control in ultra-dense WDM networks considering all technologies. Finally, this chapter is concluded in Section 7.4.

7.1 ML-based DSP assuming impairment-aware wavelength assignment

In Section 6.2.2, we introduced a wavelength-assignment scheme that is aware of the number of spectrum-narrowing events to mitigate the impact of spectrum narrowing. In this way, we control the number of spectrum-narrowing events so as not to exceed the prescribed limitation. Since the limitation depends on the demodulation framework, we apply the RNN-based demodulation framework described in Chapter 4.

We evaluate the performance of the RNN-based demodulation framework. Figure 7.1 depicts the simulation setup. The modulator creates a 32-Gbaud DP-16QAM signal. The spectrum is shaped by a root-raised cosine filter whose roll-off factor is 0.01. The linewidth of the transmitter laser is 100 kHz. The target signal is added to the network via a WSS and combined with two non-target signals whose frequencies are adjacent to that of the target signal. The channel spacing of the WDM signals is set to 37.5 GHz to evaluate the spectrum narrowing effect in ultra-dense WDM networks.

The maximum number of spectrum-narrowing events triggered by adjacent paths, N_s , is controlled. Spectrum narrowing occurs when a signal traverses the former N_s nodes. Note that spectrum narrowing was caused at the node/s closest to the source node considering the worst case. At the

node causing spectrum narrowing, the WSS filter is created by convoluting two filter functions, where a rectangular function with 37.5-GHz bandwidth and a Gaussian function with 7-GHz 3-dB bandwidth are used. The port isolation of the WSS is set to 40 dB. After power compensation with an EDFA, the signals are launched into a 100-km single-mode fiber (SMF). Here, the noise figure of the EDFA is set to 5 dB. We assumed the Kerr effect as fiber nonlinearity, it is characterized by the widely used Manakov model. The loss coefficient, chromatic-dispersion parameter, and nonlinear coefficient of the SMF are, respectively, 0.2 dB/km, 16 ps/nm/km, and 1.5 /W/km. The transmission performance is calculated by the typical split-step Fourier method. We assume widely deployed 8×8-port optical nodes, where the broadcast-and-select (B&S) and route-and-select (R&S) architectures are evaluated. Each B&S node and R&S node have one and two spectrum-narrowing events, respectively. After the signal passes through multiple nodes, the target signal is dropped by a splitter in the B&S node structure or by a WSS in the R&S node structure. Next, the target signal is coherently detected by an optical receiver. The linewidth of local oscillator is 100 kHz. In the DSP circuit within the receiver, chromatic dispersion is countered by a non-adaptive filter. Then, the adaptive filter with 64 delayed taps conducts polarization recovery and signal-spectrum reshaping. Then, the carrier phase and frequency offset are estimated. Finally, the signal is recovered by the bi-RNN model. The model is trained by using 480,000 symbols and tested by 120,000 symbols. We used the pseudorandom number generator called Mersenne Twister. The BER threshold of forward error correction is set to 0.01.

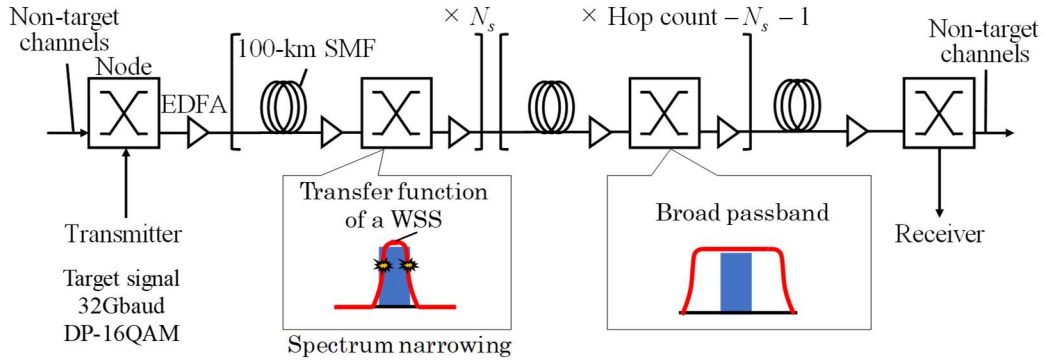


Figure 7.1 Simulation setup.

We verify the effectiveness of our RNN-based demodulation framework. The typical symbol decision based on the Euclidean distance is also evaluated as a reference. The RNN parameters of k , N_{layer} , and N_{neuron} are set to 32, 2, and 32, respectively. Both the R&S node and the B&S node are examined, with the filter function described in section III.A. We use the RNN model whose

output layer is based on regression. Figure 7.2 and Figure 7.3 show BER as a function of transmission distance and hop count for ultra-dense WDM networks and quasi-Nyquist WDM networks, respectively. We observe that the maximum transmissible reach is extended in both cases compared to the reference scheme. Since the RNN-based demodulation method enhances the performance of demodulation, we can also apply the lower-cost FEC. Our scheme extends the acceptable node-hop count and transmissible distance in conjunction with the RWA/RSA algorithm that is aware of system impairments as shown in the following sections.

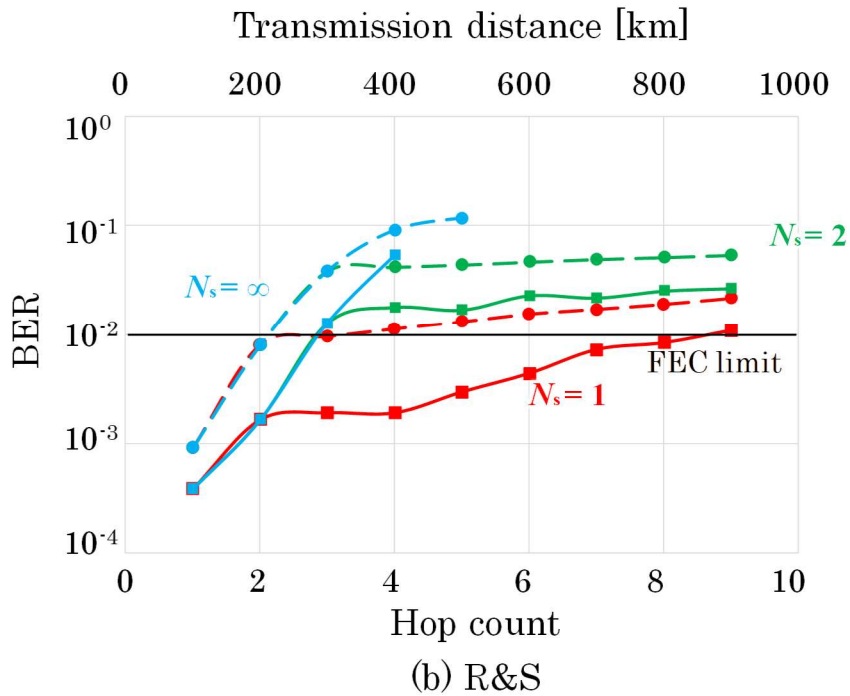
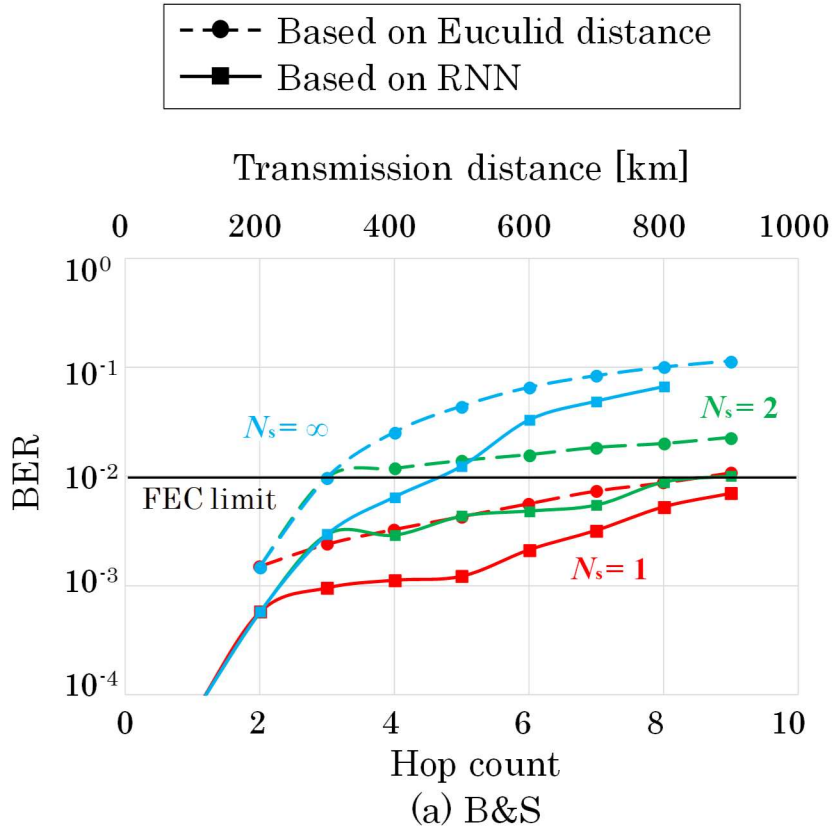


Figure 7.2 BER vs. transmission distance for ultra-dense WDM networks.

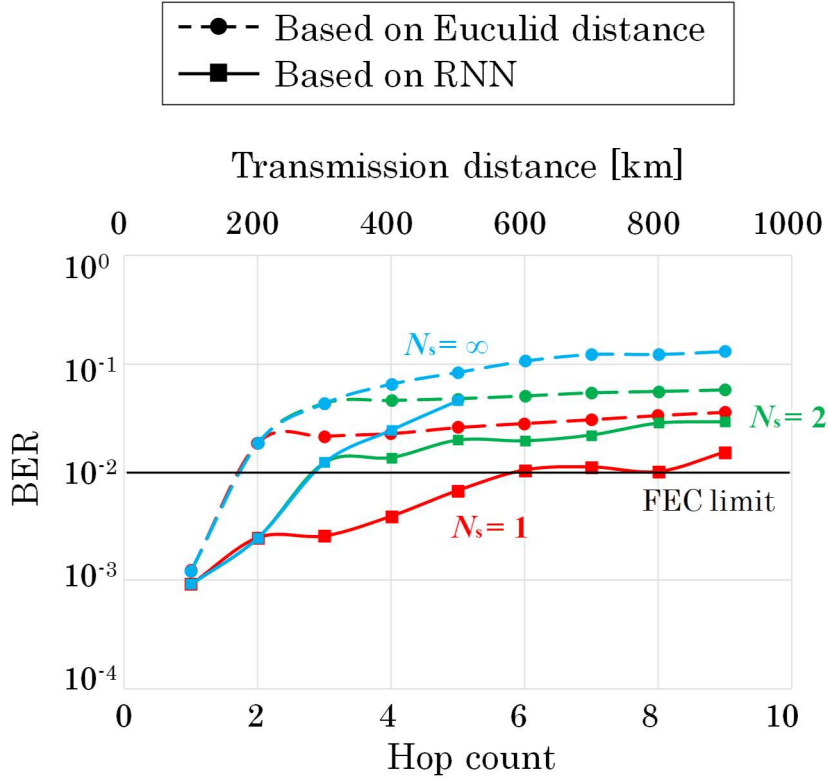


Figure 7.3 BER vs. transmission distance for quasi-Nyquist WDM networks.

7.2 Network design based on sub-networks

To introduce the ultra-dense WDM into mesh networks, the impact of spectrum narrowing should be mitigated by applying network design method based on sub-networks. The ILP-based sub-network design scheme detailed in Chapter 5 can be straightforwardly integrated with the other technologies. In the following evaluations, the sub-network discussed in Chapter 5 are utilized.

7.3 Dynamic path control in ultra-dense WDM networks

We evaluate the validity of the integrated networks in dynamic path operation scenarios. The transmission in the 4.8 THz bandwidth range is assumed. We examined several metro-scale networks: a 3×3 regular-mesh network, 2×6 regular-mesh network, US-metro Verizon network, and Kanto network. Each path comprises a 100-Gbps 32-Gbaud DP-QPSK signal. The maximum number of paths accommodated per fiber, \mathcal{W} , is 96 (50-GHz spacing) or 128 (37.5-GHz spacing) for the conventional DWDM network and the ultra-dense WDM network, respectively. In ultra-

dense WDM networks, the allowable number of spectrum-narrowing events induced by adjacent-path add operation, N_s , is set to 1 considering adequate transmission distances. The fiber arrangement is yielded by ILP; the traffic intensity for the network design, D_{static} , is selected so that the traffic volume exceeds the fiber capacity on several links, *i.e.*, multiple fibers will be laid on these links. The effectiveness of our proposal is evaluated for several $D_{dynamic}$ values drawn from $[0, D_{static}]$, where $D_{dynamic}$ is the traffic intensity for dynamic path demands, and $[\cdot, \cdot]$ stands for the closed interval. Path requests are generated in accordance with a Poisson process and the holding time of each connection follows a negative exponential distribution. The blocking ratio is calculated by the path setup requests whose number exceeds 900,000; this offers virtually average performance. The route selection corresponds to the selection of a sub-network in the network architecture described in Chapter 5. First, we select one of the sub-networks based on the k -shortest path algorithm. Then, the wavelength-assignment algorithm aware of the number of spectrum narrowing events as shown in Section 6.2.4 is applied in the selected sub-network. In the conventional scheme, a route is selected based on the k -shortest path algorithm and a wavelength is selected in a first-fit manner. Different from the proposal, the express routing can be done on a wavelength basis. As sufficient guardbands are inserted between channels, we do not impose any routing restriction due to spectrum narrowing, *i.e.*, $N_s = \infty$. For 37.5-GHz spacing ultra-dense WDM, in addition to the spectrum narrowing condition of $N_s = 1$, an alternative configuration with $N_s = \infty$ is evaluated to find the upper limit of the performance and to elucidate the deterioration caused by the limitations imposed on adjacent-path add operations.

Figure 7.4 shows the blocking-ratio variation as a function of the number of path requests; the specific value of D_{static} for each topology is shown as example. In each network, the accommodation efficiency is not significantly penalized compared to $N_s = \infty$; that is, the impact of spectrum narrowing is almost negligible thanks to the spectrum-narrowing-aware dynamic path control method. We evaluated the proposal using other D_{static} values; however, we did not observe notable sensitivity to D_{static} . Regarding topology sensitivity, the magnitude of the improvement decreases in networks whose graph diameter is large because the spectrum narrowing condition worsens. Since the selectivity of route and wavelength is penalized by fiber-granular routing, several paths need to be circumvented; however, the gain from denser path accommodation can overwhelm this penalty. As a result, the ultra-dense WDM enhances the network capacity by up to 31.0% compared to the conventional DWDM networks.

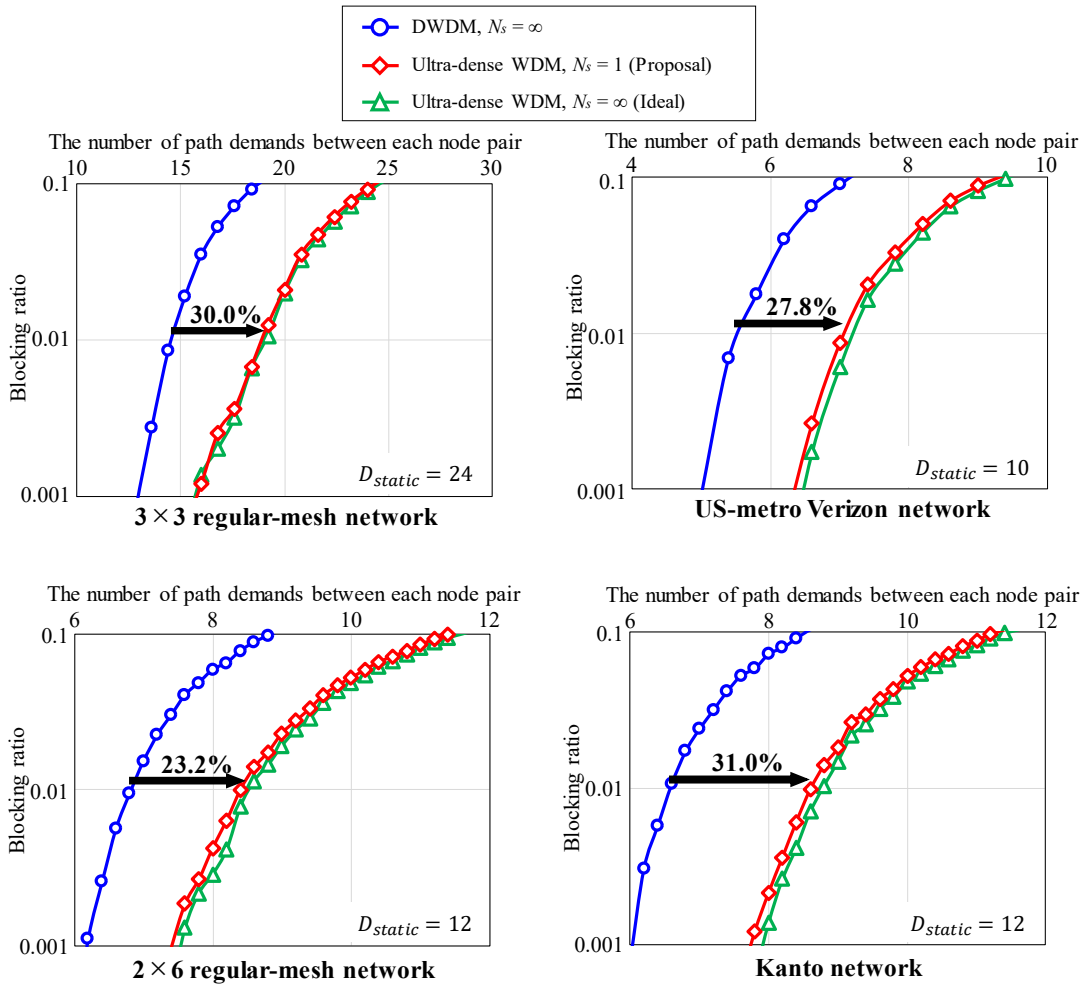


Figure 7.4 Blocking-ratio variations.

7.4 Conclusion

In this chapter, we elucidated the effectiveness of the proposed ultra-dense WDM network realized by the integration of three technologies. A highly efficient WDM network architecture allows us to utilize widely deployed WSSs. Intensive network analyses based on computer simulations showed that our network architecture improves the spectral efficiency of 100-Gbps networks by 31.0%.

Chapter 8

Conclusion

Throughout the investigations presented in the dissertation, network capacity enhancement is shown to provide a means for creating future bandwidth abundant communication networks. In Chapter 1, we showed the background of optical fiber communications network. In Chapter 2, the fundamentals of optical path network were provided. Chapter 3 described the pros and cons of ultra-dense WDM network. In Chapter 4, Chapter 5, and Chapter 6, the proposed methods were detailed and evaluated. In Chapter 4, we clarified the receiver-side DSP can mitigate the impact of signal impairments. By using a bidirectional RNN to learn the signal deterioration pattern, signal can be appropriately demodulated even for the low-quality signals. The proposal has improved the robustness against spectral narrowing and succeeded in expanding the application range of ultra-dense WDM. In Chapter 5, we proposed a network architecture and its design scheme. In the proposal, both the wavelength-granular routing and the waveband-granular routing are cooperated to minimize the effect of spectral narrowing while enabling an appropriate routing flexibility. By formulating the conditions based on ILP, the optimum configurations for optical cross-connect can be obtained. As a result, ultra-dense WDM can be applied even in mesh network topologies that would be strongly affected by spectral narrowing. Chapter 6, we proposed a path-control algorithm that minimizes the probability of spectrum narrowing caused in ultra-dense WDM networks. In this way, the maximum number of spectrum-narrowing events for each path is controlled. The effectiveness of the proposed ultra-dense WDM networks is verified thorough network simulations and transmission experiments. By integrating these three schemes as described in Chapter 7, the impact of signal impairments can be mitigated and controlled, enabling a truly efficient ultra-dense WDM network architecture. Since the proposed method can be implemented with only a slight change in the DSP circuit, the introduction of the proposed method to commercial systems can be expected to installed at an early stage. There is little room for improving spectral-efficiency by reducing guardbands. To further enhance the network capacity, we need to integrate the proposal with the other methods such as space-division multiplexing using multi-core fibers and higher-order modulation formats.

Acknowledgement

The completion of this dissertation could not have been possible without the kind support and help of many people. I would like to extend my sincere thanks to all of them.

First and foremost, I would like to express my deepest gratitude to my academic supervisor, professor Hiroshi Hasegawa and associate professor Yojiro Mori, who gave me their great guidance, invaluable advices, and support over the past six years. I would also like to offer my special thanks to professor emeritus Ken-ichi Sato. Without their instructions and caring, this dissertation would not have been possible.

I would also like to thank my colleagues in Hasegawa laboratory and Ms. Kurata for their kind support and sharing for both my academic and personal life in Nagoya; they helped me to their best and provided me with comfortable and friendly environment.

Last but not least, I am greatly thankful to my parents for always supporting me and paving the way for my achievements. I cannot thank enough all the people who helped me with their valuable assistance during my study in Nagoya University.

List of Publications

Journals

- [1] Ryuta Shiraki, Yojiro Mori, Hiroshi Hasegawa, “RNN-based demodulation framework for spectrum narrowing in ultra-dense WDM networks,” *IEEE Photonics Technology Letters*, Vol. 34, Issue 18, pp. 993-996, August 2022.
- [2] Ryuta Shiraki, Yojiro Mori, Hiroshi Hasegawa, Ken-ichi Sato, Paolo Monti, “Design and control of highly spectrally efficient photonic networks enabled by fiber-granular routing on overlaid ring-shaped topologies,” *IEEE/OSA Journal of Optical Communications and Networking*, Vol. 13, Issue 11, pp. 233-243, November 2021.
- [3] Yojiro Mori, Eiji Honda, Ryuta Shiraki, Keijiro Suzuki, Hiroyuki Matsuura, Hitoshi Kawashima, Shu Namiki, Kazuhiro Ikeda, Ken-ichi Sato, “Wavelength-division demultiplexing enhanced by silicon-photonic tunable filters in ultra-wideband optical-path network,” *IEEE/OSA Journal of Lightwave Technology*, Vol. 38, Issue 5, pp.1002-1009, October 2019.
- [4] Ryuta Shiraki, Yojiro Mori, Hiroshi Hasegawa, Ken-ichi Sato, “Design and evaluation of quasi-Nyquist WDM networks utilizing widely deployed wavelength-selective switches,” *OSA Optics Express*, Vol. 27, Issue 13, pp. 18549-18560, June 2019.

International conference

- [5] Ryuta Shiraki, Yojiro Mori, and Hiroshi Hasegawa, “[Invited] Optical path management based on machine learning in optical networks,” in Photonics West, paper 12429-23, San Francisco, USA, February 2023.
- [6] Kenji Cruzado, Ryuta Shiraki, Yojiro Mori, Takafumi Tanaka, Katsuaki Higashimori, Fumikazu Inuzuka, Takuya Ohara, Hiroshi Hasegawa, “Reinforcement-learning-based network design and control with stepwise reward variation and link-adjacency embedding,” in European Conference on Optical Communications (ECOC), paper We2B.3, Basel, Switzerland, September 2022.
- [7] Jun Sakano, Ryuta Shiraki, Yojiro Mori, Hiroshi Hasegawa, “Constellation-shaped 64QAM robust against phase noise in intra-datacenter networks,” in Photonics in Switching and Computing (PSC), paper WF3, Toyama, Japan, July 2022.
- [8] Takeshi Matsuo, Ryuta Shiraki, Yojiro Mori, Hiroshi Hasegawa, “Design and dynamic control of fiber-granular routing networks with next-generation optical paths,” in Optical Fiber Communication Conference (OFC), paper W3F.6, San Diego, USA, March 2022.
- [9] Takeshi Matsuo, Ryuta Shiraki, Yojiro Mori, Hiroshi Hasegawa, “Performance evaluation of dynamic fiber-granular routing networks with next-generation optical paths,” in Optoelectronic and Communications Conference (OECC), paper T2A.8, virtual, July 2021.
- [10] Ryuta Shiraki, Yojiro Mori, Hiroshi Hasegawa, Ken-ichi Sato, “Dynamically controlled flexible-grid networks based on semi-flexible spectrum assignment and network-state-value evaluation,” in Optical Fiber Communication Conference (OFC), paper M1B.4, San Diego, USA, March 2020.
- [11] Ryuta Shiraki, Yojiro Mori, Hiroshi Hasegawa, Ken-ichi Sato, Paolo Monti, “Highly spectrally efficient metro networks that adopt fiber-level granular routing on overlaid line-/ring-shaped virtual topologies,” in Photonics West, paper 11308-17, San Francisco, USA, February 2020.
- [12] Ryuta Shiraki, Yojiro Mori, Hiroshi Hasegawa, Ken-ichi Sato, “Dynamic control of transparent optical networks with adaptive state-value assessment enabled by reinforcement learning,” in International Conference on Transparent Optical Network (ICTON), paper Sa.A3.4, Angers, France, July 2019.

- [13] Ryuta Shiraki, Yojiro Mori, Hiroshi Hasegawa, Ken-ichi Sato, “Quasi-Nyquist WDM network using widely deployed wavelength-selective switches,” in Extremely Advanced Transmission Technologies (EXAT), paper P-24, Mie, Japan, May 2019.
- [14] Ryuta Shiraki, Yojiro Mori, Hiroshi Hasegawa, Ken-ichi Sato, “Demonstration of quasi-Nyquist WDM networks using widely deployed wavelength-selective switches,” in Optical Fiber Communication Conference (OFC), paper M1A.7, San Diego, USA, March 2019.
- [15] Ryuta Shiraki, Shuhei Yamaoka, Yojiro Mori, Hiroshi Hasegawa, Ken-ichi Sato, “Novel network architecture enabling quasi-Nyquist wavelength-division multiplexing,” in Photonics West, paper 10946-11, San Francisco, USA, February 2019.
- [16] Yojiro Mori, Mungun-Erdene Ganbold, Ryuta Shiraki, Kejiro Suzuki, Hiroyuki Matsuura, Hitoshi Kawashima, Shu Namiki, Kazuhiro Ikeda, Ken-ichi Sato, “Fast optical circuit switch using monolithically integrated silicon-photonics space switch and wavelength-tuneable filter,” in European Conference on Optical Communications (ECOC), paper Mo3H.4, Rome, Italy, September 2018.
- [17] Ryuta Shiraki, Yojiro Mori, Hiroshi Hasegawa, Ken-ichi Sato, “Architecture and design of quasi-Nyquist WDM networks with flexible grid granular switching,” in Photonics in Switching and Computing (PSC), paper Fr3A.5, Limassol, Cyprus, September 2018.

Domestic conference

- [18] 樋口 怜治, 白木 隆太, 森 洋二郎, 長谷川 浩, “短距離コヒーレント光通信システムに適する変復調方式,” 電子情報通信学会フォトニックネットワーク研究会, オンライン, 2022 年 11 月.
- [19] 松尾 武, 白木 隆太, 森 洋二郎, 長谷川 浩, “ファイバ粒度ルーティング光ネットワークの動的制御特性,” 電子情報通信学会フォトニックネットワーク研究会, オンライン, 2022 年 11 月.

- [20] 石川 誉聡, 白木 隆太, 森 洋二郎, 長谷川 浩, “スペクトラム狭窄の影響を緩和する予等化フィルタの生成法,” 電子情報通信学会フォトニックネットワーク研究会, PN2022-8, 北海道, 2022 年 8 月.
- [21] クルザド ケンジ, 白木 隆太, 森 洋二郎, 田中 貴章, 東森 一晃, 犬塚 史一, 大原 拓也, 長谷川 浩, “階段型報酬制御とリンク隣接性を用いた光ネットワーク知的设计・制御法,” 電子情報通信学会フォトニックネットワーク研究会, PN2022-14, 北海道, 2022 年 8 月.
- [22] 松尾 武, 白木 隆太, 森 洋二郎, 長谷川 浩, “ファイバ粒度ルーティングネットワークの設計法,” 電気・電子・情報関係学会 東海支部連合大会, L2-6, オンライン, 2022 年 8 月.
- [23] 松尾 武, 白木 隆太, 森 洋二郎, 長谷川 浩, “ファイバ粒度ルーティング光ネットワークの動的制御特性,” 電子情報通信学会フォトニックネットワーク研究会 学生ワークショップ, pn2022-stws-5, オンライン, 2022 年 3 月.
- [24] 松尾 武, 白木 隆太, 森 洋二郎, 長谷川 浩, “ファイバスイッチング型光ネットワークにおける超大容量光パスの動的制御,” 電子情報通信学会フォトニックネットワーク研究会, PN2021-20, pp. 46-50, オンライン, 2021 年 8 月.
- [25] 白木 隆太, 森 洋二郎, 長谷川 浩, 佐藤 健一, “ [依頼講演] 強化学習に基づく光ネットワーク設計 ～ 知的経路スペクトラム選択法 ～,” 電子情報通信学会フォトニックネットワーク研究会, PN2020-9, pp. 27-31, オンライン, 2020 年 6 月.
- [26] 白木 隆太, 森 洋二郎, 長谷川 浩, 佐藤 健一, “フォトニックネットワークの知的制御 –強化学習に基づく経路・波長選択法–,” 電子情報通信学会超知性ネットワークに関する分野横断型研究会, 2019-11-RISING, 東京, 2019 年 11 月.
- [27] 白木 隆太, 森 洋二郎, 長谷川 浩, 佐藤 健一, “強化学習に基づく通信需要分布適応型動的な光パス制御法,” 電子情報通信学会フォトニックネットワーク研究会, PN2019-27, 神奈川, 2019 年 11 月.
- [28] 白木 隆太, 森 洋二郎, 長谷川 浩, 佐藤 健一, “既設波長選択スイッチを用いた準ナイキスト波長分割多重ネットワークの実証,” 電子情報通信学会総合大会, B-12-3, 東京, 2019 年 3 月.

- [29] 白木 隆太, 山岡 修平, 森 洋二郎, 長谷川 浩, 佐藤 健一, “準ナイキスト波長分割多重ネットワークアーキテクチャおよび設計法,” 電子情報通信学会フォトニックネットワーク研究会, PN2018-21, 北海道, 2018 年 9 月.
- [30] 白木 隆太, 森 洋二郎, 長谷川 浩, 佐藤 健一, “リング網における超高密度波長多重と光パス収容法,” 電子情報通信学会総合大会, B-12-14, 東京, 2018 年 3 月.
- [31] 白木 隆太, 森 洋二郎, 長谷川 浩, 佐藤 健一, “超高密度波長多重リング網における動的な光パス収容法,” 電子情報通信学会フォトニックネットワーク研究会, pn2018-stws-3, 鹿児島, 2018 年 3 月.

Awards

- [32] 白木 隆太, IEEE Nagoya Section Conference Presentation Award, 2020 年.
- [33] 白木 隆太, 電子情報通信学会第六回 JPN デザインコンテスト奨励賞, 2020 年.
- [34] 白木 隆太, 電気通信普及財団 テレコムシステム技術学生賞, 2020 年.
- [35] Ryuta Shiraki, Best Student Oral Presentation Award in International Conference on Transparent Optical Network (ICTON), 2019
- [36] 白木 隆太, 電子情報通信学会東海支部学生研究奨励賞, 2019 年.
- [37] 白木 隆太, 名古屋大学電気電子情報工学科研究発表会 最優秀賞, 2018 年.

Patent

- [38] 森 洋二郎, 長谷川 浩, 久野 拓真, 白木 隆太, “信号処理回路、デジタルコヒーレント受信器およびデジタルコヒーレント通信システム,” 特願 2021-028629., 2021 年 02 月